

การศึกษาเชิงทฤษฎีของคีโท-อินอลไอโซเมอไรเซชันในเอช-แซดเอสเอ็ม-5

โดยวิธีดีเอฟทีและอนเน็ยม



นายอัฒศักดิ์ รัตนสัมฤทธิ์

วิทยานิพนธ์นี้เป็นส่วนหนึ่งของการศึกษาตามหลักสูตรปริญญาวิทยาศาสตรมหาบัณฑิต

สาขาวิชาปิโตรเคมีและวิทยาศาสตร์พอลิเมอร์

คณะวิทยาศาสตร์ จุฬาลงกรณ์มหาวิทยาลัย

ปีการศึกษา 2548

ISBN 974-53-2044-7

ลิขสิทธิ์ของจุฬาลงกรณ์มหาวิทยาลัย

THEORETICAL STUDY OF KETO-ENOL ISOMERIZATION IN H-ZSM-5
USING DFT AND ONIOM METHODS



Mr. Attasak Rattanasumrit

สถาบันวิทยบริการ
จุฬาลงกรณ์มหาวิทยาลัย

A Thesis Submitted in Partial Fulfillment of the Requirements
for the Degree of Master of Science in Petrochemistry and Polymer Science
Faculty of Science
Chulalongkorn University
Academic Year 2005
ISBN 974-53-2044-7

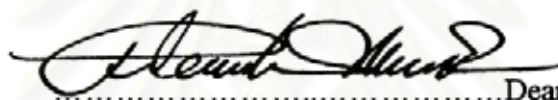
Thesis Title THEORETICAL STUDY OF KETO-ENOL ISOMERIZATION
IN H-ZSM-5 USING DFT AND ONIOM METHODS

By Mr. Attasak Rattanasumrit

Field of study Petrochemistry and Polymer Science

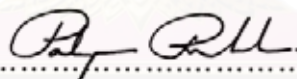
Thesis Advisor Associate Professor Vithaya Ruangpornvisuti, Dr.rer.nat.

Accepted by the Faculty of Science, Chulalongkorn University in Partial
Fulfillment of the Requirements for the Master's Degree

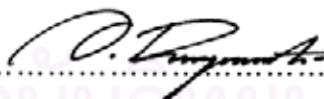


.....Dean of the Faculty of Science
(Professor Piamsak Menasveta, Ph.D.)

THESIS COMMITTEE



.....Chairman
(Professor Pattarapan Prasassarakich, Ph.D.)



.....Thesis Advisor
(Associate Professor Vithaya Ruangpornvisuti, Dr.rer.nat.)



.....Member
(Associate Professor Wimonrat Trakarnpruk, Ph.D.)



.....Member
(Associate Professor Buncha Pulpoka, Ph.D.)

อัครศักดิ์ รัตนสัมฤทธิ์: การศึกษาเชิงทฤษฎีของคีโต-อินอลไอโซเมอไรเซชันในเฮช-ซมดเอส
 เอ็ม-5โดยวิธีดีเอฟทีและออนเนียม (THEORETICAL STUDY OF KETO-ENOL
 ISOMERIZATION IN H-ZSM-5 USING DFT AND ONIOM METHODS).
 อ.ที่ปรึกษา: รศ.ดร.วิทยา เรืองพรวิสุทธิ, 142 หน้า. ISBN 974-53-2044-7

การเปลี่ยนอะซีทัลดีไฮด์เป็นไฮดรอกซีเอทิลีน อะซีโตนเป็น 2-ไฮดรอกซีโพรพิลีน บิวทานโนน
 เป็น 2-ไฮดรอกซีบิวทีน 2-เพนทานโนนเป็น 2-ไฮดรอกซีเพนทีน 3-เมทิล-2-บิวทานโนนเป็น 2-ไฮดรอกซี-
 3-เมทิล-บิวทีน และอะซีโตนเป็น 2-ไฮดรอกซีฟีนิลเอทิลีน โดยเร่งปฏิกิริยาด้วยซีโอไลต์ชนิด
 เฮช-ซมดเอสเอ็ม-5 ได้ศึกษาด้วยวิธีทางเคมีควอนตัม จากการคำนวณโครงสร้างที่เสถียรที่สุดของ
 สารแต่ละสปีชีส์เมื่อทำปฏิกิริยากับซีโอไลต์ชนิดเฮช-ซมดเอสเอ็ม-5 ขนาดโมเดลคลัสเตอร์ 3T
 และ 5T ที่คำนวณด้วยวิธีดีเอฟทีชนิด B3LYP/6-31G(d) และขนาดโมเดลคลัสเตอร์ 50/3T และ
 72/3T ที่คำนวณด้วยวิธีออนเนียมชนิด ONIOM(B3LYP/6-31G(d):AM1) พบว่าปฏิกิริยาที่เกิดขึ้นมี
 3 ขั้นตอนโดยค่าทางเทอร์โมไดนามิกส์ของปฏิกิริยาแต่ละขั้นและค่าคงที่สมดุลของปฏิกิริยาที่ได้
 จากการคำนวณจากปฏิกิริยาสำหรับทุกระบบพบว่าเป็นปฏิกิริยาดูดความร้อน

สถาบันวิทยบริการ
 จุฬาลงกรณ์มหาวิทยาลัย

สาขา วิศวกรรมและวิทยาศาสตร์พลีเมอรัล.....ลายมือชื่อนิสิต.....

ปีการศึกษา.....2548.....ลายมือชื่ออาจารย์ที่ปรึกษา.....

4672501623: PETROCHEMISTRY AND POLYMER SCIENCE PROGRAM

KEY WORD: KETO-ENOL ISOMERIZATION/ H-ZSM-5/ DFT/ ONIOM

ATTASAK RATTANASUMRIT: THEORETICAL STUDY OF KETO-ENOL ISOMERIZATION IN H-ZSM-5 USING DFT AND ONIOM METHODS.

THESIS ADVISOR: ASSOC. PROF. VITHAYA RUANGPORNVISUTI, Dr.rer.nat., 142 pp. ISBN 974-53-2044-7

Conversions of acetaldehyde to hydroxyethylene, acetone to 2-hydroxypropylene, butanone to 2-hydroxybutene, 2-pentanone to 2-hydroxypentene, 3-methyl-2-butanone to 2-hydroxy-3-methylbutene and acetophenone to 2-hydroxyphenylethylene catalyzed by H-ZSM-5 have been theoretically studied using quantum chemical methods. Geometry optimizations of species reacting with H-ZSM-5 using of 3T and 5T cluster models computed at the B3LYP/6-31G(d) level and 50/3T and 72/3T cluster models computed at the ONIOM(B3LYP/6-31G(d):AM1) level have been carried out. Three steps of the reaction mechanism were found and thermodynamic properties of each reaction step and equilibrium constant of overall reaction have been obtained. The overall reaction of the conversion for all systems is endothermic.

สถาบันวิทยบริการ
จุฬาลงกรณ์มหาวิทยาลัย

Field of Study Petrochemistry and Polymer Science Student's signature A. Rattanasumrit

Academic year 2005 Advisor's signature P. Ruangpornvisuti

ACKNOWLEDGEMENTS

First, I would like to express my sincere gratitude to my advisor Associate Professor Dr. Vithaya Ruangpornvisuti for his continuous attention and guidance thought the years of my study. I deeply appreciate the support, encouragement and valuable advice of my committee members, Professor Dr. Pattarapan Prasassarakich, Associate Professor Dr. Wimonrat Trakarnpruk and Associate Professor Dr. Buncha Pulpoka. I also acknowledge Dr. Aticha Chaisuwan who gives me first impression of 'zeolite' as well as Mr. Banchob Wannoo who always assists in intensive quantum and computational chemistry details.

Special appreciation is extended to my colleagues at Supramolecular Chemistry Research Unit (SCRU), Department of Chemistry, Faculty of Science, Chulalongkorn University, Bangkok, Thailand for their kind, friendship, support and encouragement throughout my study.

I gratefully acknowledge the financial assistance from research grant from the Graduate School, Chulalongkorn University for giving an encouragement of present work. The generous supply of computing time by, personal computers at Supramolecular Chemistry Research Unit, Chulalongkorn University is also gratefully acknowledged for research support.

Finally, I would like to dedicate this thesis to my parent, Vithoon and Arunee Rattanasumrit, and my lovely younger sister, Rakarwee Rattanasumrit. Their love and support for me is priceless. I hope my family is proud of my success.

สถาบันวิทยบริการ
จุฬาลงกรณ์มหาวิทยาลัย

CONTENTS

	Page
ABSTRACT IN THAI.....	iv
ABSTRACT IN ENGLISH.....	v
ACKNOWLEDGEMENTS.....	vi
CONTENTS.....	vii
LIST OF FIGURES.....	x
LIST OF TABLES.....	xiii
LIST OF ABBREVIATIONS.....	xv
CHAPTER I: INTRODUCTION.....	1
1.1 Background.....	1
1.2 Zeolite.....	2
1.2.1 Structure of zeolites.....	3
1.2.2 Properties of zeolites.....	7
1.2.2.1 Shape and size selectivity.....	7
1.2.2.2 Cation-exchange.....	9
1.2.2.3 Acid sites (acidity).....	9
1.2.3 ZSM-5 (Zeolite Socony Mobil-5).....	12
1.3 Keto-enol isomerization.....	13
1.4 Literature reviews.....	14
1.4.1 Experimental studied.....	14
1.4.2 Computational studied.....	16
1.5 Objectives.....	20
CHAPTER II: THEORY.....	21
2.1 Molecular mechanics (MM).....	21
UFF (Universal force field).....	22
2.2 Quantum mechanics (QM).....	24
2.2.1 Time-independent Schrödinger equation.....	25

	Page
2.2.2 The Born-Oppenheimer approximation.....	26
2.2.3 Antisymmetry of the wavefunction on exchange of two electrons.....	29
2.2.4 The Slater determinant.....	30
2.2.5 Hartree – Fock equation.....	31
2.2.5.1 The coulomb and exchange operators.....	31
2.2.5.2 The Fock operator.....	32
2.2.6 Restricted closed – shell Hartree-Fock: The Roothaan equation.....	34
Closed – shell Hartree-Fock: Restricted spin orbitals.....	34
2.2.7 The Roothaan equations.....	37
2.2.8 The charge density.....	39
2.2.9 Expression for the Fock matrix.....	40
2.2.10 Orthogonalization of the basis.....	42
2.2.11 Basis sets.....	46
2.2.12 The variational method.....	48
2.3 Semi-empirical methods.....	50
2.4 Density functional theory.....	52
2.4.1 The Hohenberg-Kohn theorem.....	53
2.4.2 The Kohn-Sham equations.....	53
2.4.3 DFT exchange and correlations.....	56
2.4.4 Hybrid functionals.....	57
2.5 ONIOM method.....	59
2.5.1 ONIOM energy definition.....	59
2.5.2 Treatment of link atoms.....	61
CHAPTER III: DETAILS OF THE CALCULATIONS.....	63
3.1 Non-catalytic, water-catalyzed and zeolite models.....	63
3.2 Methods of calculations.....	63

	Page
CHAPTER IV: RESULTS AND DISCUSSION	67
4.1 Geometrical structures, energetics and thermodynamic quantities.....	67
4.1.1 Cluster results.....	68
4.1.2 ONIOM calculations.....	83
4.2 Molecular arrangement on different cluster models.....	96
4.3 Reaction coordinate.....	96
CHAPTER V: CONCLUSIONS AND SUGGESTIONS	106
REFERENCES	108
APPENDICES	115
Appendix A.....	116
Appendix B.....	122
Appendix C.....	127
CURRICULUM VITAE	142



สถาบันวิทยบริการ
จุฬาลงกรณ์มหาวิทยาลัย

LIST OF FIGURES

Figure	Page
1.1 The primary building unit of the zeolite.....	4
1.2 Secondary building units found in zeolite structures.....	4
1.3 Various types of zeolite pores and channels.....	6
1.4 Active sites of zeolite structure: (a) Si atom was substituted by Al atom (b) protonated form of zeolite.....	7
1.5 Diagram depicting the three types of selectivity: (a) reactant, (b) product and (c) transition state shape selectivity.....	8
1.6 Diagram depicting the cation-exchange on the surface of the zeolite.....	9
1.7 Diagram of the “surface” of a zeolite framework.....	10
1.8 The mechanism of framework dealumination.....	11
1.9 The structure of ZSM-5 showing two different channel structures: (a) framework (b) channel system (the straight channel and the zigzag channels).....	12
1.10 Examples of keto-enol equilibrium.....	13
1.11 Mechanism of keto-enol isomerization catalyzed by acid catalyst.....	14
2.1 The ONIOM extrapolation scheme for a molecular system partitioned into (left) and three (right) layers.....	60
2.2 Definition of different atom sets within the ONIOM scheme.....	61
3.1 Atomic numbering for (a) reactants, (b) products, (c) water, (d) 3T and (e) 5T clusters of H-ZSM-5.....	64
3.2 The real and model (3T: color regions) systems of (a) 50/3T and (b) 72/3T cluster of H-ZSM-5 for the two-layered ONIOM(MO:MO) calculations.....	65
4.1 Reaction steps of keto-enol isomerization of reactants (a) acetaldehyde, (b) acetone, (c) butanone, (d) 2-pentanone, (e) 3-methyl-2-butanone and (f) acetophenone interacting with water molecule.....	71
4.2 Reaction steps of keto-enol isomerization of reactant acetaldehyde interacting with 3T (top) and 5T (bottom) cluster models.....	75
4.3 Reaction steps of keto-enol isomerization of reactant acetone interacting with 3T (top) and 5T (bottom) cluster models.....	75

Figure	Page
4.4 Reaction steps of keto-enol isomerization of reactant butanone interacting with 3T (top) and 5T (bottom) cluster models.....	76
4.5 Reaction steps of keto-enol isomerization of reactant 2-pentanone interacting with 3T (top) and 5T (bottom) cluster models.....	76
4.6 Reaction steps of keto-enol isomerization of reactant 3-methyl-2-butanone interacting with 3T (top) and 5T (bottom) cluster models.....	77
4.7 Reaction steps of keto-enol isomerization of reactant acetophenone interacting with 3T (top) and 5T (bottom) cluster models.....	77
4.8 Reaction steps of keto-enol isomerization of reactants (a) acetaldehyde, (b) acetone, (c) butanone, (d) 2-pentanone, (e) 3-methyl-2-butanone and (f) acetophenone interacting with 50/3T cluster model of H-ZSM-5.....	85
4.9 Reaction steps of keto-enol isomerization of reactants (a) acetaldehyde, (b) acetone, (c) butanone, (d) 2-pentanone, (e) 3-methyl-2-butanone and (f) acetophenone interacting with 72/3T cluster model of H-ZSM-5.....	90
4.10 Potential energy surface for keto-enol isomerization of (a) acetaldehyde, (b) acetone, (c) butanone, (d) 2-pentanone (e) 3-methyl-2-butanone and (f) acetophenone in gas phase (model 1).....	98
4.11 Potential energy surface for keto-enol isomerization of (a) acetaldehyde, (b) acetone, (c) butanone, (d) 2-pentanone, (e) 3-methyl-2-butanone and (f) acetophenone catalyzed by water (model 2).....	99
4.12 Potential energy surface for keto-enol isomerization of (a) acetaldehyde, (b) acetone, (c) butanone, (d) 2-pentanone, (e) 3-methyl-2-butanone and (f) acetophenone in the 3T cluster model of H-ZSM-5 (model 3).....	100
4.13 Potential energy surface for keto-enol isomerization of (a) acetaldehyde, (b) acetone, (c) butanone, (d) 2-pentanone, (e) 3-methyl-2-butanone and (f) acetophenone in the 5T cluster model of H-ZSM-5 (model 4).....	101

Figure	Page
4.14 Potential energy surface for keto-enol isomerization of (a) acetaldehyde, (b) acetone, (c) butanone, (d) 2-pentanone, (e) 3-methyl-2-butanone and (f) acetophenone in the 50/3T cluster model of H-ZSM-5 (model 5).....	102
4.15 Potential energy surface for keto-enol isomerization of (a) acetaldehyde, (b) acetone, (c) butanone, (d) 2-pentanone, (e) 3-methyl-2-butanone and (f) acetophenone in the 72/3T cluster model of H-ZSM-5 (model 6).....	103
4.16 Activation energy of keto-enol isomerization of acetaldehyde in H-ZSM-5 zeolite plotted as a function of size of the cluster models.....	105
B-1 Front views of the molecular electrostatic potential (in au), (a) 3T ; (b) 5T.....	123
B-2 Front views of the molecular electrostatic potential (in au), (a) 3T-acetaldehyde ; (b) 5T-acetaldehyde.....	124
B-3 Front views of the molecular electrostatic potential (in au), (a) 3T-TS ; (b) 5T-TS..	125
B-4 Front views of the molecular electrostatic potential (in au), (a) 3T-hydroxyethylene ; (b) 5T-hydroxyethylene.....	126
C-1 3T, 5T and 72T cluster models of H-ZSM-5.....	139
C-2 3T, 5T and 50T cluster models of H-ZSM-5.....	141

LIST OF TABLES

Table	Page
1.1 Zeolite and their secondary building units. The nomenclature used is consistent with that presented in Figure 1.2.....	5
4.1 Geometrical data for various species of free form, form of transition states and product of various systems in gas phase.....	68
4.2 Relative energies and thermodynamic quantities of related species of various systems (model 1).....	70
4.3 Geometrical data for various species of free form, form of transition states and product of various systems catalyzed by water.....	72
4.4 Relative energies and thermodynamic quantities of related species of various systems (model 2).....	74
4.5 Computed stretching vibrational frequencies of hydroxyl groups at O2 and O3 atoms and the selected geometry parameters (bond distances and bond angles) on the 3T (model 3) and 5T (model 4) cluster models of H-ZSM-5.....	80
4.6 Relative energies and thermodynamic quantities of related species of various systems (model 3 and model 4).....	82
4.7 Computed stretching vibrational frequencies of hydroxyl groups at O2 and O3 atoms and selected geometry parameters (bond distances and bond angles) on 50/3T (model 5) cluster model of H-ZSM-5, ONIOM(B3LYP:AM1).....	87
4.8 Relative energies and thermodynamic quantities of related species of various systems (model 5), ONIOM(B3LYP:AM1).....	89
4.9 Computed stretching vibrational frequencies of hydroxyl groups at O2 and O3 atoms and selected geometry parameters (bond distances and bond angles) on 72/3T (model 6) cluster model of H-ZSM-5, ONIOM(B3LYP:AM1).....	92
4.10 Relative energies and thermodynamic quantities of related species of various systems (model 6), ONIOM(B3LYP:AM1).....	94
4.11 Activation energies of related model of various systems.....	104
A-1 Unit cell of 72T cluster.....	117
A-2 Dipole moment of all reactants and all products.....	120

Figure	Page
A-3 Computed stretching vibrational frequencies of hydroxyl groups at O2 and O3 atoms and selected geometry parameters (bond distances and bond angles) on 50/3T (model 5) and 72/3T (model 6) cluster models of H-ZSM-5.....	121
A-4 Relative energies and thermodynamic quantities of related species of various systems.....	121



สถาบันวิทยบริการ
จุฬาลงกรณ์มหาวิทยาลัย

LIST OF ABBREVIATIONS

au	=	Atomic units
AM1	=	Austin model 1
B3LYP	=	Becke's three parameter hybrid functional using the LYP correlation function
BLYP	=	Beck-Lee-Yang-Parr function
BSSE	=	Basis set superposition error
CBS	=	Complete basis set
CP	=	Counterpoise method
DFT	=	Density functional theory
ECP	=	Effective core potential
E-ONIOM	=	Embedded ONIOM
FQEC	=	Full quantum embedded cluster
FT-IR	=	Fourier transform infrared
GGA	=	Generalized gradient approximation
HF	=	Hartree-Fock
IMOMO	=	Integrated molecular orbital-molecular orbital
IR	=	Infrared spectroscopy
IRC	=	Intrinsic reaction coordinate
kcal/mol	=	Kilocalorie per mole
KS	=	Kohn-Sham
LCAO	=	Linear combination of atomic orbitals
LDA	=	Local density approximation
LSD	=	Local spin density approximation
LYP	=	Lee-Yang-Parr functional
MAS NMR	=	Magic angle spinning nuclear magnetic resonance
MFI	=	Mobil-five
MM	=	Molecular mechanics
MNDO	=	Modified neglect of differential overlap
MO	=	Molecular orbital

MP2	=	The second-order Møller-Plesset perturbation theory
NMR	=	Nuclear magnetic resonance
ONIOM	=	Our own N-layered integrated molecular orbital and molecular mechanics
ppm	=	Parts per million
QM	=	Quantum mechanics
QM/MM	=	Quantum mechanical/molecular mechanical
QM-Pot	=	Combined quantum mechanics - interatomic potential functions
SBU	=	Secondary building unit
SCF	=	Self-consistent field
STO	=	Slater type orbital
STO-3G	=	Slater type orbital approximated by 3 gaussian type orbitals
STQN	=	Synchronous transit-guided quasi-newton
TPD	=	Temperature programmed desorption
UFF	=	Universal force field
UV	=	Ultraviolet
VWN	=	Vosko-Wilk-Nusair functional
XRD	=	X-ray diffraction
ZPE	=	Zero-point energy
ZSM-5	=	Zeolite Socony Mobil-5

CHAPTER I

INTRODUCTION

1.1 Background

Various reactions can be catalyzed by acid and base catalysts such as H_2SO_4 , H_3PO_4 , NaOH etc. However, these corrosive catalysts cause a number of problems concerning handling, safety, corrosion and waste disposal. Therefore, the conventional liquid-acid catalysts are progressively being replaced by heterogeneous catalysts. Many types of catalysts have been used for many reactions such as various metal oxides and various zeolites. In recent years, there have been considerable academic and industrial research efforts carried out in the field of zeolite catalysis.

The few last decade up to present, zeolites have played very important role in the petroleum and petrochemical industries. They have been known as the one of the most important heterogeneous catalysts. [1-4] Therefore, zeolites were widely studied for their acidic properties of Brønsted acid sites [5-6] using several techniques. [7-21] ZSM-5 (Zeolite Socony Mobil-5) is one of the most useful catalysts that have been widely used in the petroleum and petrochemical industries. ZSM-5 is a representative member of a new class of high-silica zeolites having considerable significance as catalyst materials. Examples of their uses include the conversion of methanol to gasoline (MTG), dewaxing of distillates, and the interconversion of aromatic compounds. Proton-exchanged zeolites present high acidity, and so, they are commonly used in acid-catalyzed reactions such as double bond migration, skeletal reorganization, or aldol condensation. [1, 2]

To elucidate the information of the zeolite structure and the chemistry of the active site of zeolitic catalysts, the wide range of experimental techniques have been used such as UV, IR, NMR, XRD and TPD techniques. As an alternative, theoretical methods and computational technologies have been developed as a practical tool to retrieve information of the system at the molecular level. Theoretical interest in zeolites originates from the need to understand their function as catalysts, adsorbents, and ion-exchangers, and from a vision of making improved materials by design. This is not possible without knowledge of the relationship between structure, properties, and

reactivity. Although numerous experiments have been made many questions still remain unsolved. The crystal structure of certain complex solids can be solved only with the aid of modeling techniques. Numerous theoretical models, including the periodic calculations, have been proposed to study the crystalline zeolite. Such a large deviation indicates an important effect of the extended framework in stabilizing the adsorption complex. To accurately include the effects of the extended zeolite framework on the catalytic properties, one can employ the periodic electronic structure methods such as the periodic density functional theory (DFT) methodology. However, due to the large unit cells of typical zeolites, such calculations are often computationally unfeasible. On the other hand, the hybrid methods, such as the embedded cluster or combined quantum mechanics/molecular mechanics (QM/MM) methods, as well as the more general ONIOM (Our-own-N-layer Integrated molecular Orbital + molecular Mechanics) [22] provide a cost effective computational strategy for including the effects of the zeolite framework.

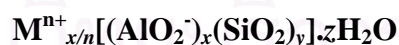
1.2 Zeolite

Zeolite was discovered in 1756 by the Swedish mineralogist, Boron Axel F. Cronstrdt, as the natural minerals. The word “zeolite” is Greek in origin, derived from the words “zein” and “lithos” meaning “to boil” and “rock”. Many new types of natural minerals have been discovered and a large number of synthetic zeolites have been developed for specifically commercial proposes. The synthetic zeolite was interested in the application of shape selective zeolite catalyst in the petrochemical companies such as Union Carbide and Mobil. In the 1950s and early 1960s, Union Carbide Company made several discoveries which proved to be of great economic significance and propelled them to the forefront of zeolite science. Milton and Breck of the Linde division of the Union Carbide company, over a period of 5 years, developed and characterized three novel zeolites classified as types A, X and Y, which have become 3 of the most profitable synthetic zeolites. In 1962 Mobil Oil introduced the use of synthetic of zeolite X as a cracking catalyst. In 1969 Grace described the first modification chemistry based on steaming zeolite Y to form an “ultrastable” Y. In 1967-1969 Mobil Oil reported the synthesis of the high silica

zeolites beta and ZSM-5. In 1974 Henkel introduced zeolite A in detergents as a replacement for the environmentally suspect phosphates. By 1977 industry-wide 22,000 tons of zeolite Y was in use in catalytic cracking. In 1977 Union Carbide introduced zeolite for ion-exchange separations.

1.2.1 Structure of zeolites

Zeolites are three-dimensional, microporous, crystalline aluminosilicate materials constructed from tetrahedral units (primary building units; Figure 1.1), TO_4 , such as $[\text{SiO}_4]^{4-}$ and $[\text{AlO}_4]^{5-}$. Each of tetrahedral centers is connected via oxygen atom formed Si-O-Si and Si-O-Al bridges. These tetrahedra are linked together by corner sharing of Si or Al atoms in various ways, forming a secondary building unit (SBU; Figure 1.2). Most zeolite frameworks can be generated from several different SBU. A secondary building unit consists of selected geometric groupings of those tetrahedra, which can be used to describe all of known zeolite structures. Descriptions of known zeolite structure based on their SBU are listed in Table 1.1. The various types of zeolites are built up from different composition and framework to generate different pores and channels which demonstrate the ability to prevent or allow the program of a reaction (Figure 1.3). A representative unit cell formula for the composition of a zeolite is:



where M is the exchangeable cation of valence n; y/x is the Si/Al molar ratio, and is equal to or greater than 1 because Al^{3+} does not occupy adjacent tetrahedral sites, otherwise the negatively charged units next to each other will be obtained; and z is the number of water molecules located in the channels and cavities inside a zeolite.

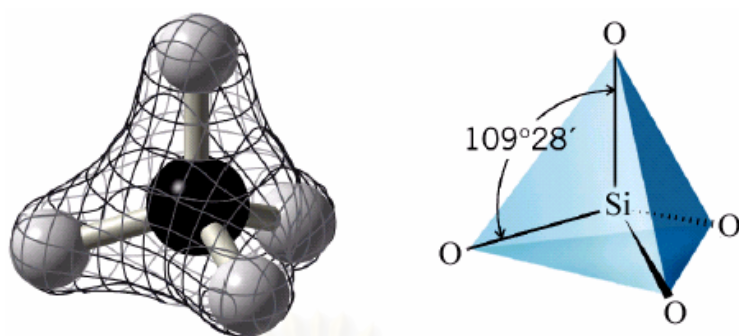


Figure 1.1 The primary building unit of the zeolite.

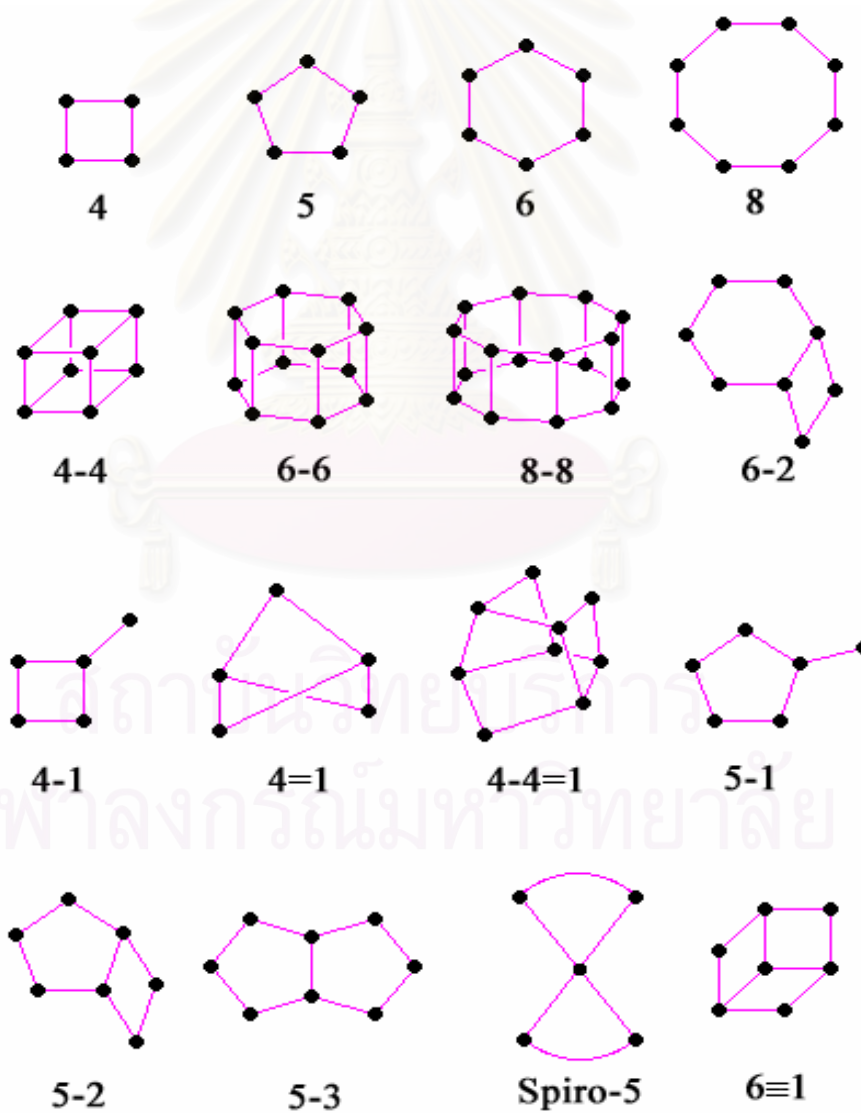


Figure 1.2 Secondary building units found in zeolite structures.

Table 1.1 Zeolite and their secondary building units. The nomenclature used is consistent with that presented in Figure 1.2.

Zeolite	Secondary building units								
	4	6	8	4-4	6-6	8-8	4-1	5-1	4-4-1
Analcime	X	X							
ZSM-5								X	
Mordenite								X	
Sodalite	X	X							
Type A	X	X	X	X					
Stilbite									X
Cancrinite							X		
Faujasite	X	X			X				
Chabasite	X	X			X				
Merlionite	X		X			X			

Exceptions of type of zeolites, the active site region also shows the dramatic effect in the properties of zeolites. The difference of oxidation state of Si^{4+} and Al^{3+} in zeolites is the crucial reason for the active site occurring. The charges imbalance occurs when the Si^{3+} substituted by Al^{4+} , and to maintain the system natural, each $[\text{AlO}_4]^{5-}$ tetrahedral center needs a balancing positive charge such as proton or monovalence cation (Figure 1.4). These compensation species present the specific active sites of zeolite in various applications. If the charge compensating cation is H^+ , a bridged hydroxyl group, $(\text{Si}-\text{O}(\text{H})-\text{Al})$, is formed, which functions as a strong Brønsted acid site. Due to these acid sites, zeolites are solid acids and are used as catalysts. The catalytic activity of zeolites is often related to strength of the acid sites, which depends on chemical composition and topology of zeolite frameworks. There are numerous naturally occurring and synthetic zeolites. However, most zeolites used commercially are produced synthetically, each with a unique structure. Zeolites have void and space (cavities or channels) that can host cations, water or other molecules.

Zeolites are widely used industrially as a catalyst for a variety of reactions and separation processes. The active site of zeolite also plays a crucial role in catalyzing the reactions.

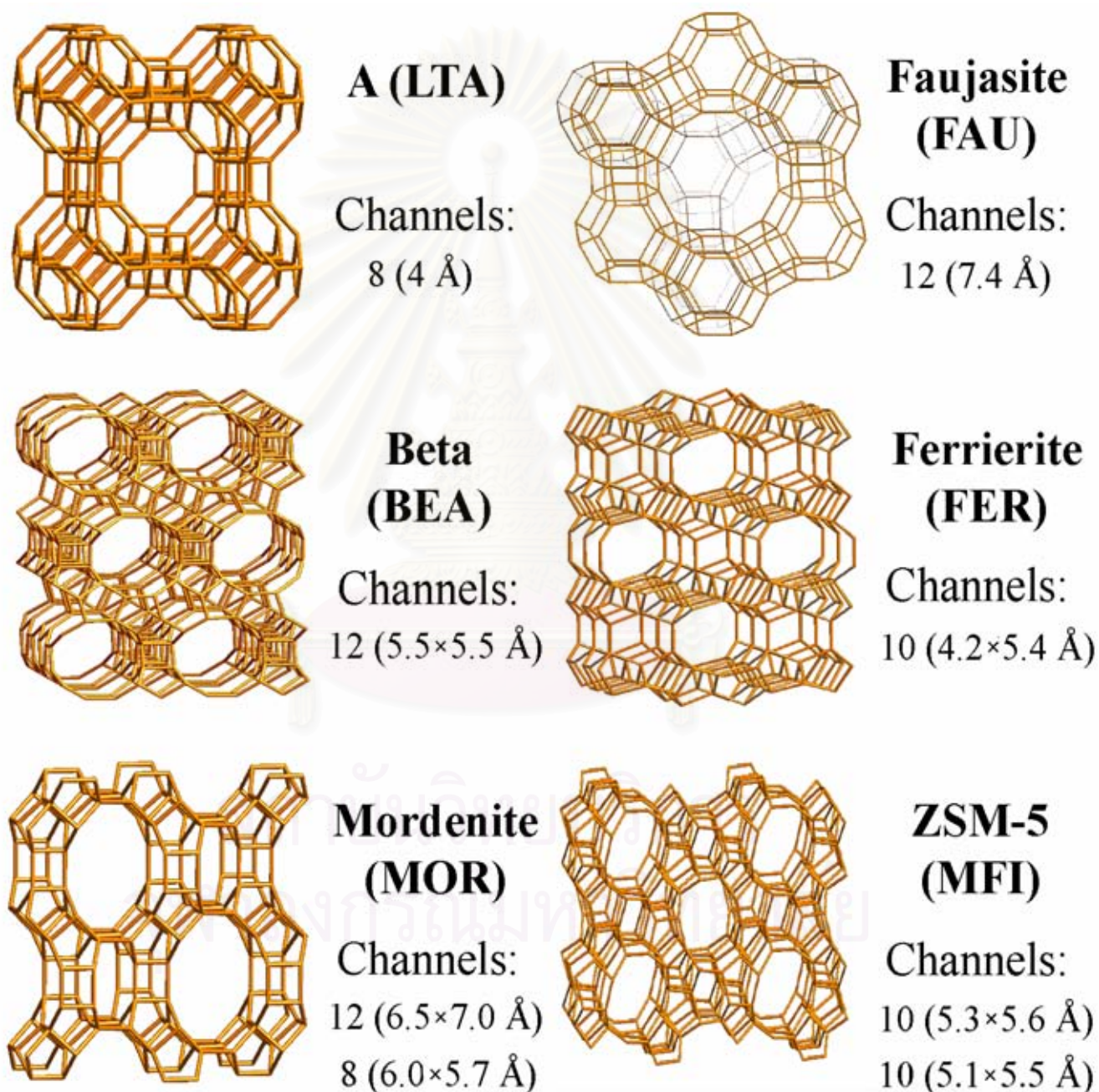


Figure 1.3 Various types of zeolite pores and channels.

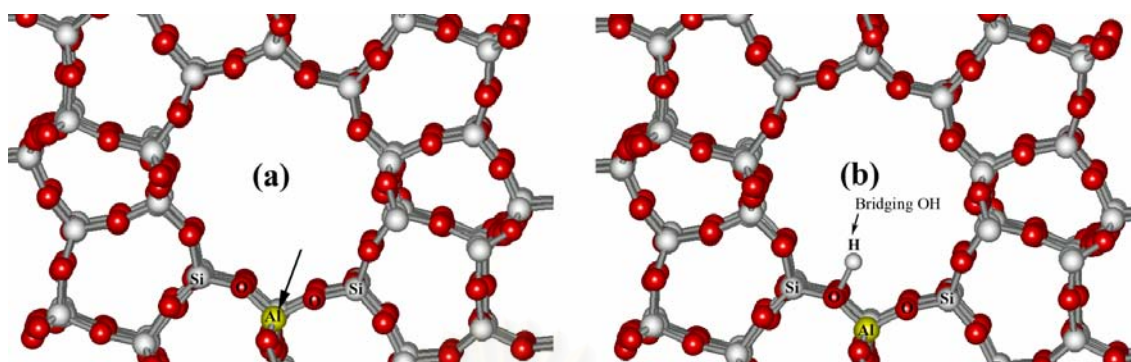


Figure 1.4 Active sites of zeolite structure: (a) Si atom was substituted by Al atom (b) protonated form of zeolite.

1.2.2 Properties of zeolites [23]

1.2.2.1 Shape and size selectivity

Shape and size selectivity plays a very important role in catalysis. Highly crystalline and regular channel structures are among the principal features that molecular sieves used as catalysts offer over other materials.

There are three types of shape selectivity: reactant shape selectivity, product shape selectivity, and transition-state shape selectivity. These types of selectivity are depicted in Figure 1.5. Reactant shape selectivity results from the limited diffusion of some of the reactants, which cannot effectively enter and diffuse inside the crystal. Product shape selectivity occurs when slowly diffusing product molecules cannot rapidly escape from the crystal, and undergo secondary reactions. Restricted transition-state shape selectivity is a kinetic effect arising from the local environment around the active site, i.e. the rate constant for a certain reaction mechanism is reduced if the necessary transition state is too bulky to form readily.

The critical diameter (as opposed to the length) of the molecules is important in predicting shape selectivity. However, molecules are deformable and can pass through smaller opening than their critical diameter. Hence not only size but also the dynamics and structure of the molecules must be taken into account.

An equivalent to activation energy exists for the diffusion of molecules inside the molecular sieve because the temperature-dependent translational energy of

molecule (as move through the force fields in the pores) must increase significantly as the dimensions of the molecular configuration approach the void dimensions of the crystal. It should be noted that the effective diffusivity varies with molecular type; adsorption affinity affects diffusivity, and rapidly reacting molecules (such as olefins) show diffusion mass transfer limitations inside the structure due to their extreme reactivity.

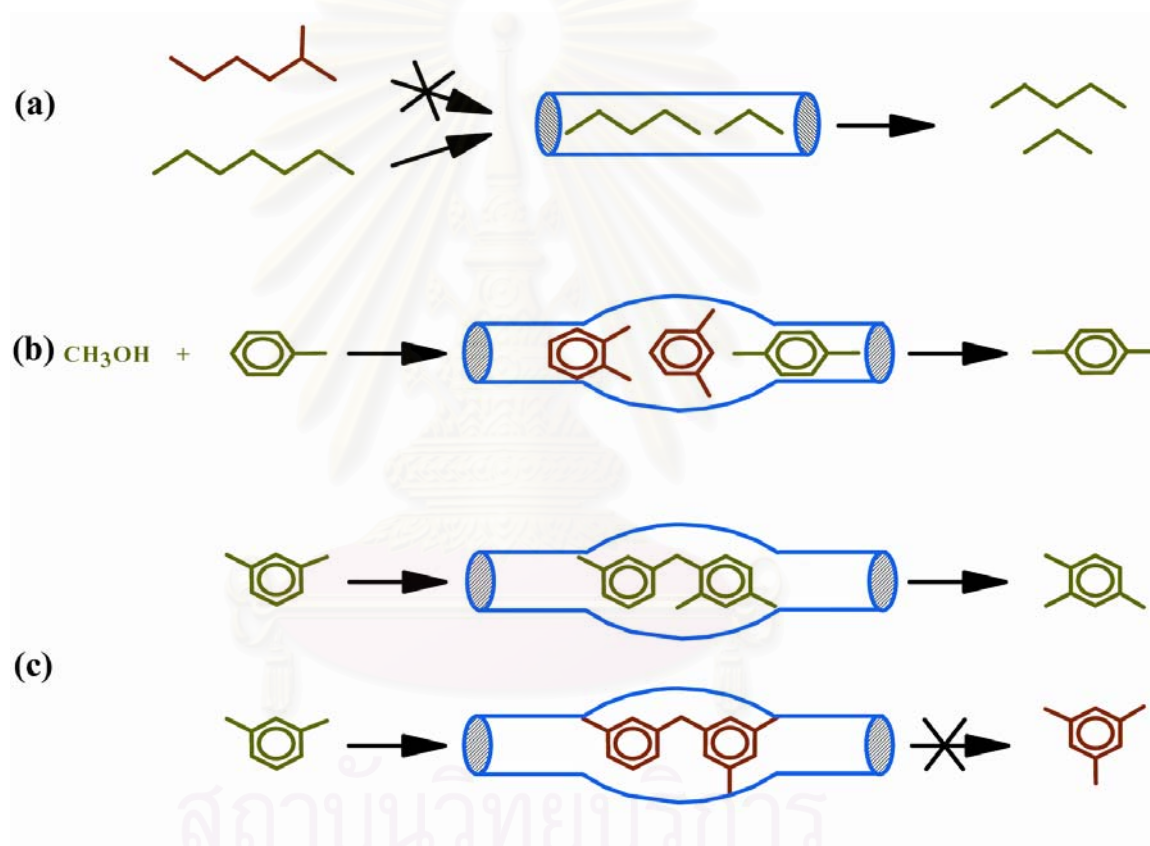


Figure 1.5 Diagram depicting the three types of selectivity: (a) reactant, (b) product and (c) transition state shape selectivity.

The effective size and relative accessibility of the pore and cavities can be altered by partially blocking the pore and/or by changing the molecular sieve crystal size. The effect of shape selective are especially induced by the above two methods when the diffusivities of these species differ significantly.

1.2.2.2 Cation-exchange

On the surface of the zeolite, there are the cations that neutralize the negative charge created by the AlO_2^- tetrahedra in the structure. Typical cations include, the alkaline (Na^+ , K^+ , Rb^+ , Cs^+) and alkaline earth (Mg^{2+} , Ca^{2+}) cations. The cations are on the surface that can exchange to the other cations that are shown in the Figure 1.6.

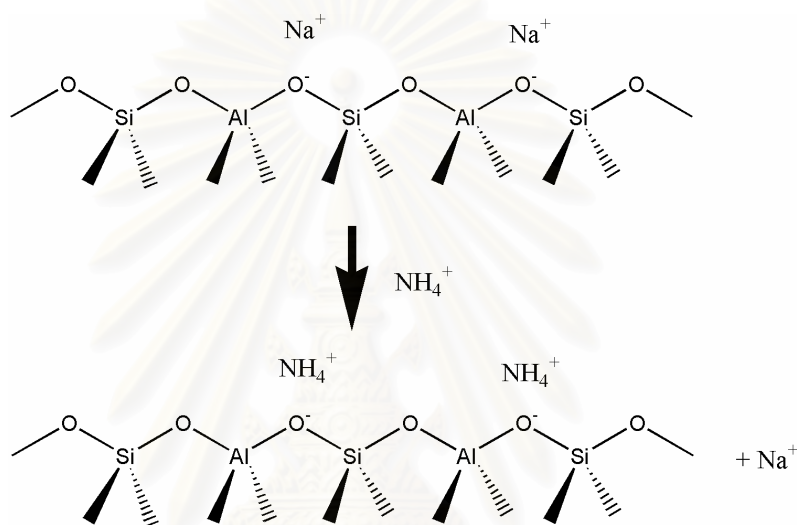


Figure 1.6 Diagram depicting the cation-exchange on the surface of the zeolite.

1.2.2.3 Acid sites (acidity)

All of the variation pretreatment conditions as well as synthesis and post-treatments (hydrothermal, thermal and chemical), affect the ultimate acidity an activity observed in the zeolite molecular sieves. Both Brønsted and Lewis acid sites are exhibited in these materials, with assertions by various investigations that:

1. Brønsted acid sites are the active center.
2. Lewis acid sites are the active center.
3. Brønsted and Lewis acid sites together act as the active centers.
4. Cations or the other types of sites in small concentrations act in the conjunction with the Brønsted/Lewis acid sites to function as the active center.

Dealumination by acid treatment results in material having similar properties with dealuminated zeolites resulting from dehydroxylation as shown in Figure 1.8. In general, chemical treatments, including acid extraction of aluminum from zeolite framework, usually affect the external surface of crystal. Hydrochloric acid treatment, for example, removes aluminum to yield a silica-rich external surface.

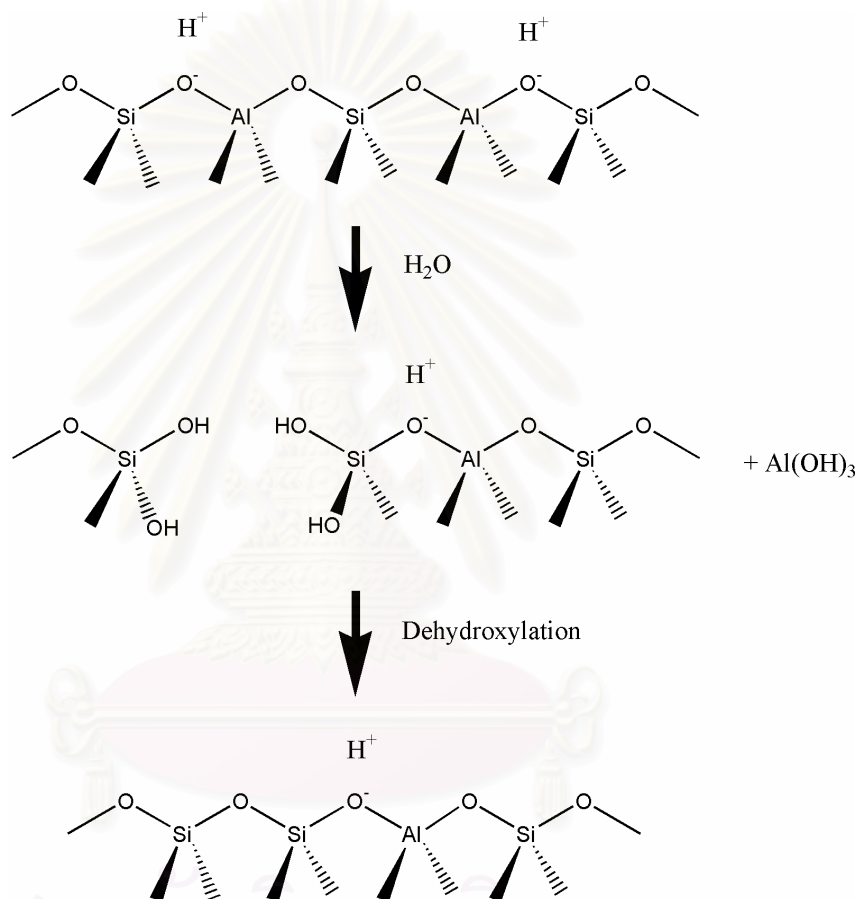


Figure 1.8 The mechanism of framework dealumination.

The products of dealumination can be extracted from the molecular sieve pores by the use of acid. However, the removal of the aluminum from the lattice has been claimed to produce a “nest” of four Si-O-H silanols. Dehydroxylation is believed to accomplish at the area of the silanol “nest”, followed by reconnection of Si-O-Si bonds. As a result the unit cell of zeolites is contracted.

1.2.3 ZSM-5 (Zeolite Socony Mobil-5)

ZSM-5 (Zeolite Socony Mobil-5 is discovered by Mobil Oil Company) is a commercial name of MFI zeolite with high silica to alumina ratio, and H-ZSM-5 is ZSM-5, which is compensated negative charge by H^+ . The dimensions of the pores and channels are of the order of a nanometer ($1 \text{ nm} = 10 \text{ \AA}$). In some cases, the channels of the internal surface form intersections that are considerably larger than their channels. For example, the diameter of the roughly cylindrical pores and channels of zeolites having the MFI topology as ZSM-5 are about 5 \AA (Figure 1.9), but the diameter of the roughly spherical intersection is about 9 \AA which act as nanoscopic catalytic reactors. ZSM-5 has two types of channel, both formed by 10-membered oxygen rings. The first of these channel is straight channel and elliptical in cross section ($5.1 \times 5.5 \text{ \AA}$), the second pores is zigzag or sinusoidal channels and are circular ($5.4 \times 5.6 \text{ \AA}$) in cross section. The intersection of both channels is called intersection channel.

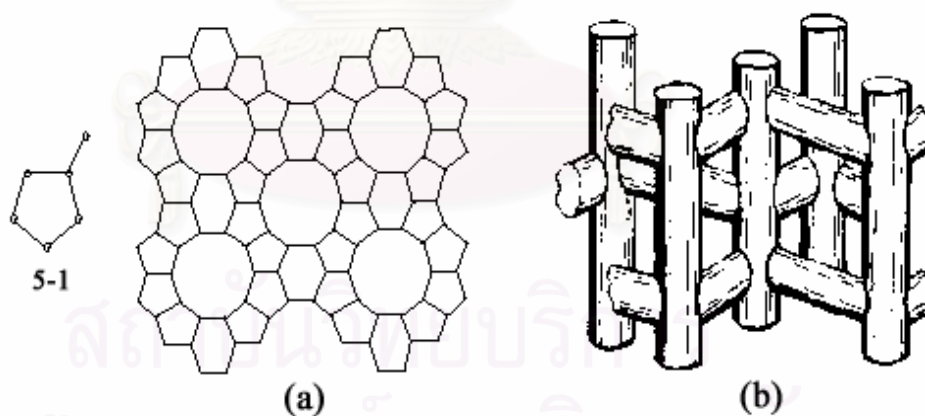


Figure 1.9 The structure of ZSM-5 showing two different channel structures: (a) framework (b) channel system (the straight channel and the zigzag channels).

1.3 Keto-enol isomerization

Aldehydes and ketones exist in solution as an equilibrium mixture of two isomeric forms, the keto form and the enol (from -ene + -ol, unsaturated alcohol) form. For simple aliphatic ketones, there is very little of the enol form present at equilibrium, as shown in Figure 1.10.

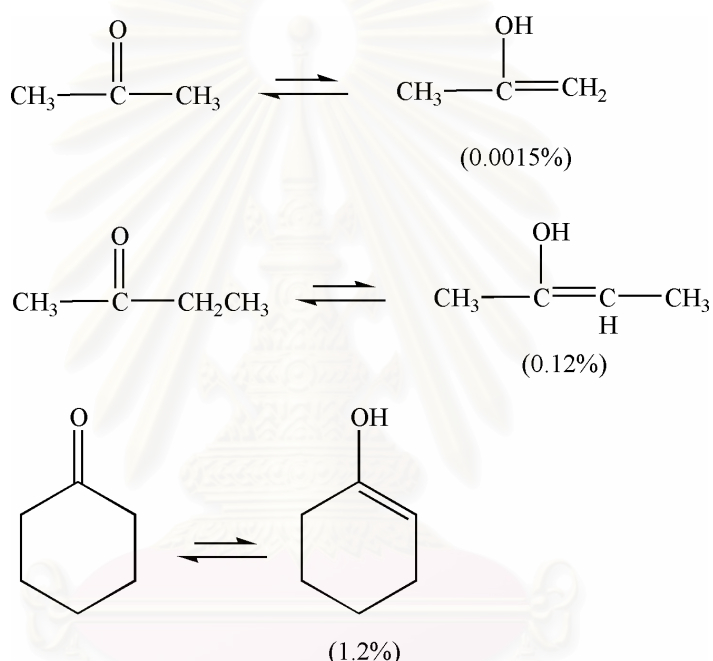


Figure 1.10 Examples of keto-enol equilibrium.

This type of isomerization, where isomers differing only by the placement of a proton and the corresponding location of a double bond, is commonly referred to as tautomerization. The isomers are known as tautomers. [24]

The aldol condensation is a very important reaction in organic synthesis because it leads to the formation of C-C bonds. Because of that, the use of different catalysts and in particular the use of zeolites for the catalysis of this reaction has been considered by several authors. [1, 25-29] The proposed mechanism for the aldol condensation in zeolites assumes that the first step is keto-enol isomerization of the aldehyde or ketone, as shown in Figure 1.11. In second step the enol reacts with an

aldehyde or ketone molecule that is coordinated to a Brønsted acid site of the zeolite. Thus, the formation of the enol form of the aldehyde or ketone molecule, through keto-enol isomerization, is a very important reaction in the aldol condensation. [30]

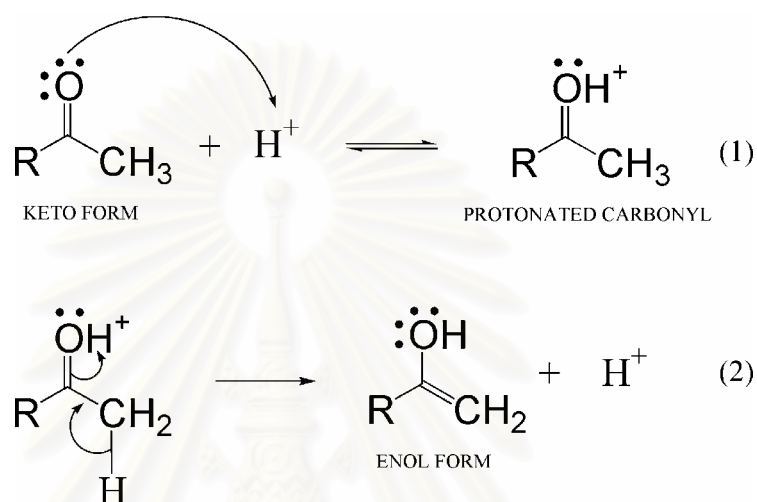


Figure 1.11 Mechanism of keto-enol isomerization catalyzed by acid catalyst.

1.4 Literature reviews

1.4.1 Experimental studied

The “ion-pair” structure of acetone on zeolite was found by Kubelkova *et al.* in 1991. [25] The carbonyl bond in ketone is perturbed far more by the bridging hydroxyl of active site of zeolite causing the formation of a protonated ketone. However, the ^{13}C NMR spectroscopy has also been used to study the condensation of acetaldehyde and acetone by Biaglow *et al.* in 1995. [26] This experiment which indicated the adsorptions of acetone and acetaldehyde with H-ZSM-5 are hydrogen bond at low converge. At room temperature acetone adsorbed on H-ZSM-5 with hydrogen bond and can be transformed to mesityl oxide at higher temperature and converge. The ^{13}C NMR chemical shift for C=O of acetone on H-ZSM-5 has been found at 223 ppm.

In 1994, Xu *et al.* [31] studied the adsorption of acetone using ^{13}C MAS NMR spectroscopy, the structure of the adsorbed acetone on H-ZSM-5 would involve strong hydrogen bonding. The proton transfer can be observed on H-ZSM-5 to mesityl oxide which is a product of aldol condensation of acetone, in the ^{13}C chemical shift. However, they observed an odd peak at 85 ppm, which disappeared when mesityl oxide formed. It is possible that the acetone can form an alkoxide intermediate. Furthermore, the ^1H MAS NMR spectroscopy (Böhlmann *et al.* in 2002 [32]; Xu *et al.* in 2003 [33]) indicated the acetone on H-ZSM-5 which was a strong interaction. The ^1H MAS NMR result showed that the enol formed as an intermediate.

The heat of adsorption for acetone on H-ZSM-5 was measured by Sepa *et al.* in 1996. [28] The average of the measurements from the lowest surface coverage up to one molecule per acid site is 31.3 ± 1.0 kcal/mol. The heat of adsorption of acetone in silicalite is equal to 16.01 ± 0.5 kcal/mol. The standard heat of reaction of acetone to form mesityl oxide is -26.68 kcal/mol of acetone.

In 1998, Panov and Fripiat [34] studied the condensation reaction of acetone on H-ZSM-5, which has been studied by FT-IR. Under identical conditions, the reaction rate is faster on alumina, and the condensation goes beyond the formation of mesityl oxide while zeolites without aluminum are poor catalysts. It seems that the reaction occurs between a molecule in the gas phase and a molecule activated on a Lewis acid and the reaction goes further than mesityl oxide.

In 2001, Dumitriu *et al.* [27] studied the aldol condensation of lower aldehydes on H-ZSM-5. The surface properties of zeolite were investigated by temperature-programmed reduction, X-ray photoelectron spectroscopy, temperature-programmed desorption of ammonia, Fourier transform infrared spectroscopy and microcalorimetry. Vapor phase aldol condensation of acetaldehyde on H-ZSM-5 has been carried out, and it has been observed that the structure features of the catalysts do play an important role in controlling conversion and selectivity. Moreover, the increase of the aluminium content in the H-ZSM-5 samples has a strong influence on the catalytic selectivity to aldol products.

1.4.2 Computational studied

The theoretical study of carbonyls on clusters zeolite was under taken by Sepa *et al.* in 1996. [28] They simulate the zeolite by a small cluster 3T consisting of a few atom surrounding the zeolite hydroxyl bond. The ab initio calculations were performed at the Hartree-Fock (HF) level using 6-31G(d) basis set functions. The interaction of acetone on H-ZSM-5 is through hydrogen-bond type.

In 1998, Barich *et al.* [35] studied the interaction of acetone with H-ZSM-5, which investigated using ^{13}C NMR and B3LYP/DZV2P techniques. The adsorption of acetone on H-ZSM-5 is by hydrogen bond formation. In this work, the acetone-zeolite cluster, the predicted value is 224.0 ppm for chemical shift of ^{13}C NMR, which is in good agreement with the experimental value of 223 ppm.

In further theoretical studies, the carbonyls on clusters zeolite were studied in various clusters by Kassab *et al.* in 1999. [29] The cluster models used were 1T, 3T and 10T calculated at HF/6-31G(d). The interaction energies of acetaldehyde and acetone were -12.17 and -11.14 kcal/mol, respectively. The complex formed is a hydrogen bond complex. In this work the mechanism silyl-ether complex formation also studied.

In 2000, Santiago *et al.* [36] studied the keto-enol isomerization of neutral acetaldehyde and ionized acetaldehyde, both isolated and catalyzed by solvent molecules have been studied using the B3LYP and MP2 levels of theory. The results show that ionization favors the enolization of acetaldehyde, although the energy barrier is still too large that the process will not be observed. In contrast, solvent molecules produce an important catalytic effect. In particular, for the methanol solvated system, the transition state of the isomerization lies below the $\text{CH}_3\text{CHO}^+ + \text{CH}_3\text{OH}$ ground-state asymptote.

In 2001, Khaliullin *et al.* [37] studied an experimental and quantum chemical calculations of the interactions of CH_4 with H-ZSM-5. Adsorption of methane on the

Brønsted acid sites of H-ZSM-5 results in a shift of the ν_1 and ν_3 vibrational bands of methane by -15 cm^{-1} and -23 cm^{-1} , respectively. A shift of -93 cm^{-1} was observed in the O-H vibrational frequency for the Brønsted acid center. Quantum chemical calculations demonstrate that these vibrational band shifts are attributed to the effects of the electrostatic field created by the atoms in the zeolite on the adsorbed methane. The methods used in this study under predict the observed heat of adsorption for CH_4 and the shift in the vibrational frequency for bridging OH group of the Brønsted acid center.

In 2002, Monford *et al.* [30] studied the keto-enol isomerization of acetaldehyde within H-ZSM-5. It has been studied using the B3LYP density functional approach and modeling the zeolite with 3T and 5T clusters. Moreover, the effect of enlarging the cluster to 63T has been considered using the ONIOM2 approach and combining the B3LYP method with the AM1 semi-empirical one. It is observed that the zeolite produces an important catalytic effect on the enolization reaction. The catalytic effect is much larger than that produced by a water molecule, due to the larger acidity of the zeolite and to smaller geometry reorganizations along the process. Results with clusters 3T and 5T are very similar. Enlarging the size of the cluster to 63 tetrahedra with the ONIOM2 approach destabilizes the keto intermediate and stabilizes the enol one, which results in a decrease of the endothermic of the reaction. The ONIOM2 procedure allows us to consider quite large clusters at a reasonable computational cost, which naturally introduce the limited flexibility of the zeolite without imposing artificial constraints.

In 2003, Panjan and Limtrakul [38] studied the influence of the framework on adsorption properties of ethylene/H-ZSM-5 system. The adsorption of ethylene on H-ZSM-5 zeolites has been investigated with six different cluster sizes. The bare 3T quantum cluster approach predicts the $[\text{C}_2\text{H}_4]/\text{H-ZSM-5}$ complexes to have the binding energies of 24.25 kcal/mol . The effect of the zeolite framework is modeled by the ONIOM2 method. They found that the extended framework significantly enhances the adsorption energy of ethylene to the zeolites. In particular, the final predicted adsorption energy of 29.14 kcal/mol for the $[\text{C}_2\text{H}_4]/\text{H-ZSM-5}$ complexes

was calculated by the ONIOM2(B3LYP/6-311++G(d,p):HF/3-21G) method. This efficient scheme performs superbly as compared with the experimental estimate of 29 kcal/mol. The results obtained in the present study suggest that the ONIOM approach yields a more accurate and practical model in studying adsorption of unsaturated hydrocarbons on zeolite.

In 2003, Raksakoon and Limtrakul [39] studied the adsorption of aromatic hydrocarbon onto H-ZSM-5. The adsorption of benzene on H-ZSM-5 zeolites has been investigated with four different cluster sizes. The bare 3T quantum cluster approach predicts the $[C_6H_6]/H-ZSM-5$ complexes to have the binding energies of 25.99 kcal/mol. The effect of the zeolite framework is modeled on the ONIOM2 method. They found that the extended framework significantly enhances the adsorption energy of benzene to the zeolites. In particular, the final predicted adsorption energy of 213.75 kcal/mol for the $[C_6H_6]/H-ZSM-5$ complexes was calculated by the ONIOM2(MP2/6-31G(d,p):HF/3-21G) scheme. This efficient scheme performs superbly as compared with the experimental estimate of 214.0 kcal/mol. The results obtained in the present study suggest that the ONIOM approach yields a more accurate and practical model in studying adsorption of unsaturated hydrocarbons on zeolites.

In 2003, Milas and Nascimento [40] studied the dehydrogenation and cracking of isobutane over HZSM-5 using the B3LYP/6-31G** level of calculation, using a 20T cluster to represent the zeolite. From the comparison of the results obtained with the 5T and 20T clusters, no major differences in the mechanism of both reactions were observed as the size of the cluster was increased. Nevertheless, as expected from the nature of the transition state, the energetic of the reactions was clearly affected by the presence of the zeolite cavity. Finally, despite the reactions having similar activation energies, the 20T calculations suggest that at more hindered acid sites the dehydrogenation reaction should be favored.

In 2003, Bhan *et al.* [41] investigated the alkoxide formation from olefins (propene, 1-hexene and 3-hexene) in H-ZSM-5. They conclude that the protonation

energy of an olefinic molecule is relatively independent of carbon number but varies significantly with the extent of interaction with the zeolite wall and steric hindrance. Hence, the protonation energy of a molecule is not only indicative of the interaction between the Brønsted acid proton and the molecule but also depends on a significant extent on the interaction of the protonated molecule with the zeolite wall. Thus, changes in zeolite structure may affect the energetics of alkoxide formation dramatically.

In 2004, Sillar and Burk [42, 43] studied the Brønsted acid sites in eight different crystallographic positions of the zeolite ZSM-5. Both types of bridged hydroxyl groups (types 1 and 2) were represented among the studied acid sites. Their calculations show that in the case of the second type of Brønsted acid site the hydrogen of the bridged hydroxyl group forms a hydrogen bond with one of the lattice oxygen atoms. In the case of the first type of bridged hydroxyl group, the distortion of the local environment around Al indicates that hydrogen atoms in the first type of bridged hydroxyl group are also influenced by an electrostatic interaction (primarily) with nearby oxygen atoms. The calculated ^1H NMR chemical shifts and stretching vibrational frequencies of bridged hydroxyl groups are in good accordance with experimental measurements, showing that the calculation method used can reproduce the properties of zeolites acid sites well. The analysis of experimental IR and ^1H NMR spectra in combination with current calculations suggests that the experimentally observable mean acidity of zeolite ZSM-5 is dependent on temperature.

In 2004, Zheng and Blowers [44] studied the ethane cracking, hydrogen exchange and de-hydrogenation reactions catalyzed by a zeolite using ab initio methods. The transition state structures were optimized using HF and MP2 methods, and the energies were obtained using a CBS composite energy method. The effects of zeolite cluster size and acidity on the activation barriers were investigated. Additionally, the choice of HF and MP2 geometry optimization methods and the effects on the barrier heights were also studied. The activation energies obtained for cracking, hydrogen exchange and dehydrogenation reactions are 71.39, 31.39 and

75.95 kcal/mol, respectively, using geometries optimized at the MP2 level. This indicates that the hydrogen exchange reaction has the lowest barrier and is the easiest reaction to happen, while the dehydrogenation reaction has the highest barrier and is the most difficult to happen.

1.5 Objectives

In this work, conversion reactions of acetaldehyde (ACD) to hydroxyethylene (HETH), acetone (ACT) to 2-hydroxypropylene (HPRO), butanone (BTN) to 2-hydroxybutene (HBUT), 2-pentanone (PTN) to 2-hydroxypentene (HPEN), 3-methyl-2-butanone (MBTN) to 2-hydroxy-3-methylbutene (HMBUT) and acetophenone (ACP) to 2-hydroxyphenylethylene (HPETH) in gas phase, catalyzed by water and H-ZSM-5 have been theoretically studied employing the calculations of B3LYP/6-31G(d) for gas phase, water-catalyzed and zeolite-catalyzed of 3T, 5T cluster models, and ONIOM(B3LYP/6-31G(d):AM1) for 50/3T and 72/3T cluster models. The energetic and thermodynamic quantities of catalytic reactions for each models have been determined via their transition structures.

The goals of this study are, firstly, to analyze the catalytic effect of H-ZSM-5 on keto-enol isomerization and compare it to that of water molecules and, secondary, to discuss the behavior of DFT method and of different theoretical strategies within ONIOM method for studying this kind of systems.

CHAPTER II

THEORY OF CALCULATION

Computational chemistry (also called molecular modeling; the two terms mean about the same thing) is a set of techniques for investigating chemical problems on a computer. [45] The computational chemistry is concerned with the calculating and predicting the properties of atomic and molecular systems. It is based on the fundamental laws of quantum mechanics and uses a variety of mathematical transformation and approximation techniques to solve the fundamental equations. This section provides an introduction overview of the theory underlying electronic structure methods.

2.1 Molecular mechanics (MM)

Molecular mechanics is based on a mathematical model of a molecule as a collection of balls (corresponding to the atoms) held together by springs (corresponding to the bonds). The *mathematical* model is thus conceptually very close to the intuitive feel for molecular energetics that one obtains when manipulating molecular models of plastic or metal: the model resists distortions from the “natural” geometry that corresponds to the bond lengths and angles imposed by the manufacturer, and in the case of space-filling models, atoms cannot be forced too closely together. The MM model clearly ignores electrons. In other words, MM uses a conceptually *mechanical* model of a molecule to find its minimum-energy geometry (for flexible molecules, the geometries of the various conformers). The form of the mathematical expression for the energy, and the parameters in it, constitute a *force field*, and MM methods are sometimes called force field methods.

UFF (Universal force field)

The parameters used to generate the Universal force field include a set of hybridization dependent atomic bond radii, a set of hybridization angles, van der Waals parameters, torsional and inversion barriers, and a set of effective nuclear charges.

The potential energy of an arbitrary geometry for a molecule is written as superposition of various two-body, three-body, and four-body interaction.

$$E_{tot} = \sum_{k,l} V_{k,l}(\vec{R}_k, \vec{R}_l) + \sum_{k,l,m} V_{k,l,m}(\vec{R}_k, \vec{R}_l, \vec{R}_m) + \sum_{k,l,m,n} V_{k,l,m,n}(\vec{R}_k, \vec{R}_l, \vec{R}_m, \vec{R}_n). \quad (1)$$

Here, the first term is the two-body term, the second term is the three-body and third term is the four-body interaction. The potential energy as sum of valence or bonded interactions and nonbonded interactions

$$E = E_R + E_\theta + E_\phi + E_\omega + E_{vdw} + E_{el}. \quad (2)$$

The valence interactions consist of bond stretching (E_R) and angular distortions that are bond angle bending (E_θ), dihedral angle torsion (E_ϕ) and inversion terms (E_ω). The nonbonded interactions consist of van der Waals (E_{vdw}) terms and electrostatic (E_{el}) terms.

The universal force field describes the bond stretch interaction as either a harmonic oscillator (Hooke's law)

$$E_R = \frac{1}{2} k_{IJ} (r - r_{IJ})^2 \quad (3)$$

or as the Morse function

$$E_R = D_{IJ} [e^{-\alpha(r-r_{IJ})} - 1]^2 \quad (4)$$

where k_{IJ} is the force constant in units of (kcal/mol)/Å, r_{IJ} is the standard or natural bond length in angstroms, D_{IJ} is the bond dissociation energy (kcal/mol), and

$$\alpha = [k_{IJ} / 2D_{IJ}]^{1/2} \quad (5)$$

The angle bend term is described with a small cosine Fourier expansion in θ

$$E_{\theta} = K_{IJK} \sum_{n=0}^m C_n \cos(n\theta) \quad (6)$$

where the C_n are coefficients, K_{IJK} are the angle bend force constants. The torsional terms for two bonds IJ and KL connected via a common bond JK is described with a small cosine Fourier expansion in ϕ

$$E_{\phi} = K_{IJKL} \sum_{n=0}^m C_n \cos(n\phi_{IJKL}) \quad (7)$$

For UFF, a one- or two-term cosine Fourier expansion in ω is used for atoms I bonded exactly to three other atoms J, K, L

$$E_{\omega} = K_{IJKL} (C_0 + C_1 \cos(\omega_{IJKL}) + C_2 \cos(2\omega_{IJKL})) \quad (8)$$

where K_{IJKL} is the force constant in (kcal/mol) and ω_{IJKL} is the angle between the IL axis and the IJK plane. The energy of van der Waals interactions, E_{vdw} , is written as the sum of interactions between pairs of nonbonded atom. A Lennard-Jones 6-12 potential is

$$E_{vdw} = \left[\frac{a}{R} \right]^6 + \left[\frac{b}{R} \right]^{12} \quad (9)$$

where a and b are constants and R is the interatomic distance. For UFF a Lennard-Jones 6-12 potential expression is used

$$E_{vdw} = D_{IJ} \left\{ -2 \left[\frac{x_{IJ}}{x} \right]^6 + \left[\frac{x_{IJ}}{x} \right]^{12} \right\} \quad (10)$$

where D_{IJ} is the well depth in kcal/mol and x_{IJ} is the van der Waals bond length in Å. The electrostatic (E_{el}) interactions are calculated by

$$E_{el} = 332.0637(Q_i Q_j / \epsilon R_{ij}) \quad (11)$$

Q_i and Q_j are charges in electron units, R_{ij} is the distance in angstroms, and ϵ is the dielectric constant. The default dielectric constant is 1 for UFF.

2.2 Quantum mechanics (QM)

The word *quantum* comes from Latin (*quantus*, “how much?”, plural *quanta*) and was first used in our sense by Max Planck in 1900, as an adjective and noun, to denote the constrained *quantities* or amounts in which energy can be emitted or absorbed. Although the term *quantum* mechanics was apparently first used by Born (of the Born-Oppenheimer approximation) in 1924, in contrast to classical mechanics, the matrix algebra and differential equation techniques that we now associate with the term were presented in 1925 and 1926.

“Mechanics” as used in physics is traditionally the study of the behavior of bodies under the action of forces like, e.g. gravity (celestial mechanics). Molecules are made of nuclei and electrons, and quantum chemistry deals, fundamentally, with the motion of electrons under the influence of the electromagnetic force exerted by nuclear charges.

Quantum mechanics (QM) is the correct mathematical description of the behavior of electrons and thus of chemistry. In theory, QM can predict any property of an

individual atom or molecule exactly. In practice, the QM equations have only been solved exactly for one electron systems. A myriad collection of methods has been developed for approximating the solution for multiple electron systems. These approximations can be very useful, but this requires an amount of sophistication on the part of the researcher to know when each approximation is valid and how accurate the results are likely to be.

The QM was formulated independently by Erwin Schrödinger and Werner Heisenberg in 1925. Schrödinger's method is formulated in terms of the partial differential equations used to describe waves (hence its name of wave mechanics). Heisenberg's method used matrices and at first glance appears very different from Schrödinger's. It was shown, however, that the two ways are mathematically equivalent. Chemistry customarily uses the wave mechanics method to develop its treatment of quantum mechanics. I will start our formulation of quantum mechanics with an introduction to wave mechanics.

The solutions to the Schrödinger equation are called wave functions and these wave functions give a complete description of any system. The Schrödinger equation can not be derived, instead it is postulated, that is, assumed to be true for the purposes of our reasoning. It is in fact the fundamental postulate of quantum mechanics.

2.2.1 Time-independent Schrödinger equation

The problems in quantum mechanics are usually concerned with many-electron system which it deals with the time-independent Schrödinger equation. The time-independent Schrödinger equation is

$$\hat{H}\Psi = E\Psi \quad (12)$$

Where \hat{H} is the Hamiltonian operator, representing all contributions of energies in the system. E is the total energy of the system. The wavefunction, Ψ , is a function of the electronic and atomic nuclei coordinates that describes the considerate system. In atomic units, the Hamiltonian for n electrons and M nuclei is the summation of kinetic energy operator and potential energy operator.

$$\hat{H} = \hat{T} + \hat{V} \quad (13)$$

\hat{T} represents the summation of kinetic energy operator of electron and atomic nuclei,

$$\hat{T} = -\frac{1}{2} \sum_{i=1}^n \nabla_i^2 - \frac{1}{2m_A} \sum_{A=1}^M \nabla_A^2 \quad (14)$$

The differential operator “del squared” in equation (14) is known as Laplacian operator. The operator del is equivalent to partial differentiation with respect to x, y and z components.

In cartesian coordinate;
$$\nabla^2 = \frac{\partial^2}{\partial x^2} + \frac{\partial^2}{\partial y^2} + \frac{\partial^2}{\partial z^2} \quad (15a)$$

In polar coordinate;
$$\nabla^2 = \frac{1}{r^2} \frac{\partial}{\partial r} \left(r^2 \frac{\partial}{\partial r} \right) + \frac{1}{r^2 \sin \theta} \frac{\partial}{\partial \theta} \left(\sin \theta \frac{\partial}{\partial \theta} \right) + \frac{1}{r^2 \sin^2 \theta} \frac{\partial^2}{\partial \phi^2} \quad (15b)$$

and \hat{V} presents the potential energy operator consist of nuclei-electron attraction, electron-electron repulsion and nuclei-nuclei repulsion.

$$\hat{V} = -\sum_{i=1}^n \sum_{A=1}^M \frac{Z_A}{r_{iA}} + \sum_{i=1}^n \sum_{j>i}^n \frac{1}{r_{ij}} + \sum_{A=1}^M \sum_{B>A}^M \frac{Z_A Z_B}{R_{AB}} \quad (16)$$

2.2.2 The Born-Oppenheimer approximation

Since nuclei are much heavier than electrons, they move much slower. To a good approximation, the electrons can adjust themselves almost simultaneously to any changes in the position of the nuclei. In the Born-Oppenheimer approximation, we consider electrons in a molecule to be moving in the field of fixed nuclei. The electronic wavefunctions thus depend only on the positions but not on the momenta of

nuclei. Therefore, the motion of electron can be decoupled from the motion of the nuclei.

$$\Psi(\{r_i\}; \{R_A\}) = \psi_{elec}(\{r_i\}; \{R_A\}) \psi_{nucl}(\{R_A\}) \quad (17)$$

Within the Born-Oppenheimer approximation, the kinetic energy of the nuclei can be neglected and the repulsion between the nuclei can be considered to be constant. The electronic wavefunction ψ_{elec} , which describes the motion of electrons and depends parametrically on the nuclei coordinates, is the solution to a Schrödinger equation involving the electronic Hamiltonian,

$$\hat{H}_{elec} \psi_{elec} = E_{elec} \psi_{elec} \quad (18)$$

The motion of nuclei is described by the nuclear wavefunction ψ_{nucl} , which is the solution to a nuclear Schrödinger equation.

$$\hat{H}_{nucl} \psi_{nucl} = E \psi_{nucl} \quad (19)$$

The electronic Hamiltonian operator \hat{H}_{elec} describing the motion of n electrons in the field of K nuclei is

$$\hat{H}_{elec} = \sum_{i=1}^n -\frac{1}{2} \nabla_i^2 - \sum_{i=1}^n \sum_{A=1}^K \frac{Z_A}{r_{iA}} + \sum_{i=1}^n \sum_{j < i}^n \frac{1}{r_{ij}} \quad (20)$$

and the nuclear Hamiltonian operator \hat{H}_{nucl} is

$$\hat{H}_{nucl} = -\sum_{A=1}^K \frac{1}{2M_A} \nabla_A^2 + E_{elec}(\{R_A\}) + \sum_{A=1}^K \sum_{B > A}^K \frac{Z_A Z_B}{R_{AB}} \quad (21)$$

Henceforth, the electronic problem of equation (18) will be concentrated only on the electronic Hamiltonian \hat{H} and the electronic wavefunctions ψ , without subscript “elec” labeled.

In the Hartree Approximation the n-electron wavefunction Ψ^{HP} is simply written as a product of one-electron wavefunctions φ_i .

$$\Psi^{HP}(x_1, x_2, \dots, x_n) = \varphi_1(x_1) \varphi_2(x_2) \dots \varphi_n(x_n) \quad (22)$$

Such a many-electron wavefunction is termed a Hartree product, with electron-one being described by the orbital φ_1 , electron-two being described by the orbital φ_2 , etc. Using the Hartree product, the energy is just the sum of the orbital energies ε_i .

$$E = \varepsilon_1 + \varepsilon_2 + \dots + \varepsilon_n \quad (23)$$

The orbital energies ε_i are obtained from

$$h(i)\varphi_j(x) = \varepsilon_j\varphi_j(x) \quad (24)$$

where $h(i)$ is the operator describing the kinetic energy and potential energy of electron i.

The Hartree product is an uncorrelated wavefunction because the probability of finding one electron at a given point in space, $|\varphi_i(x_i)|^2 dx_i$, is independent of the position of other electrons. Moreover, it takes no account of the indistinguishability of electrons.

2.2.3 Antisymmetry of the wavefunction on exchange of two electrons

In systems with more than one electron a fundamental problem arises as we cannot distinguish between the electrons. This is because we cannot specify position and linear momentum at the same time and thus cannot follow electron trajectories. Thus, we cannot really “put labels” on the electrons. In other words, quantum mechanics must still predict the same expectation values for all observables when we interchange the coordinates (three space coordinates and spin coordinate) of two electrons. For all possible values of the coordinates, we must have this means that the two wavefunctions must be the same, except for their phase, In other words, the exchange of the coordinates of two electrons can only result in a phase shift of the wavefunction.

Wavefunction in a system consisting of more than one particle. With respect to interchange of two particles, the wavefunction can be either symmetric (it remains unchanged) or antisymmetric (it just changes sign). A quantum-mechanical treatment of the helium atom agrees with experiment if and only if one postulates that the wavefunction must be antisymmetric with respect to exchange of two electrons. Furthermore, by postulating that wavefunctions in many-electron systems are generally antisymmetric with respect to exchange of two electrons one can derive the Pauli principle. This requirement for antisymmetry is therefore a generalization of the Pauli principle.

In general, the wavefunction is antisymmetric for particles with half-integral spin such as electrons, protons and neutrons. Such particles are called fermions. It can be shown that the probability to find two fermions with the same magnetic spin quantum number m_s at the same time in the same place is zero (Pauli repulsion). This is not true for two electrons with different values of m_s . In contrast, bosons with integral spin require symmetric wavefunctions. In a system of bosons, all particles can occupy the same state of lowest energy (Bose-Einstein condensation).

2.2.4 The Slater determinant

To satisfy the Pauli Exclusion principle – that the wavefunction of electrons must be antisymmetric with respect to electron-interchange, in the Hartree-Fock theory the wavefunction is given by the Slater determinants of N spin-orbitals.

$$\psi(x_1, x_2, \dots, x_n) = \frac{1}{\sqrt{n!}} \begin{vmatrix} \phi_1(x_1) & \phi_2(x_1) & \cdots & \phi_n(x_1) \\ \phi_1(x_2) & \phi_2(x_2) & \cdots & \phi_n(x_2) \\ \vdots & \vdots & & \vdots \\ \phi_1(x_n) & \phi_2(x_n) & \cdots & \phi_n(x_n) \end{vmatrix} \quad (25)$$

The factor $\frac{1}{\sqrt{n!}}$ is a normalization factor. A Slater determinant $\psi(x_1, x_2, \dots, x_n)$ can be written in short form which includes the normalization constant and only shows the diagonal elements of the determinant,

$$\psi(x_1, x_2, \dots, x_n) \equiv |\phi_1(x_1) \phi_2(x_2) \dots \phi_n(x_n)\rangle \quad (26)$$

The antisymmetric property of a Slater determinant is

$$|\dots \phi_i \dots \phi_j \dots\rangle = -|\dots \phi_j \dots \phi_i \dots\rangle. \quad (27)$$

Notation for One- and Two- Electron Integrals: If \hat{P} is any quantum mechanical operator for the property P , the expectation value of property P , denoted $\langle P \rangle$, for the system described by the wavefunction ψ is defined by

$$\langle P \rangle = \int \psi^* \hat{P} \psi d\tau \equiv \langle \psi | \hat{P} \psi \rangle \quad (28)$$

When the wavefunction ψ is expressed in a Slater determinant from equation (26) the matrix element P_{ij} is defined as

$$P_{ij} = \int \varphi_i \hat{P} \varphi_j d\tau \equiv \langle \varphi_i | \hat{P} | \varphi_j \rangle \quad (29)$$

The notation for two-electron integrals over orbitals is

$$\int dx_1 dx_2 \varphi_i^*(x_1) \varphi_j^*(x_2) \frac{1}{r_{12}} \varphi_k(x_1) \varphi_l(x_2) = \langle \varphi_i \varphi_{1j1} | \varphi_k \varphi_{l1} \rangle = \langle ij | kl \rangle \quad (30)$$

2.2.5 Hartree – Fock equation.

2.2.5.1 The coulomb and exchange operators

Hartree – Fock equation is

$$\left[h(1) + \sum_{b \neq a} \rho_b(1) - \sum_{b \neq a} \kappa_b(1) \right] \chi_a(1) = \varepsilon_a \chi_a(1) \quad (31)$$

Or

$$h(1) \chi_a(1) + \sum_{b \neq a} \left[\int dx_2 |\chi_b(2)|^2 r_{12}^{-1} \right] \chi_a(1) - \sum_{b \neq a} \left[\int dx_2 \chi_b^*(2) \chi_a(2) r_{12}^{-1} \right] \chi_a(1) = \varepsilon_a \chi_a(1) \quad (32)$$

Where

$$h(1) = -\frac{1}{2} \nabla_1^2 - \sum_A \frac{Z_A}{r_{1A}} \quad (33)$$

This term stand for a one-electron Schrödinger equation for the spin orbital (χ_a) state of a single electron field of the nuclei.

$$V_a^{coul}(1) = \sum_{b \neq a} \int dx_2 |\chi_b(2)|^2 r_{12}^{-1} \quad (34)$$

This term stands for coulomb term. The coulomb term has a simple interpretation. Suppose electron 2 occupied χ_b . The two electron potential r_{12}^{-1} felt by electron 1 and associated with instantaneous position of electron 2, which obtained by averaged the interaction r_{12}^{-1} of electron 1 and electron 2, over all space and spin coordinates x_2 of electron 2, weight by probability $dx_2 |\chi_b(2)|^2$ that electron 2 occupies the volume element dx_2 at x_2 .

Summing over all $b \neq a$ obtained the total averaged potential acting on the electron in χ_a . It is convenient to define a coulomb operator.

$$\rho_b(1) = \int dx_2 |\chi_b(2)|^2 r_{12}^{-1} \quad (35)$$

The last term in equation (32) stands for exchange integrals, defined by its effect when operating on spin orbital χ_a , introduced in form exchange operator $\kappa_b(1)$.

$$\kappa_b(1)\chi_a(1) = \left[\int dx_2 \chi_b^*(2) r_{12}^{-1} \chi_a(2) \right] \chi_b(1) \quad (36)$$

The result of operating with $\kappa_b(1)$ on $\chi_a(1)$ depends on values of $\chi_a(1)$ throughout all space.

2.2.5.2 The Fock operator.

$$\left[h(1) + \sum_{b \neq a} \rho_b(1) - \sum_{b \neq a} \kappa_b(1) \right] \chi_a(1) = \varepsilon_a \chi_a(1) \quad (37)$$

As

$$[\rho_a(1) - \kappa_a(1)]\chi_a(1) = 0 \quad (38)$$

It's mean no coulomb and exchange interaction by itself therefore, it can define Fock operator f by

$$f(1) = h(1) + \sum_b \rho_b(1) - \kappa_b(1) \quad (39)$$

so that the Hartree-Fock equations become

$$f|\chi_a\rangle = \varepsilon_a|\chi_a\rangle \quad (40)$$

This is the usual from the Hartree equation. The Fock operator $f(1)$ is the sum of a core-Hamiltonian operator $h(1)$.

And an effect one-electron potential operator called the Hartree-Fock potential $v^{HF}(1)$

$$v^{HF}(1) = \sum_b \rho_b(1) - \kappa_b(1) \quad (41)$$

That is

$$f(1) = h(1) + v^{HF}(1) \quad (42)$$

Sometimes it is convenient to write the exchange potential in term of an operator P_{12} which operate to the right, interchange electron 1 and electron 2. Thus

$$\kappa_b(1)\chi_a(1) = \left[\int dx_2 \chi_b^*(2) r_{12}^{-1} \chi_a(2) \right] \chi_b(1) \quad (43)$$

$$= \left[\int dx_2 \chi_b^*(2) r_{12}^{-1} P_{12} \chi_b(2) \right] \chi_a(1) \quad (44)$$

The exact solutions to Hartree-Fock equation correspond to the exact Hartree-Fock spin orbitals. In practice it is only possible to solve this equation exactly for atom. One normally, instead, introduce a set of basis functions for expansion of the spin orbitals and solves set of matrix equation. Only as the basis set approaches completeness, i.e., as one approach the Hartree-Fock limit, will the spin orbitals that one obtains approach the exact Hartree-Fock spin orbitals.

2.2.6 Restricted closed – shell Hartree-Fock: The Roothaan equation.

Closed – shell Hartree-Fock: Restricted spin orbitals.

A restricted set of spin orbitals has the form

$$\chi_i(x) = \psi_j(r)\alpha(\omega) \text{ and } \psi_j(r)\beta(\omega) \quad (45)$$

and the closed-shell restricted ground state is

$$|\Psi_0\rangle = |\chi_1\chi_2 \cdots \chi_{N-1}\chi_N\rangle = \left| \psi_1\psi_2 \cdots \psi_a \psi_a \cdots \psi_{N/2}\psi_{N/2} \right\rangle \quad (46)$$

Hartree-Fock equation.

$$f(x_1)\chi_i(x_1) = \varepsilon_i\chi_i(x_1) \quad (47)$$

The spin orbital $\chi_i(x_1)$ will have either the α and β spin function, Let's assume α , identical results will be obtained by assuming β

$$f(x_1)\psi_j(r_1)\alpha(\omega_1) = \varepsilon_j\psi_j(r_1)\alpha(\omega_1) \quad (48)$$

Multiplying this equation by $\alpha^*(\omega_1)$ and integrating over spin gives

$$\left[\int d\omega_1 \alpha^*(\omega_1) f(x_1) \alpha(\omega_1) \right] \psi_j(r_1) = \varepsilon_j \psi_j(r_1) \quad (49)$$

The Fock operator is

$$f(x_1) = h(r_1) + \sum_c^N \int dx_2 \chi_c^*(x_2) r_{12}^{-1} (1 - P_{12}) \chi_c(x_2) \quad (50)$$

equation (49) becomes

$$\begin{aligned} \left[\int d\omega_1 \alpha^*(\omega_1) f(x_1) \alpha(\omega_1) \right] \psi_j(r_1) &= \left[\int d\omega_1 \alpha^*(\omega_1) h(r_1) \alpha(\omega_1) \right] \psi_j(r_1) + \\ &\left[\int d\omega_1 dx_2 \alpha^*(\omega_1) \chi_c^*(x_2) r_{12}^{-1} (1 - P_{12}) \chi_c(x_2) \alpha(\omega_1) \right] \psi_j(r_1) \\ &= \varepsilon_j \psi_j(r_1) \end{aligned} \quad (51)$$

If we let $f(r_1)$ be the closed-shell Fock operator

$$f(r_1) = \int d\omega_1 \alpha^*(\omega) f(x_1) \alpha(\omega_1) \quad (52)$$

then

$$\begin{aligned} f(r_1) \psi_j(r_1) &= h(r_1) \psi_j(r_1) + \sum_c \int d\omega_1 dx_2 \alpha^*(\omega_1) \chi_c^*(x_2) r_{12}^{-1} \chi_c(x_2) \alpha(\omega_1) \psi_j(r_1) \\ &\quad - \sum_c \int d\omega_1 dx_2 \alpha^*(\omega_1) \chi_c^*(x_2) r_{12}^{-1} \chi_c(x_1) \alpha(\omega_2) \psi_j(r_2) \\ &= \varepsilon_j \psi_j(r_1) \end{aligned} \quad (53)$$

The sum over occupied spin orbitals includes an equal sum over those with the α spin function and those with the β spin function

$$\sum_c^N \rightarrow \sum_c^{N/2} + \sum_{\bar{c}}^{N/2} \quad (54)$$

and therefore

$$\begin{aligned}
f(r_1)\psi_j(r_1) &= h(r_1)\psi_j(r_1) \\
&+ \sum_c^{N/2} \int d\omega_1 d\omega_2 dr_2 \alpha^*(\omega_1)\psi_c^*(r_2)\alpha^*(\omega_2)r_{12}^{-1}\psi_c(r_2)\alpha(\omega_2)\alpha(\omega_1)\psi_j(r_1) \\
&+ \sum_c^{N/2} \int d\omega_1 d\omega_2 dr_2 \alpha^*(\omega_1)\psi_c^*(r_2)\beta^*(\omega_2)r_{12}^{-1}\psi_c(r_2)\beta(\omega_2)\alpha(\omega_1)\psi_j(r_1) \\
&- \sum_c^{N/2} \int d\omega_1 d\omega_2 dr_2 \alpha^*(\omega_1)\psi_c^*(r_2)\alpha^*(\omega_2)r_{12}^{-1}\psi_c(r_1)\alpha(\omega_1)\alpha(\omega_2)\psi_j(r_2) \\
&- \sum_c^{N/2} \int d\omega_1 d\omega_2 dr_2 \alpha^*(\omega_1)\psi_c^*(r_2)\beta^*(\omega_2)r_{12}^{-1}\psi_c(r_1)\beta(\omega_1)\alpha(\omega_2)\psi_j(r_2) \\
&= \varepsilon_j\psi_j(r_1) \quad (55)
\end{aligned}$$

The last term of equation (55) disappears. This reflects the fact that there is only an exchange interaction between electrons of parallel spin.

Or, equivalently,

$$\begin{aligned}
f(r_1)\psi_j(r_1) &= h(r_1)\psi_j(r_1) + \left[2 \sum_c^{N/2} \int dr_2 \psi_c^*(r_2)r_{12}^{-1}\psi_c(r_2) \right] \psi_j(r_1) \\
&- \left[\sum_c^{N/2} \int dr_2 \psi_c^*(r_2)r_{12}^{-1}\psi_j(r_2) \right] \psi_c(r_1) \\
&= \varepsilon_j\psi_j(r_1) \\
f(1) &= h(1) + \sum_a^{N/2} 2J_a(1) - K_a(1) \quad (56)
\end{aligned}$$

2.2.7 The Roothaan equations

The contribution of Roothaan was to show how, by introducing a set of known spatial basis functions

$$\psi_i = \sum_{\mu}^K C_{\mu i} \phi_{\mu} \quad i = 1, 2, 3, \dots, K \quad (57)$$

If the set ϕ_{μ} was complete, this would be an exact expansion, and any complete could be used. Unfortunately, one is always restricted, for practical computational reasons, to a finite set of K basis function.

Substituting equation (57) to Hartree-Fock equation.

$$f(r_i)\psi_i(r_i) = \varepsilon_i\psi_i(r_i)$$

give

$$f(1)\sum_{\nu} C_{\nu i} \phi_{\nu}(1) = \varepsilon_i \sum_{\nu} C_{\nu i} \phi_{\nu}(1) \quad (58)$$

multiplying $\phi_{\mu}^*(1)$ on left and integrating

$$\sum_{\nu} C_{\nu i} \int dr_1 \phi_{\mu}^*(1) f(1) \phi_{\nu}(1) = \varepsilon_i \sum_{\nu} C_{\nu i} \int dr_1 \phi_{\mu}^* \phi_{\nu}(1) \quad (59)$$

now define two matrices

1. The overlap matrix S has elements

$$S_{\mu\nu} = \int dr_1 \phi_{\mu}^*(1) \phi_{\nu}(1) \quad (60)$$

2. The Fock matrix F has elements

$$F_{\mu\nu} = \int dr_1 \phi_\mu^*(1) f(1) \phi_\nu(1) \quad (61)$$

With these definition of F and S we can now write the integrated Hartree-Fock equation (58) as

$$\sum_\nu F_{\mu\nu} C_{\nu i} = \varepsilon_i \sum_\nu S_{\mu\nu} C_{\nu i} \quad i = 1, 2, 3, \dots, K \quad (62)$$

There are the Roothaan equations, which can be written more compactly as the single matrix equation.

$$FC = SC \varepsilon \quad (63)$$

Where C is a $K \times K$ square matrix of the expansion coefficients $C_{\mu i}$

$$C = \begin{bmatrix} C_{11} & C_{12} & \dots & C_{1K} \\ C_{21} & C_{22} & \dots & C_{2K} \\ \vdots & \vdots & \ddots & \vdots \\ C_{K1} & C_{K2} & \dots & C_{KK} \end{bmatrix}$$

and ε is a diagonal matrix of the orbital energies ε_i

$$\varepsilon = \begin{bmatrix} \varepsilon_1 & & & \\ & \varepsilon_2 & & \\ & & \ddots & \\ & & & \varepsilon_K \end{bmatrix}$$

2.2.8 The charge density

If we have a closed-shell molecule described by a single determinant wave function with each occupied molecular orbital ψ_a containing two electrons then the total charge density is just.

$$\rho(r) = 2 \sum_a^{N/2} |\psi_a(r)|^2 \quad (64)$$

The integral of this charge density is just the total number of electrons.

$$\int dr \rho(r) = 2 \sum_a^{N/2} \int dr |\psi_a(r)|^2 = 2 \sum_a^{N/2} 1 = N \quad (65)$$

For a single determinant, these equations show that total charge density is just a sum of charge for each of the electrons.

$$\psi_i = \sum_{\mu}^K C_{\mu i} \phi_{\mu} \quad I = 1, 2, 3, \dots, K \quad (66)$$

Let us now insert the molecular orbital expansion equation (66) into expression equation (64) for charge density,

$$\begin{aligned} \rho(r) &= 2 \sum_a^{N/2} \psi_a^*(r) \psi_a(r) \\ &= 2 \sum_a^{N/2} \sum_v C_{va}^* \phi_v^*(r) \sum_{\mu} C_{\mu a} \phi_{\mu}(r) \\ &= \sum_{\mu\nu} \left[2 \sum_a^{N/2} C_{\mu a} C_{va}^* \right] \phi_{\mu}(r) \phi_{\nu}^*(r) \end{aligned}$$

$$= \sum_{\mu\nu} P_{\mu\nu} \phi_{\mu}(r) \phi_{\nu}^*(r) \quad (67)$$

Where we have defined a density matrix

$$P_{\mu\nu} = 2 \sum_a^{N/2} C_{\mu a} C_{\nu a} \quad (68)$$

2.2.9 Expression for the Fock matrix

The Fock matrix F is the matrix representation of the Fock operator

$$f(1) = h(1) + \sum_a^{N/2} 2J_a(1) - K_a(1)$$

in the basis ϕ_{μ} , i.e.,

$$\begin{aligned} F_{\mu\nu} &= \int dr_1 \phi_{\mu}^*(1) f(1) \phi_{\nu}(1) \\ &= \int dr_1 \phi_{\mu}^*(1) h(1) \phi_{\nu}(1) + \sum_a^{N/2} \int dr_1 \phi_{\mu}^*(1) [2J_a(1) - K_a(1)] \phi_{\nu}(1) \\ &= H_{\mu\nu}^{core} + \sum_a^{N/2} 2(\mu\nu|aa) - (\mu a|a\nu) \end{aligned} \quad (69)$$

where we have defined a core-Hamiltonian matrix

$$H_{\mu\nu}^{core} = \int dr_1 \phi_{\mu}^*(1) h(1) \phi_{\nu}(1) \quad (70)$$

The elements of the core-Hamiltonian matrix are integrals involving the one-electron operator $h(1)$, describing the kinetic energy and nuclear attraction of an electron, i.e.,

$$h(1) = -\frac{1}{2}\nabla_1^2 - \sum_A \frac{Z_A}{|r_1 - R_A|} \quad (71)$$

Calculating the element of the core-Hamiltonian matrix thus involves the kinetics energy integrals

$$T_{\mu\nu} = \int dr_1 \phi_\mu^*(1) \left[-\frac{1}{2}\nabla_1^2 \right] \phi_\nu(1) \quad (72)$$

and the nuclear attraction integrals

$$V_{\mu\nu}^{nucl} = \int dr_1 \phi_\mu^*(1) \left[-\sum_A \frac{Z_A}{|r_1 - R_A|} \right] \phi_\nu(1) \quad (73)$$

where

$$H_{\mu\nu}^{core} = T_{\mu\nu} + V_{\mu\nu}^{nucl} \quad (74)$$

Unlike the full Fock matrix, need only to be evaluated ones as it remain constant during iterative calculation.

To return to expression equation (69) for Fock matrix, we now insert the linear expression for the molecular orbitals equation (75).

$$\psi_i = \sum_{\mu}^K C_{\mu i} \phi_{\mu} \quad i = 1, 2, 3, \dots, K \quad (75)$$

$$\begin{aligned} F_{\mu\nu} &= \int dr_1 \phi_{\mu}^* f(1) \phi_{\nu} \\ &= \int dr_1 \phi_{\mu}^*(1) h(1) \phi_{\nu}(1) + \sum_a^{N/2} \int dr_1 \phi_{\mu}^*(1) [2J_a(1) - K_a(1)] \phi_{\nu}(1) \\ &= H_{\mu\nu}^{core} + \sum_a^{N/2} 2(\mu\nu|aa) - (\mu a|a\nu) \end{aligned} \quad (76)$$

into the two-electron terms to get

$$\begin{aligned}
 F_{\mu\nu} &= H_{\mu\nu}^{core} + \sum_a \sum_{\lambda\sigma}^{N/2} C_{\lambda a} C_{\sigma a}^* [2(\mu\nu|\lambda\sigma) - (\mu\lambda|\sigma\nu)] \\
 &= H_{\mu\nu}^{core} + \sum_{\lambda\sigma} P_{\lambda\sigma} [(\mu\nu|\lambda\sigma) - 1/2(\mu\lambda|\sigma\nu)] \\
 &= H_{\mu\mu}^{core} + G_{\mu\nu}
 \end{aligned} \tag{77}$$

where $G_{\mu\nu}$ is the two-electron part of Fock matrix. The Final expression is Fock matrix contain $H_{\mu\nu}^{core}$ which is fixed,

Given basis set , and a two-electron part G which depends on the density matrix P and a set of two-electron integrals.

$$(\mu\nu|\lambda\sigma) = \int dr_1 dr_2 \phi_\mu^*(1) \phi_\nu(1) r_{12}^{-1} \phi_\lambda^*(2) \phi_\sigma(2)$$

Because of their large number, the evaluation and manipulation of these two-electron integrals is the major difficulty in Hartree-Fock calculations.

2.2.10 Orthogonalization of the basis

The basis sets that are used in molecular calculations are not orthonormal sets. The basis functions are normalized, but there are not orthogonal to each other. This gives rise to overlap matrix in Roothaan's equations. In order to put Roothaan equations into form of the usual matrix eigenvalue problem, we need to consider procedure for orthogonalizing the basis functions

If we have a set of function ϕ_μ that are not orthogonal, i.e.,

$$\int dr \phi_\mu^*(r) \phi_\nu(r) = S_{\mu\nu} \tag{78}$$

then it will always be possible to find a transformation matrix X such that a transformed set of functions ϕ'_μ

$$\phi'_\mu = \sum_v^K X_{\mu v} \phi_v \quad \mu = 1, 2, \dots, K \quad (79)$$

do form an orthogonal set, i.e.,

$$\int dr \phi'_\mu{}^*(r) \phi'_\nu(r) = \delta_{\mu\nu} \quad (80)$$

substitute equation (79) in equation (80)

$$\begin{aligned} \int dr \phi'_\mu{}^*(r) \phi'_\nu(r) &= \int dr \left[\sum_\lambda X_{\lambda\mu}^* \phi_\lambda^*(r) \right] \left[\sum_\sigma X_{\sigma\nu} \phi_\sigma(r) \right] \\ &= \sum_\lambda \sum_\sigma X_{\lambda\mu}^* \int dr \phi_\lambda^*(r) \phi_\sigma(r) X_{\sigma\nu} \\ &= \sum_\lambda \sum_\sigma X_{\lambda\mu}^* S_{\lambda\sigma} X_{\sigma\nu} = \delta_{\mu\nu} \end{aligned} \quad (81)$$

can be written as the matrix equation

$$X' S X = 1 \quad (82)$$

$$S k = s k \quad (83)$$

$$S = \begin{bmatrix} \phi_{\lambda 1} & \phi_{\lambda 2} & \cdots \\ \vdots & & \\ & & \phi_{\lambda \sigma} \end{bmatrix}_{\lambda \sigma}$$

We wish to find all column vectors k (the eigenvectors of S) and corresponding numbers s (the eigenvalues of S) such that

$$k^\alpha = \begin{bmatrix} k_1^\alpha \\ k_2^\alpha \\ \vdots \\ \vdots \\ k_i^\alpha \end{bmatrix}, \alpha = 1, 2, 3, \dots, \lambda$$

$$s_\alpha \text{ when } \alpha = 1, 2, 3, \dots, \lambda$$

$$(S - sI)k = 0 ; I = \text{identity matrix} \quad (84)$$

$$|S - sI| = 0$$

Once we have found the eigenvalues, we can find the corresponding eigenvectors by substituting each s_α into equation (84) and solving the resulting equations for k^α

Let us now construct a matrix U (Unitary matrix) defined $U_{i\alpha} = k_i^\alpha$

$$U = \begin{bmatrix} k_1^1 & k_1^2 & \cdots & k_1^N \\ k_2^1 & k_2^2 & \cdots & k_2^N \\ \vdots & \vdots & \ddots & \vdots \\ k_N^1 & k_N^2 & \cdots & k_N^N \end{bmatrix}$$

$$X \equiv S^{-1/2} = US^{-1/2}U'$$

we can form $S^{-1/2}$ by diagonalizing S to form s , the taking inverse square root of each of the eigenvalues give $s^{-1/2}$ to form $S^{-1/2}$

$$U' S U = s = \begin{bmatrix} s_1 & & & \\ & s_2 & & \\ & & \ddots & \\ & & & s_\alpha \end{bmatrix}$$

$$S = U s U' = U \begin{bmatrix} s_1 & & & \\ & s_2 & & \\ & & \ddots & \\ & & & s_\alpha \end{bmatrix} U'$$

$$X \equiv S^{-1/2} = U s^{-1/2} U' = U \begin{bmatrix} s_1^{-1/2} & & & \\ & s_2^{-1/2} & & \\ & & \ddots & \\ & & & s_\alpha^{-1/2} \end{bmatrix} U'$$

One way of dealing with the problem of a nonorthogonal basis set would thus be to orthogonalize the function ϕ_μ to obtain the transformed basis functions ϕ'_μ then calculate $(\mu' \nu' | \lambda' \sigma')$ obtain new coefficient matrix C' related to the old coefficient matrix by

$$C' = X^{-1} C \quad C = X C' \quad (85)$$

substituting this equation into Roothaan equations gives

$$F X C' = S X C' \varepsilon$$

multiplying equation on the left by X' gives

$$X' F X C' = X' S X C' \varepsilon \quad (86)$$

$$F' = X' F X \quad (87)$$

$$F' C' = \varepsilon C' \quad (88)$$

There is transformed Roothaan equations, which can solve for C' by diagonalizing F' . Given C' , then C can be obtained by $C = X C'$

Given F we use $F' = X' F X$ ($X \equiv S^{-1/2} = U S^{-1/2} U'$)

$$F' C' = \varepsilon C'$$

$$C' = X^{-1} C \quad C = X C'$$

to solve Roothaan equations $FC = SC\varepsilon$ for C and ε the intermediate are F' and C'

$$\psi_i = \sum_{\mu=1}^K C'_{\mu} \phi'_{\mu} \quad i = 1, 2, \dots, K$$

$$F'_{\mu\nu} = \int dr_1 \phi_{\mu}^*(1) f(1) \phi_{\nu}(1) \quad (89)$$

2.2.11 Basis sets

In general, a basis set is an assortment of mathematical functions used to solve a differential equation. In quantum chemical calculations, the term 'basis set' which applied to a collection of contracted Gaussians representing atomic orbitals, are optimized to reproduce the desired chemical properties of a system.

Standard *ab initio* software packages generally provide a choice of basis sets that vary both in size and in their description of the electrons in different atomic orbitals. Larger basis sets include more and a greater range of basis functions. Therefore, larger basis sets can better refine the approximation to the 'true' molecular wave function, but require correspondingly more computer resources. Alternatively,

accurate wave functions may be obtained from different treatments of electrons in atoms. For instance, molecules containing large atoms ($Z > 30$) are often modeled using basis sets incorporating approximate treatments of inner-shell electrons which account for relativistic phenomena.

'Minimal' basis sets contain the minimum number of AO basis functions needed to describe each atom (*e.g.*, 1s for H and He; 1s, 2s, 2px, 2py, 2pz for Li to Ne). An example of a minimal basis sets is STO-3G, which uses three Gaussian-type functions (3G) per basis function to approximate the atomic Slater-type orbitals. Although minimal basis sets are not recommended for consistent and accurate predictions of molecular energies, their simple structure provides a good tool for visualizing qualitative aspects of chemical bonding. Improvements on minimal basis sets are described below.

Split valence basis sets

In split valence basis sets, additional basis functions (one contracted Gaussian plus some primitive Gaussians) are allocated to each valence atomic orbital. The resultant linear combination allows the atomic orbitals to adjust independently for a given molecular environment. Split valence basis sets are characterized by the number of functions assigned to valence orbitals. 'Double zeta' basis sets use two basis functions to describe valence electrons, 'triple zeta' use three functions, and so forth. Basis sets developed by Pople and coworkers are denoted by the number of Gaussian functions used to describe inner and outer shell electron. Thus '6-31G' describes an inner shell atomic orbital with a contracted Gaussian composed of six primitive Gaussians, an inner valence shell with a contracted Gaussian composed of three primitives, and an outer valence shell with one primitive. Other split-valence sets include 3-21G, 4-31G, and 6-31G.

Polarized basis sets

Polarization functions can be added to basis sets to allow for non-uniform displacement of charge away from atomic nuclei, thereby improving descriptions of chemical bonding. Polarization functions describe orbitals of higher angular momentum quantum number than those required for the isolated atom (*e.g.*, *p*-type functions for H and He, and *d*-type functions for atoms with $Z > 2$), and are added to the valence electron shells. For example, the 6-31G(d) basis set is constructed by adding six *d*-type Gaussian primitives to the 6-31G description of each non-hydrogen atom. The 6-31G(d,p) is identical to 6-31G(d) for heavy atoms, but adds a set of Gaussian *p*-type functions to hydrogen and helium atoms. The addition of *p*-orbitals to hydrogen is particularly important in systems where hydrogen is bridging atom.

Diffuse basis sets

Species with significant electron density far removed from the nuclear centers (*e.g.*, anions, lone pairs and excited states) require diffuse functions to account for the outermost weakly bound electrons. Diffuse basis sets are recommended for calculations of electron affinities, proton affinities, inversion barriers and bond angles in anions. The addition of diffuse *s*- and *p*-type Gaussian functions to non-hydrogen atoms is denoted by a plus sign-as in '3-21+G'. Further addition of diffuse functions to both hydrogen and larger atoms is indicated by a double plus.

2.2.12 The variation method

The variation principle is an important approach to find approximate solution to Schrödinger's equation. It states that the expectation value or average value of the energy for an approximation wave function always lies above or equal the exact solution of Schrödinger equation for the same Hamiltonian operator. This means that if

we have a trial wave function that contains adjustable parameters and we adjust them to minimize the expectation value of the energy, then we are approaching the exact result.

The expectation value or average value of the energy, E_a can be calculated by

$$\langle E \rangle = \frac{\int \psi_a^* \hat{H} \psi_a d\tau}{\int \psi_a^* \psi_a d\tau} = \frac{\langle \psi_a | \hat{H} | \psi_a \rangle}{\langle \psi_a | \psi_a \rangle} \quad (90)$$

The trial wave function can be expressed in terms of a linear combination of the exact eigenfunctions of ψ_i

$$\psi_a = \sum_i c_i \psi_i \quad (91)$$

Now consider the integral

$$\begin{aligned} \int \psi_a^* (\hat{H} - E_0) \psi_a d\tau &= \sum_i \sum_v c_i^* c_v \int \psi_i^* (\hat{H} - E_0) \psi_v d\tau \\ &= \sum_i \sum_v c_i^* c_v (E_i - E_0) \int \psi_i^* \psi_v d\tau \\ &= \sum_i c_i^* c_i (E_i - E_0) \geq 0 \end{aligned} \quad (92)$$

Since the E_0 is the lowest eigenvalue, $E_i - E_0$ can never be negative. The quantity of $c_i^* c_i$ is always positive or zero ($|c_i|^2 \geq 0$) and $E_i \geq E_0$, hence,

$$\int \psi_a^* (\hat{H} - E_0) \psi_a d\tau \geq 0 \quad (93)$$

from which follows the variation principle which states that for a trial wavefunction ψ , the energy, E , computed as the expectation value of the Hamiltonian is an upper bound to the exact ground state energy, E_0 , (i.e. $E_a - E_0$). This also gives insight into how to and the best approximate wavefunctions, as

$$E_a = E_0 \Leftrightarrow \psi_a = \psi_0 \quad (94)$$

Therefore, minimization of the energy, E_a , with respect to all allowed variable parameters in ψ_a will give the best ground state energy and wavefunction. This is the most important result.

2.3 Semi-empirical methods

Semi-empirical methods increase the speed of computation by using approximations of *ab initio* techniques (*e.g.*, by limiting choices of molecular orbitals or considering only valence electrons) which have been fitted to experimental data (for instance, structure and formation energies of organic molecules). Until recently, the size of many energetic molecules placed them beyond the scope of *ab initio* calculations. However, semi-empirical methods have been calibrated to typical organic or biological systems and tend to be inaccurate for problems involving hydrogen bonding, chemical transitions or nitrated compounds.

Several semi-empirical methods are available and appear in commercially available computational chemistry software packages such as HyperChem [46] and Chem3D. [47] Some of the more common semi-empirical methods can be grouped according to their treatment of electron-electron interactions.

The extended Hückel method

Extended Hückel calculations neglect all electron-electron interactions, making them computationally fast but not very accurate. The model provides a qualitative estimate of the shapes and relative energies of molecular orbitals, and approximates the spatial distribution of electron density. Extended Hückel models are good for chemical visualization and can be applied to ‘frontier orbital’ treatments of chemical reactivity.

Neglect of differential overlap (NDO)

NDO models neglect some but not all of the electron-electron interactions. The Hartree-Fock Self-Consistent Field (HF-SCF) method is used to solve the Schrödinger equation with various approximations:

- *Complete NDO (CNDO)* – the product of two atomic orbitals on different atoms is set equal to zero everywhere.
- *Intermediate NDO (INDO)* – differential overlap between orbitals on the same atom are taken into account in the description of electron-electron repulsion, but differential overlap between orbitals on different atoms is neglected.
- *Modified INDO, version 3 (MINDO/3)* – reparameterized version of INDO optimized to predict good enthalpies of formation and reasonable molecular geometries for a range of chemical systems, in particular, sulphur-containing compounds, carbocations, and polynitro organic compounds. [48]
- *Zerner's INDO methods (ZINDO/1 and ZINDO/S)* – Michael Zerner's (University of Florida) versions of INDO developed for use with molecular systems containing transition metals.

Neglect of diatomic differential overlap (NDDO)

NDDO methods build upon the INDO model by including the overlap density between two orbitals on one atom interacting with the overlap density between two orbitals on the same or another atom.

- *Modified NDO (MNDO)* – a method introduced to correct some of the problems associated with MINDO/3. In general, MNDO overestimates activation barriers to chemical reactions.
- *Austin Method, version 1 (AM1)* – a reparameterised version of MNDO which includes changes in nuclear repulsion terms.
- *Parameterization Model, version 3 (PM3)* – a second reparameterization of MNDO, functionally similar to AM1, but with some significant improvements. The PM3 Hamiltonian contains essentially the same elements as that for AM1, but the

parameters for the PM3 model are derived using an automated parameterization procedure. By contrast, many of the parameters in AM1 were obtained by applying chemical knowledge and 'intuition'. As a consequence, some of the parameters have significantly different values in AM1 and PM3, even though both methods use the same functional form and they both predict various thermodynamic and structural properties to approximately the same level of accuracy. Some problems do remain with PM3. One of the most important of these is the rotational barrier of the amide bond, which is much too low and in some cases almost non-existent. This problem can be corrected through the use of an empirical torsional potential. There has been considerable debate over the relative merits of the AM1 and PM3 approaches to parameterization.

2.4 Density functional theory

According to the density functional theory proposed by Hohenberg and Kohn in 1964, the total energy of a system at the ground-state can be expressed as a functional of the electron density. Moreover, every observation of a stationary quantum mechanical system can be calculated from the ground-state density alone, while the ground-state density can be calculated using the variation method. However, for the time being, it seems that there is no way to avoid wavefunctions in molecular calculations and for accurate calculations they have to be used as a mapping step between the energy (and other observations) and the electron density. The DFT has come to prominence over the last decade as a method potentially capable of very accurate results at low cost. Parr and Yang (1994) in practice, approximations are required to implement the theory, and a significantly variable accuracy results. Calibration studies are therefore required to establish the likely accuracy in a given class of systems.

2.4.1 The Hohenberg-Kohn theorem

Within a Born-Oppenheimer approximation, the ground state of the system is a result of the positions of the nuclei. In the quantum mechanics hamiltonian equation (13) the kinetic energy of electrons (\hat{T}_e) and the electron-electron interaction (\hat{V}_{ee}) adjust themselves to the external potential (\hat{V}_{ext}) to get the lowest total energy. Thus, the external potential can be uniquely determined from knowledge of the electron density. The Hohenberg-Kohn theorem (1964) states that if N interacting electrons move in an external potential V_{ext} , the ground-state electron density $\rho_0(r)$ minimizes the functional

$$E[\rho] = F[\rho] + \int \rho(r)V_{ext}(r)dr \quad (95)$$

In equation (95) $F[\rho]$ is a universal functional of $\rho(r)$ and the minimum value of the functional E is E_0 , the exact ground-state electronic energy.

$$\hat{F} = \hat{T}_e + \hat{V}_{ee} = \sum_i -\frac{1}{2}\nabla_i^2 + \sum_{i \neq j} \frac{1}{|r_i - r_j|} \quad (96)$$

and by using the variation principle, the density can be obtained.

2.4.2 The Kohn-Sham equations

Kohn and Sham (1965) introduced a method based on the Hohenberg-Kohn theorem that allows one to minimize the functional $E[n(r)]$ by varying $\rho(r)$ over all the densities containing N electrons. They derived a coupled set of differential equations enabling the ground state density $\rho_0(r)$ to be found. Kohn and Sham separated $F[\rho(r)]$ in equation (95) into three distinct parts, so that the functional E becomes

$$E[\rho(r)] = T_s[\rho(r)] + \frac{1}{2} \iint \frac{\rho(r)\rho(r')}{|r-r'|} dr dr' + E_{xc}[\rho(r)] + \int \rho(r)V_{ext}(r)dr \quad (97)$$

where $T_s[\rho(r)]$ is defined as the kinetic energy of a non-interacting electron gas with density $\rho(r)$,

$$T_s[\rho(r)] = -\frac{1}{2} \sum_i \psi_i^*(r) \nabla^2 \psi_i(r) dr \quad (98)$$

and $E_{xc}[\rho(r)]$ is the exchange-correlation energy functional. Introducing a normalization constraint on the electron density, $\int \rho(r)dr = N$, by the Lagrange's method of undetermined multiplier, we obtain

$$\delta \{ E[\rho(r)] - \mu \left[\int \rho(r)dr - N \right] \} = 0 \quad (99)$$

where μ is an undetermined Lagrange multiplier. The number of electrons in the system is constant so $\delta N = 0$. Then equation (99) reduces to

$$\delta E[\rho(r)] - \mu \delta \left(\int \rho(r)dr \right) = 0 \quad (100)$$

Using the definition of the differential of the functional $\delta F = \int \frac{\delta F}{\delta f(x)} \delta f(x) dx$, and the fact that the differential and the integral signs may be interchanged,

$$\int \frac{\delta E[\rho(r)]}{\delta \rho(r)} \delta \rho(r) dr - \mu \int \delta \rho(r) dr = 0 \quad (101)$$

$$\int \left\{ \frac{\delta E[\rho(r)]}{\delta \rho(r)} - \mu \right\} \delta \rho(r) dr = 0 \Rightarrow \frac{\delta E[\rho(r)]}{\delta \rho(r)} = \mu \quad (102)$$

Equation (102) may now be rewritten in terms of an effective potential, $V_{eff}(r)$,

$$\frac{\delta T_s[\rho(r)]}{\delta \rho(r)} + V_{eff}(r) = \mu \quad (103)$$

where

$$V_{eff}(r) = V_{ext}(r) + \int \frac{\rho(r')}{|r-r'|} dr' + V_{xc}(r) \quad (104)$$

and

$$V_{xc}(r) = \frac{\delta E_{xc}[\rho(r)]}{\delta \rho(r)} \quad (105)$$

To find the ground state energy, $E_0(r)$, and the ground state density, $\rho_0(r)$, the one electron Schrödinger equation

$$\left(-\frac{1}{2} \nabla_i^2 + V_{eff}(r) \right) \phi_i(r) = \varepsilon_i \phi_i(r) \quad (106)$$

should be solved self-consistently with

$$\rho(r) = \sum_{i=1}^N |\phi_i(r)|^2 \quad (107)$$

Similar to the SCF procedure in the Hartree-Fock method, the density $\rho(r)$ can be solved iteratively. A self-consistent solution is required due to the dependence of $V_{eff}(r)$ on $\rho(r)$. The single SCF cycle involves following steps:

1. Start with a guess density (for the 1st iteration, superposition of atomic densities is typically used).
2. Establish a grid for charge density and exchanger correlation potential.
3. Compute KS matrix elements and overlap integrals matrix.
4. Solve the equations for expansion coefficients to obtain KS orbitals.
5. Calculate new density $\rho = \sum_{i=occ} |\phi_i(r)|^2$.
6. If density or energy changed substantially, go to step 1.

7. If the SCF cycle converged and geometry optimization is not requested, go to step 10.
8. Calculate derivatives of energy versus atom coordinates, and update atom coordinates.
9. If gradients are still large, or positions of nuclei moved appreciably, go to step 1.
10. Calculate required properties.

2.4.3 DFT exchange and correlations

The form of E_{xc} is in general unknown and its exact value has been calculated for only a few very simple systems. In the density functional theory, the exchange energy is defined as

$$E_X[\rho] = \langle \phi[\rho] | \hat{V}_{ee} | \phi[\rho] \rangle - U[\rho] \quad (108)$$

when $U[\rho]$ is the Hartree piece of the columbic potential. The correlation term is defined as the remaining unknown piece of the energy:

$$E_C[\rho] = F[\rho] - T_s[\rho] - U[\rho] - E_X[\rho] \quad (109)$$

Due to the definition of $F[\rho]$, the correlation energy consists of two separate contributions:

$$E_C[\rho] = T_C[\rho] + U_C[\rho] \quad (110)$$

when $T_C[\rho]$ and $U_C[\rho]$ are the kinetic contribution and the potential contribution, respectively, of the correlation energy.

In electronic structure calculations, E_{xc} is most commonly approximated within the local density approximation or generalized-gradient approximation. Ziegler (1991) In the local density approximation (LDA), the value of $E_{xc}[\rho(r)]$ is approximated by the exchange-correlation energy of an electron in homogeneous electron gas of the same density $\rho(r)$, *i.e.*

$$E_{xc}^{LDA}[\rho(r)] = \int \epsilon_{xc}(\rho(r))\rho(r)dr \quad (111)$$

The most accurate data for $\epsilon_{xc}(\rho(r))$ is calculated from Quantum Monte Carlo calculations. For systems with slowly varying charge densities this approximation generally gives very good results. An obvious approach to improving the LDA, so called generalized gradient approximation (GGA), is to include gradient corrections by making E_{xc} a functional of the density and its gradient:

$$E_{xc}^{GGA}[\rho(r)] = \int \epsilon_{xc}(\rho(r))\rho(r)dr + \int F_{xc}[\rho(r), |\nabla\rho(r)|]dr \quad (112)$$

where F_{xc} is a correction chosen to satisfy one or several known limits for E_{xc} . Clearly, there is no unique recipe for the F_{xc} , and several functionals have been proposed in the literature. The development of improved functionals is currently a very active area of research and although incremental improvements are likely, it is far from clear whether the research will be successful in providing the substantial increase in accuracy that is desired.

2.4.4 Hybrid functionals

From the Hamiltonian equation and the definition of the exchange-correlation energy, an exact connection can be made between the E_{xc} and the corresponding potential connecting the non-interacting reference and the actual system. The resulting

equation is called the ACF -- Adiabatic connection formula and involves an integration over the parameter λ which turns on the electron-electron interaction

$$E_{XC} = \int_0^1 \langle \psi_\lambda | V_{XC}(\lambda) | \psi_\lambda \rangle d\lambda \quad (113)$$

In the $\lambda=0$ limit, the electrons are non-interacting and there is consequently no correlation. Since the Kohn-Sham wavefunction is simply a single Slater determinant of orbitals then if the KS orbitals are identical to the HF orbitals, the exact exchange energy is precisely the HF exchange energy:

$$E_X[\phi_i; \lambda = 0] = -\frac{1}{2} \sum_{\sigma} \sum_{i,j} \int d^3r \int d^3r' \frac{\phi_{i\sigma}^*(r) \phi_{j\sigma}^*(r') \phi_{i\sigma}(r') \phi_{j\sigma}(r)}{|r-r'|} = E_X^{exact} \quad (114)$$

The approximation of exchange-correlation can be made by summing E_{XC} terms of different values of λ within the limit $\lambda = 0$ to 1. The choice of terms is arbitrary. Hybrid functionals includes a mixture of Hartree-Fock Exchange with DFT exchange-correlation.

B3LYP functional uses Becke's exchange functional with part of the Hartree-Fock exchange mixed in and a scaling factor on the correlation part but using the LYP correlation function. The exchange-correlation energy has the form of

$$AE_X^{Slater} + (1-A)E_X^{HF} + B\Delta E_X^{Beck} + (1-C)E_C^{VWN} + CE_C^{LYP} \quad (115)$$

where the exchange includes the Slater exchange E_X^{Slater} , or local spin density exchange, along with corrections involving the gradient of the density and the correlation is provided by the LYP and VWN correlations. The constants A , B , and C are those determined by fitting to the G1 molecule set. The values of the three parameters are determined by fitting to the 56 atomization energies, 42 ionization

potentials, 8 proton affinities, and 10 first-row atomic energies in the G1 molecule set, computing values of $A=0.80$, $B=0.72$, and $C=0.81$.

2.5 ONIOM method

ONIOM (**O**ur **N**-layer **I**ntegrated molecular **O**rbital + molecular **M**echanics) is the hybrid method of Morokuma and co-workers that enables different levels of theory to be applied to different parts of a molecule/system and combined to produce a consistent energy expression. The objective is to perform a high-level calculation on just a small part of the system and to include the effects of the remainder at lower levels of theory, with the end result being of similar accuracy to a high-level calculation on the full system.

2.5.1 ONIOM energy definition

The basic idea behind ONIOM approach can be explained most easily when it is considered as an extrapolation scheme in a two-dimensional space, spanned by the size of the system on one axis and the level of theory on the other axis. Figure 2.1 shows the extrapolation procedure schematically. The goal is to describe the real system at the highest level of theory, i.e. the approximation of the target E_4 (point 4) in a system partitioned into the two-layer ONIOM or E_9 (point 9) in the system consisting of three layers. In the case of two layers, the extrapolated energy E_{ONIOM2} is then defined as:

$$E_{\text{ONIOM2}} = E_3 - E_1 + E_2$$

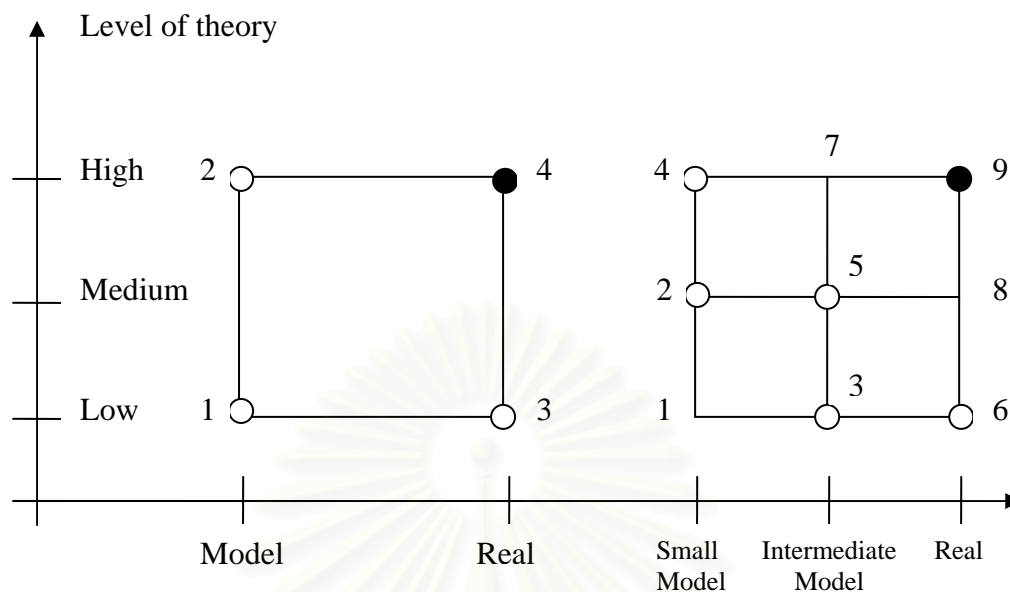


Figure 2.1 The ONIOM extrapolation scheme for a molecular system partitioned into (left) and three (right) layers.

Where E_3 is the energy of the entire (real) system calculated at the low level method and E_1 and E_2 are the energies of the model system determined at the low and high level of theory, respectively. E_{ONIOM2} is an approximation to the true energy of the real system E_4 :

$$E_4 = E_{\text{ONIOM2}} + D \quad (116)$$

Thus, if the error D of the extrapolation procedure is constant for two different structure (e.g., between reactant and transition state) their relative energy ΔE_4 will be evaluated correctly by using the ONIOM energy ΔE_{ONIOM2} .

For a system partitioned into three different layers, the expression for the total energy E_{ONIOM3} as an approximation for E_9 read:

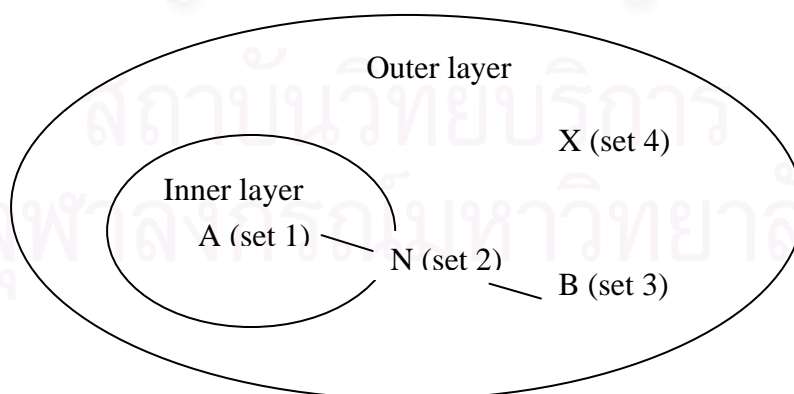
$$E_{\text{ONIOM3}} = E_6 - E_3 + E_5 - E_2 + E_4 \quad (117)$$

Since the evaluation of E_1 (the smallest model system at the lowest level of theory) does not require much computational effort, its value can be used to determine the effect of the three-layer approach as compared to a two-layer partitioning with points 1, 4, and 6. If the energy different between the two- and three-layer extrapolation is constant, a two layer partitioning with the intermediate layer omitted would give comparable accurate results.

2.5.2 Treatment of link atoms.

As mentioned before, an important and critical feature of all combination scheme is the treatment of the link atoms. For the following discussion, We first introduce some useful definition adopting a two layer ONIOM scheme as an example, as illustrated in Figure 2.2. The methodology in the case of a three-layer ONIOM is exactly the same and will not be discuss explicitly.

The atoms present both in the model system and the real system are called set 1 atoms and their coordinates are donated by R_1 . The set 2 atoms are the artificially introduced link atoms. They only occur in the model system and their coordinate are described by R_2 . In the real system they are replaced by the atom describes by R_3 . Atoms belong to the outer layer and are not substituted



Model System = inner layer + link atoms

Real System = inner layer + outer layer

Figure 2.2 Definition of different atom sets within the ONIOM scheme.

by link atoms are called set 4 atoms with coordinate R_4 . The geometry of the real system is thus described by R_1 , R_3 and R_4 and they are the independent coordinates for the ONIOM energy

$$E_{\text{ONIOM}} = E_{\text{ONIOM}}(R_1, R_3, R_4) \quad (118)$$

In order to generate the model system, described by R_1 and the link atom R_2 , we define R_2 as a function of R_1 and R_3 :

$$R_2 = f(R_1, R_3) \quad (119)$$

The explicit functional of the R_2 dependency can be chosen arbitrarily. However, considering the fact that link atoms are introduced to mimic the corresponding covalent bonds of the real system, they should follow the movement of the atom they replace. Therefore we adopt the following coupling scheme. If atoms A belong to set 1 and atoms B belong to set 3, the set 2 link atom is placed onto the bond axis A-B. In terms of internal coordinates we choose the same bond angles and dihedral angles for set 2 atoms as for set 3. Therefore, in the model calculations the link atoms are always aligned along the bond vectors of the real system. For the exact position r_2 of the single H atom on A-B bond ($r_3 - r_1$), we introduce a fixed scale factor (or distance parameter) g . Hence,

$$r_2 = r_1 + g(r_3 - r_1) \quad (120)$$

CHAPTER III

DETAILS OF THE CALCULATIONS

3.1 Non-catalytic, water-catalyzed and zeolite models

Six models of computations of the conversion reactions are comparatively considered. Models 1 and 2 are assigned as non-catalytic and water-catalyzed models, respectively. Model 1 is a tautomerization in the gas phase and model 2 is a tautomerization catalyzed by a water molecule. Models 3, 4, 5 and 6 are geometrical models of the H-ZSM-5 zeolite. Models 3 and 4 are respectively a 3T $[(\text{H}_3\text{SiOAl}(\text{OH})_2\text{OSiH}_3)]$ and 5T $[(\text{H}_3\text{SiO})_4\text{Al}]$ cluster models of which involved species are computed using density functional theory (DFT) method. The 3T and 5T clusters are defined as shown in Figure 3.1. Model 5 and 6 are respectively a 50/3T (176 atoms) and 72/3T (245 atoms) cluster models representing a window of the zigzag channel intersecting the straight channel, shown in Figure 3.2 which involved reactions are computed using the two-layered ONIOM method.

3.2 Methods of calculations

Full geometry optimizations of all species relating to gas phase, water catalyzed and H-ZSM-5 catalyzed of 3T and 5T cluster models were carried out for all stationary points using DFT method. The DFT calculations have been performed with the Becke's three parameters hybrid density functional using the Lee, Yang and Parr correlation functional (B3LYP). [49, 50] Due to the limitation of computational resources and time consumption, the active region is treated more accurately with the DFT method, while interaction in the rest of the model is approximated by a less accurate method.

Geometry optimizations of the 50/3T and 72/3T cluster models have been carried out the hybrid ONIOM methodology. [51-53] This ONIOM2(MO:MO) approach subdivides the real system in two different layers, each one being described at a high and low levels of theory. The active site of H-ZSM-5 zeolite and reacting

compounds called the models system is described at the highest level of theory whereas the rest of the zeolite is computed at a lower level. The real and model systems of H-ZSM-5 zeolite and reacting compounds used for the two-layered ONIOM(MO:MO) calculations are shown in Figure 3.2. The energies computed at the B3LYP/6-31G(d) and ONIOM2(B3LYP/6-31G(d):AM1) [54, 55] have been carried out with the zero-point vibrational energy corrections.

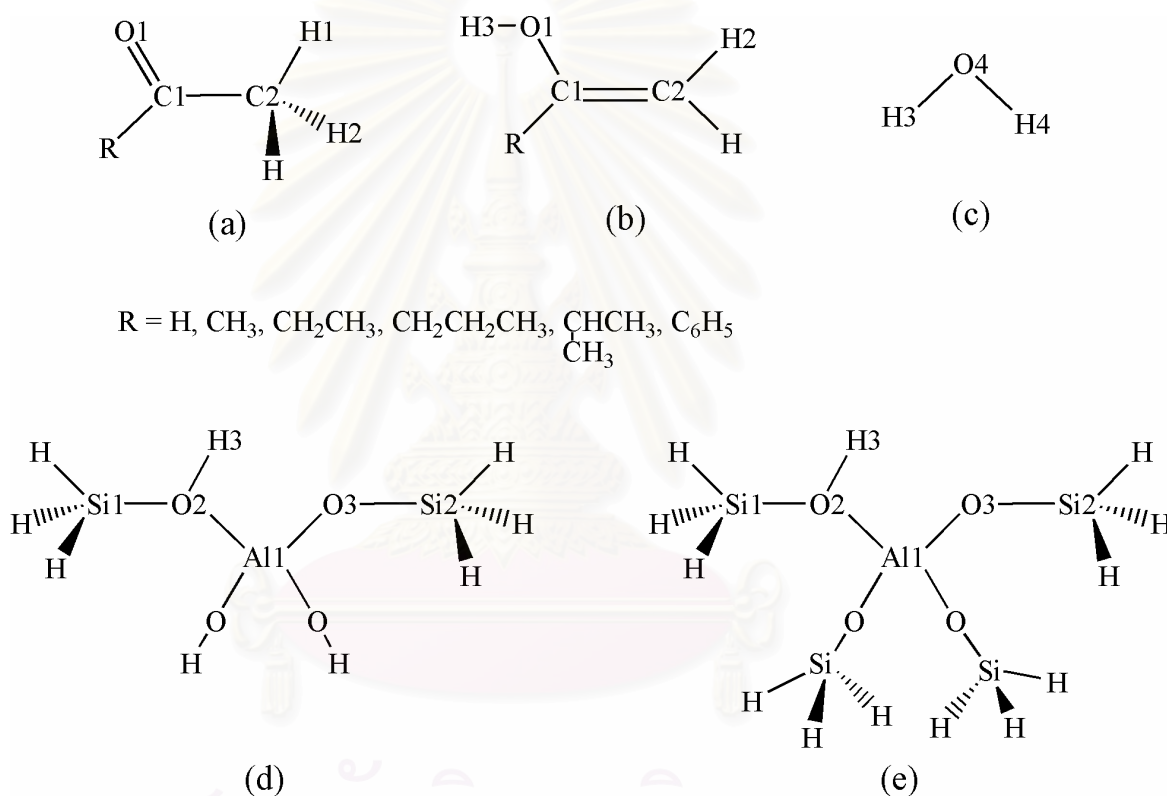


Figure 3.1 Atomic numbering for (a) reactants, (b) products, (c) water, (d) 3T and (e) 5T clusters of H-ZSM-5.

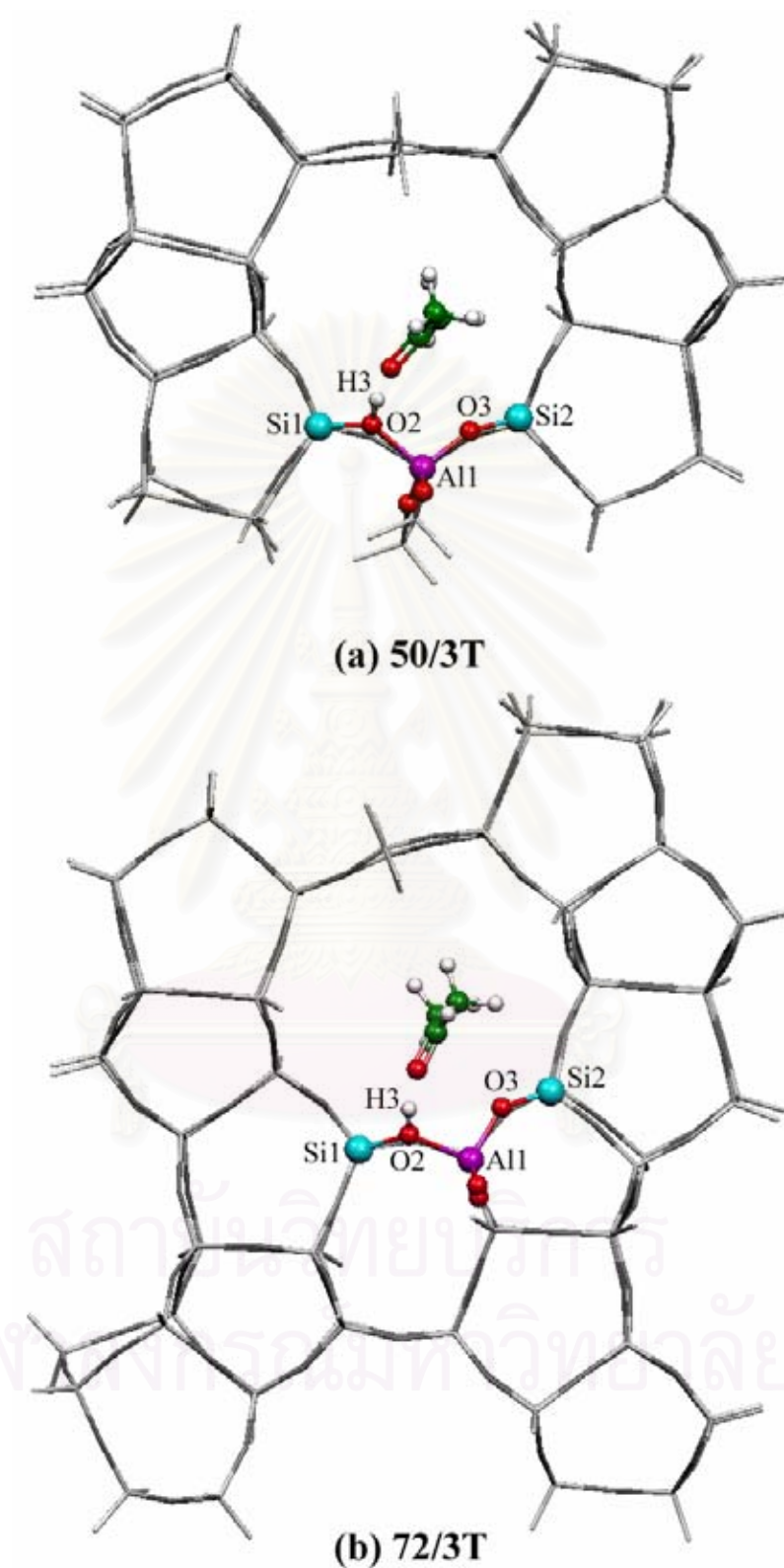


Figure 3.2 The real and model (3T: color regions) systems of (a) 50/3T and (b) 72/3T cluster of H-ZSM-5 for the two-layered ONIOM(MO:MO) calculations.

The total energy of the whole system can be expressed within the framework of the ONIOM methodology developed by Morokuma and co-workers. [22]

$$E_{ONIOM} = E_{Low}^{Real} + (E_{High}^{Model} - E_{Low}^{Model})$$

where the superscript *Real* means the whole system and the superscript *Model* means the active region, which would be treated with the higher level of calculation. Subscripts *High* and *Low* mean high- and low- level methodologies used in the ONIOM calculation.

The transition state structures of the 3T and 5T cluster models optimized at B3LYP/6-31G(d) level of theory have been located using the reaction coordinate method referred to the synchronous transit-guided quasi-newton (STQN) calculation. [56] The transition states were confirmed by one imaginary frequency. The intrinsic reaction coordinate (IRC) method [57] was used to track minimum energy paths from transition structures to the corresponding minimum. For the 50/3T and 72/3T cluster models, the transition structures of all related species have been located using the B3LYP/6-31G(d) optimized transition structure of the 3T cluster model as an initial geometry of the computation. The reaction energy ΔE^{298} , standard enthalpy ΔH^{298} and Gibbs free energy changes ΔG^{298} of all reactions have been derived from the frequency calculations at B3LYP/6-31G(d) level of theory. The reaction entropies ΔS^{298} of all reactions were computed using a thermodynamic equation $\Delta S^{298} = (\Delta H^{298} - \Delta G^{298})/T$. All computations were performed using the GAUSSIAN 03 program package. [58] The MOLDEN 3.7 program [59] was utilized to observe molecular energies and geometries convergence via the Gaussian output files. The molecular graphics of all species were generated with the MOLEKEL 4.3 program. [60]

CHAPTER IV

RESULTS AND DISCUSSION

Conversion reactions of acetaldehyde (ACD) to hydroxyethylene (HETH), acetone (ACT) to 2-hydroxypropylene (HPRO), butanone (BTN) to 2-hydroxybutene (HBUT), 2-pentanone (PTN) to 2-hydroxypentene (HPEN), 3-methyl-2-butanone (MBTN) to 2-hydroxy-3-methylbutene (HMBUT) and acetophenone (ACP) to 2-hydroxyphenylethylene (HPETH) were investigated as non-catalytic (model 1) and water-catalyzed (model 2) and on the 3T (model 3), 5T (model 4), 50/3T (model 5) and 72/3T (model 6) clusters of the acid sites of H-ZSM-5 catalyst. The systems of conversion reactions according to the reactants acetaldehyde, acetone, butanone, 2-pentanone, 3-methyl-2-butanone and acetophenone are also called as the ACD system, ACT system, BTN system, PTN system, MBTN system and ACP system respectively. Relative energies and thermodynamic properties of the various systems and models were determined and compared.

4.1 Geometrical structures, energetics and thermodynamic quantities

The geometrical structures of reactants acetaldehyde, acetone, butanone, 2-pentanone, 3-methyl-2-butanone and acetophenone were optimized at B3LYP/6-31G(d) level of theory. Geometrical data of these reactants and their corresponding transition structures and products in gas phase and in keto-enol isomerization reactions catalyzed by water are listed in Table 4.1 and 4.3, respectively; their atomic numbering are shown in Figure 3.1. Relative energies and thermodynamic quantities of related species of systems acetaldehyde, acetone, butanone, 2-pentanone, 3-methyl-2-butanone and acetophenone in gas phase and in keto-enol isomerization reactions catalyzed by water are listed in Table 4.2 and 4.4, respectively. The geometrical structures of the involved species (water, intermediate1, transition state, intermediate2) in the systems acetaldehyde (ACD system), acetone (ACT system), butanone (BTN system), 2-pentanone (PTN system), 3-methyl-2-butanone (MBTN system) and acetophenone (ACP system) of the model 2 are shown in Figure 4.1.

4.1.1 Cluster results

In this study, it was found keto-enol isomerization reaction catalyzed by H-ZSM-5 of acetophenone (ACP system), which was not complete because the steric and electronic effect of ACP system. (see dipole moment of all reactants in Table A-2) The transition state of ACP system was not converted by these effects. The geometrical structures of the involved species (zeolite, intermediate1, transition state, intermediate2) in the systems acetaldehyde (ACD system), acetone (ACT system), butanone (BTN system), 2-pentanone (PTN system), 3-methyl-2-butanone (MBTN system) and acetophenone (ACP system) of the models 3 and 4 are shown in Figure 4.2, 4.3, 4.4, 4.5, 4.6 and 4.7, respectively.

Table 4.1 Geometrical data for various species of free form, form of transition states and product of various systems in gas phase.

System/parameter ^a	REA	TS	PRO
ACD system			
Bond distance (Å)			
C1-C2	1.508	1.411	1.332
C1-O1	1.210	1.280	1.360
C2-H1	1.090	1.520	-
O1-H1	2.570	1.290	-
O1-H2	-	-	2.630
Bond Angle (Degree)			
O1-C1-C2	124.520	110.770	122.310
H1-C2-C1	110.280	-	-
H2-C2-C1	-	112.570	121.300
ACT system			
Bond distance (Å)			
C1-C2	1.525	1.423	1.336
C1-O1	1.210	1.290	1.370
C2-H1	1.090	1.510	-
O1-H1	2.680	1.270	-
O1-H2	-	-	2.570
Bond Angle (Degree)			
O1-C1-C2	120.370	108.830	119.060
H1-C2-C1	108.760	-	-
H2-C2-C1	-	112.290	121.870
BTN system			
Bond distance (Å)			
C1-C2	1.519	1.423	1.336
C1-O1	1.210	1.290	1.370
C2-H1	1.090	1.510	-
O1-H1	2.530	1.260	-
O1-H2	-	-	2.580

Table 4.1 (cont.)

System/parameter ^a	REA	TS	PRO
Bond Angle (Degree)			
O1-C1-C2	121.710	108.760	119.310
H1-C2-C1	109.930	-	-
H2-C2-C1	-	112.420	121.070
<i>PTN system</i>			
Bond distance (Å)			
C1-C2	1.521	1.423	1.336
C1-O1	1.210	1.290	1.370
C2-H1	1.090	1.510	-
O1-H1	2.520	1.270	-
O1-H2	-	-	2.580
Bond Angle (Degree)			
O1-C1-C2	121.510	108.700	119.300
H1-C2-C1	109.790	-	-
H2-C2-C1	-	112.450	121.120
<i>MBTN system</i>			
Bond distance (Å)			
C1-C2	1.520	1.424	1.338
C1-O1	1.210	1.290	1.370
C2-H1	1.090	1.510	-
O1-H1	2.530	1.260	-
O1-H2	-	-	2.680
Bond Angle (Degree)			
O1-C1-C2	121.510	108.630	123.690
H1-C2-C1	110.080	-	-
H2-C2-C1	-	112.540	122.160
<i>ACP system</i>			
Bond distance (Å)			
C1-C2	1.521	1.427	1.340
C1-O1	1.220	1.300	1.370
C2-H1	1.090	1.500	-
O1-H1	2.480	1.260	-
O1-H2	-	-	2.560
Bond Angle (Degree)			
O1-C1-C2	120.290	108.100	118.790
H1-C2-C1	108.460	-	-
H2-C2-C1	-	112.540	120.320

^a Atomic numbering are shown in Figure 3.1.

Table 4.2 Relative energies and thermodynamic quantities of related species of various systems.

System/energy ^a	ΔE^{298} , ^b	ΔH^{298} , ^b	ΔG^{298} , ^b	ΔS^{298} , ^c	log K
<i>ACD system</i>					
ACD	0.00	0.00	0.00	0.00	
TS_M1	69.38	69.03	69.80	-2.60	
HETH	17.77	17.76	17.94	1.99	-13.14
<i>ACT system</i>					
ACT	0.00	0.00	0.00	0.00	
TS_M1	65.92	66.52	65.22	4.35	
HPRO	20.09	20.52	19.78	-1.88	-14.19
<i>BTN system</i>					
BTN	0.00	0.00	0.00	0.00	
TS_M1	66.22	65.89	66.78	-2.98	
HBUT	18.76	18.66	19.35	0.66	-14.18
<i>PTN system</i>					
PTN	0.00	0.00	0.00	0.00	
TS_M1	67.87	67.49	68.66	-3.92	
HPEN	20.38	20.19	21.38	-0.08	-15.67
<i>MBTN system</i>					
MBTN	0.00	0.00	0.00	0.00	
TS_M1	67.25	66.98	66.52	1.55	
HMBUT	17.49	17.23	18.15	-4.62	-13.30
<i>ACP system</i>					
ACP	0.00	0.00	0.00	0.00	
TS_M1	65.59	65.32	65.93	-2.06	
HPETH	19.90	19.79	20.19	0.72	-14.79

^a For gas phase (model 1).

^b In kcal/mol. ^c In cal/mol K.

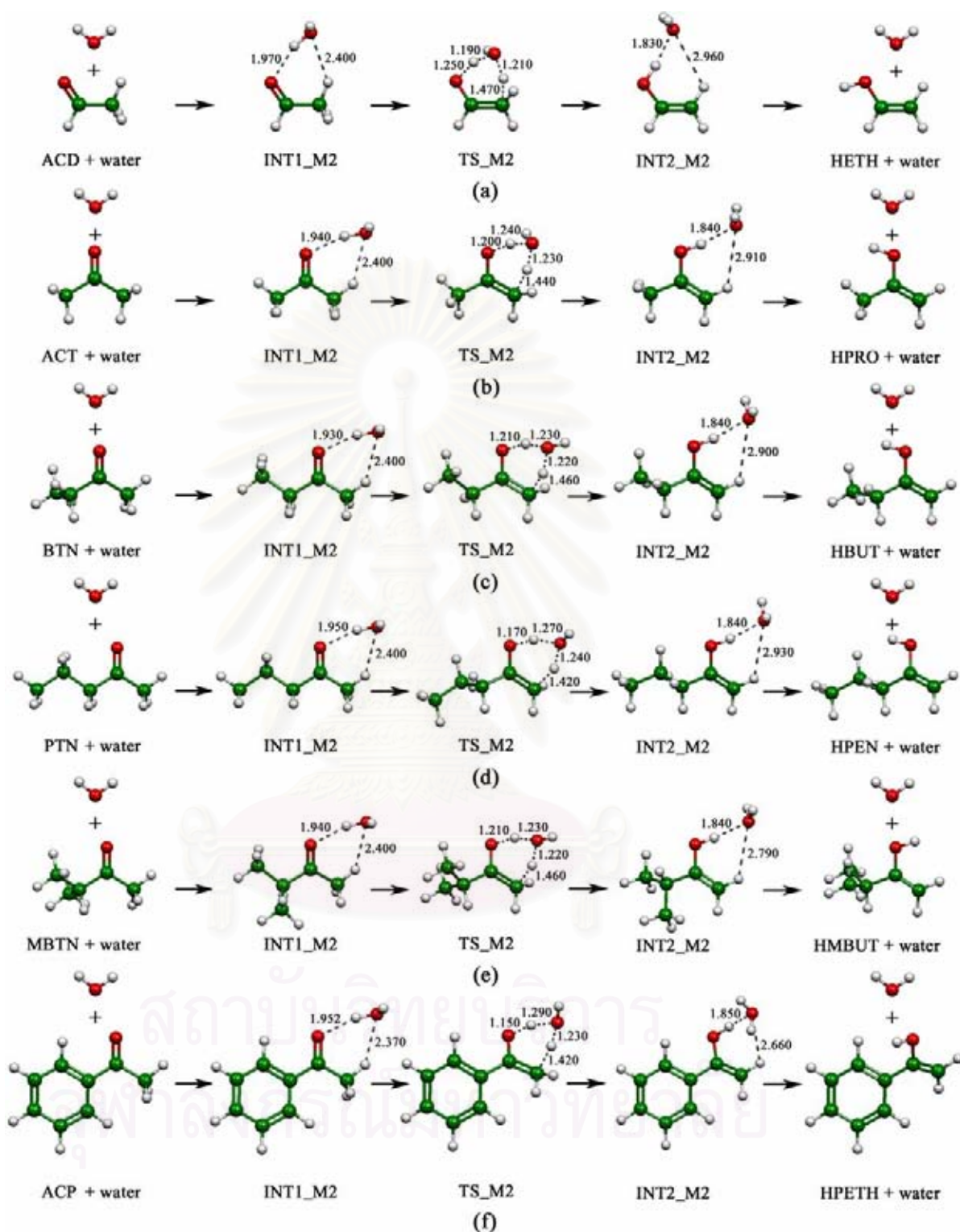


Figure 4.1 Reaction steps of keto-enol isomerization of reactants (a) acetaldehyde, (b) acetone, (c) butanone, (d) 2-pentanone, (e) 3-methyl-2-butanone and (f) acetophenone interacting with water molecule.

Table 4.3 Geometrical data for various species of free form, form of transition states and product of various systems catalyzed by water.

System/parameter ^a	INT1	TS	INT2
<i>ACD system</i>			
Bond distance (Å)			
C1-C2	1.502	1.409	1.337
C1-O1	1.210	1.280	1.350
C2-H1	1.090	1.470	-
O1-H1	2.580	2.350	-
O4-H1	2.400	1.210	-
O1-H3	1.970	1.250	0.980
O4-H3	-	1.190	1.830
O4-H2	-	-	2.960
C2-H2	-	-	1.080
Bond Angle (Degree)			
O1-C1-C2	125.050	123.280	127.470
H1-C2-C1	110.580	-	-
H2-C2-C1	-	116.480	122.110
<i>ACT system</i>			
Bond distance (Å)			
C1-C2	1.515	1.417	1.341
C1-O1	1.220	1.280	1.360
C2-H1	1.090	1.440	-
O1-H1	2.530	2.340	-
O4-H1	2.400	1.230	-
O1-H3	1.940	1.200	0.980
O4-H3	-	1.240	1.840
O4-H2	-	-	2.910
C2-H2	-	-	1.080
Bond Angle (Degree)			
O1-C1-C2	121.890	120.520	124.440
H1-C2-C1	109.890	-	-
H2-C2-C1	-	115.530	121.810
<i>BTN system</i>			
Bond distance (Å)			
C1-C2	1.516	1.419	1.341
C1-O1	1.220	1.280	1.360
C2-H1	1.090	1.460	-
O1-H1	2.530	2.340	-
O4-H1	2.400	1.220	-
O1-H3	1.930	1.210	0.980
O4-H3	-	1.230	1.840
O4-H2	-	-	2.900
C2-H2	-	-	1.080
Bond Angle (Degree)			
O1-C1-C2	121.750	120.230	124.300
H1-C2-C1	109.900	-	-
H2-C2-C1	-	115.360	121.910
<i>PTN system</i>			
Bond distance (Å)			
C1-C2	1.516	1.423	1.341
C1-O1	1.220	1.290	1.360
C2-H1	1.090	1.420	-
O1-H1	2.540	2.360	-
O4-H1	2.400	1.240	-
O1-H3	1.950	1.170	0.980
O4-H3	-	1.270	1.840
O4-H2	-	-	2.930
C2-H2	-	-	1.080

Table 4.3 (cont.)

System/parameter ^a	INT1	TS	INT2
Bond Angle (Degree)			
O1-C1-C2	121.830	120.870	124.290
H1-C2-C1	110.130	-	-
H2-C2-C1	-	114.660	121.920
<i>MBTN system</i>			
Bond distance (Å)			
C1-C2	1.517	1.418	1.341
C1-O1	1.220	1.280	1.360
C2-H1	1.090	1.460	-
O1-H1	2.520	2.340	-
O4-H1	2.400	1.220	-
O1-H3	1.940	1.210	0.980
O4-H3	-	1.230	1.840
O4-H2	-	-	2.790
C2-H2	-	-	1.080
Bond Angle (Degree)			
O1-C1-C2	121.290	120.150	123.520
H1-C2-C1	109.750	-	-
H2-C2-C1	-	115.490	121.290
<i>ACP system</i>			
Bond distance (Å)			
C1-C2	1.516	1.427	1.350
C1-O1	1.220	1.290	1.360
C2-H1	1.090	1.420	-
O1-H1	2.490	2.350	-
O4-H1	2.370	1.230	-
O1-H3	1.950	1.150	0.980
O4-H3	-	1.290	1.850
O4-H2	-	-	2.660
C2-H2	-	-	1.080
Bond Angle (Degree)			
O1-C1-C2	120.580	120.060	123.250
H1-C2-C1	108.620	-	-
H2-C2-C1	-	114.550	121.480

^a Atomic numbering are shown in Figure 3.1.

สถาบันวิทยบริการ
จุฬาลงกรณ์มหาวิทยาลัย

Table 4.4 Relative energies and thermodynamic quantities of related species of various systems.

System/energy ^a	ΔE^{298} , ^b	ΔH^{298} , ^b	ΔG^{298} , ^b	ΔS^{298} , ^c	log K
<i>ACD system</i>					
ACD + water	0.00	0.00	0.00	0.00	
INT1_M2	-5.95	-6.43	2.00	-28.26	
TS_M2	32.12	30.11	42.05	-40.04	
INT2_M2	8.71	8.35	16.01	-25.70	
HETH + water	17.77	17.76	17.94	-0.60	-10.26
<i>ACT system</i>					
ACT + water	0.00	0.00	0.00	0.00	
INT1_M2	-8.30	-7.80	-1.47	-21.24	
TS_M2	29.99	29.02	39.03	-33.59	
INT2_M2	8.71	9.26	15.11	-19.63	
HPRO + water	20.09	20.52	19.78	2.48	-12.14
<i>BTN system</i>					
BTN + water	0.00	0.00	0.00	0.00	
INT1_M2	-8.17	-8.54	-0.10	-28.30	
TS_M2	31.13	29.25	41.50	-41.09	
INT2_M2	9.60	8.73	18.55	-32.94	
HBUT + water	18.76	18.66	19.35	-2.32	-13.67
<i>PTN system</i>					
PTN + water	0.00	0.00	0.00	0.00	
INT1_M2	-6.36	-6.79	2.09	-29.80	
TS_M2	35.23	33.33	45.87	-42.05	
INT2_M2	11.26	10.90	19.00	-27.18	
HPEN + water	20.38	20.19	21.38	-4.00	-12.39
<i>MBTN system</i>					
MBTN + water	0.00	0.00	0.00	0.00	
INT1_M2	-6.26	-7.17	2.83	-33.53	
TS_M2	32.02	30.18	42.08	-39.92	
INT2_M2	11.04	10.67	18.64	-26.71	
HMBUT + water	17.49	17.23	18.15	-3.07	-11.58
<i>ACP system</i>					
ACP + water	0.00	0.00	0.00	0.00	
INT1_M2	-6.45	-6.81	1.69	-28.50	
TS_M2	33.18	31.46	43.28	-39.63	
INT2_M2	11.66	11.13	20.10	-30.11	
HPETH + water	19.90	19.79	20.19	-1.33	-13.49

^a For water (model 2).

^b In kcal/mol. ^c In cal/mol K.

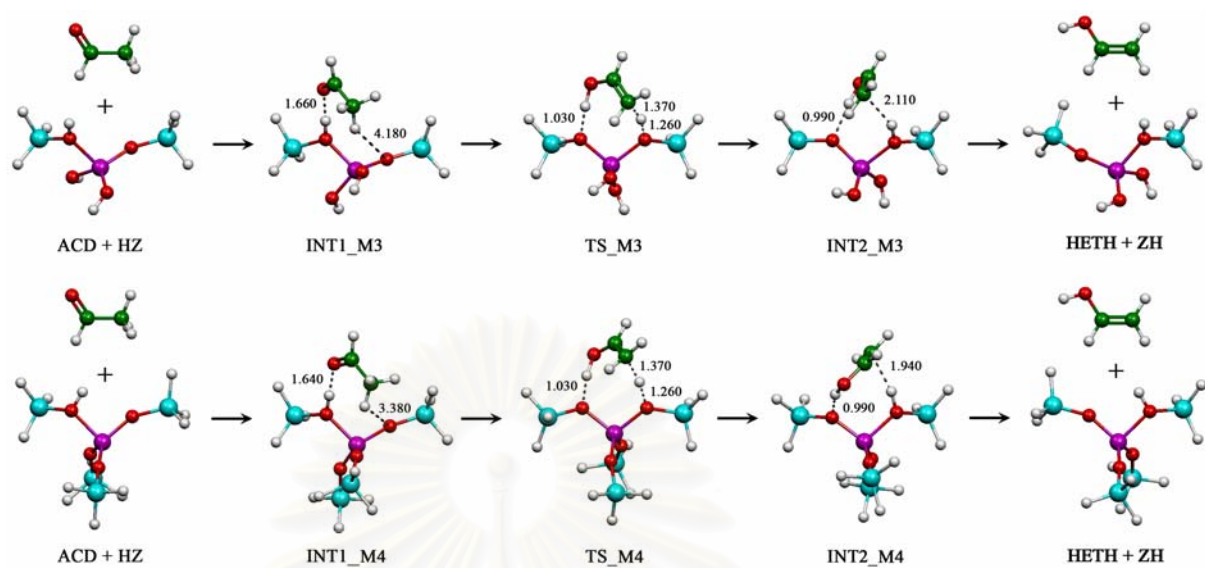


Figure 4.2 Reaction steps of keto-enol isomerization of reactant acetaldehyde interacting with 3T (top) and 5T (bottom) cluster models.

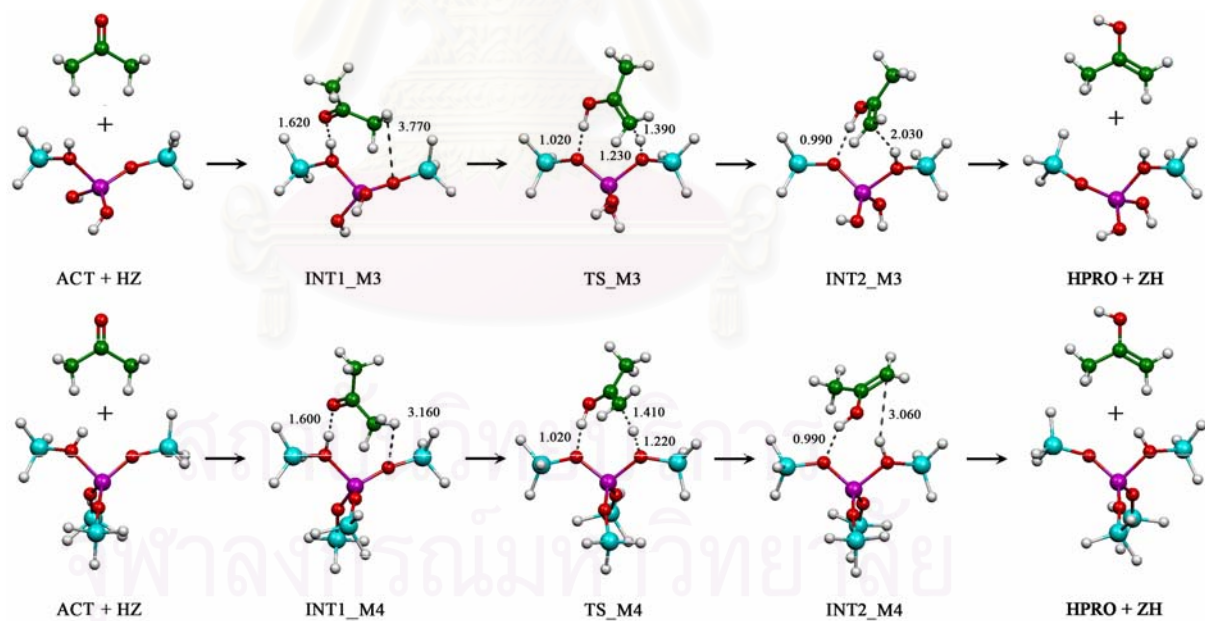


Figure 4.3 Reaction steps of keto-enol isomerization of reactant acetone interacting with 3T (top) and 5T (bottom) cluster models.

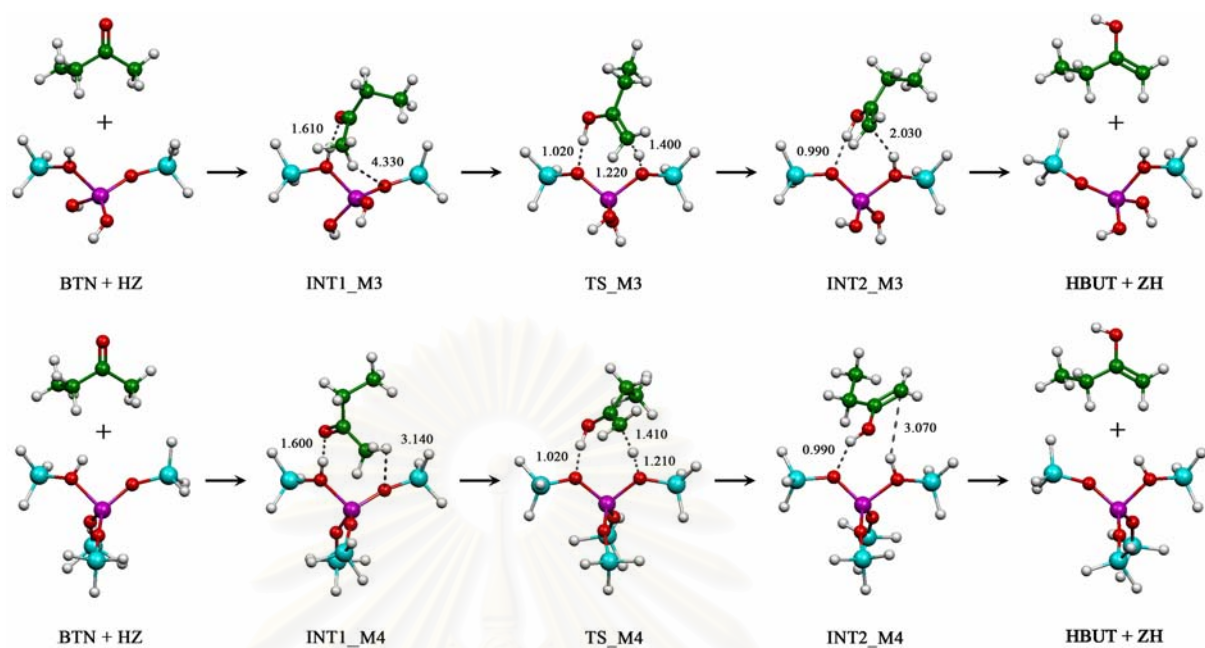


Figure 4.4 Reaction steps of keto-enol isomerization of reactant butanone interacting with 3T (top) and 5T (bottom) cluster models.

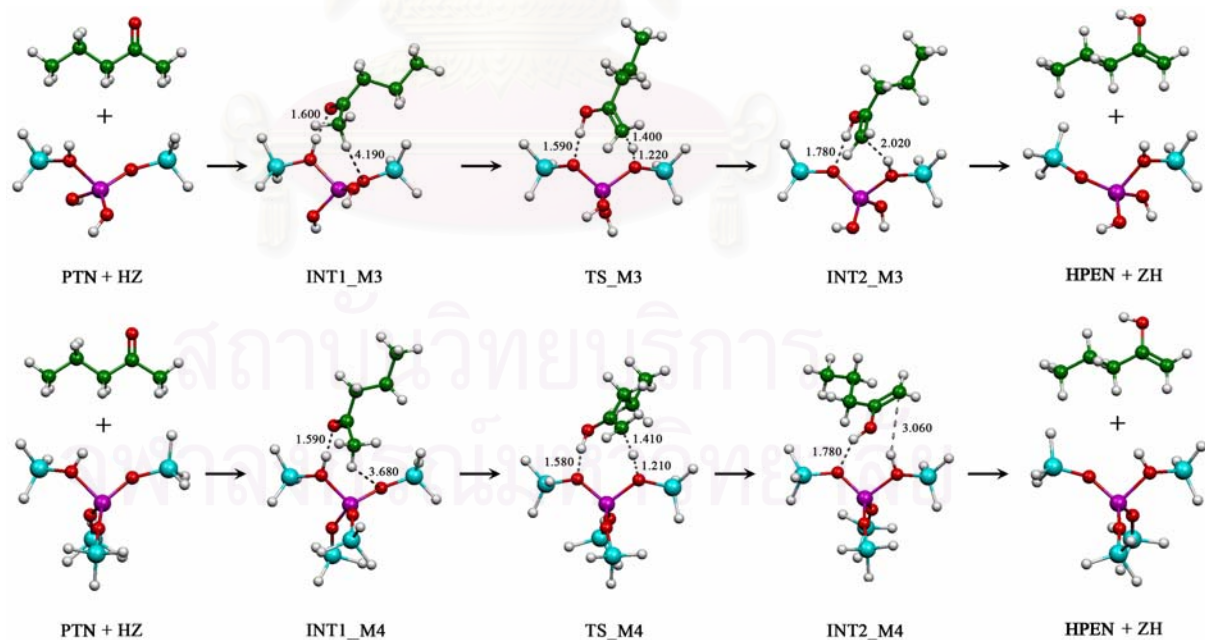


Figure 4.5 Reaction steps of keto-enol isomerization of reactant 2-pentanone interacting with 3T (top) and 5T (bottom) cluster models.

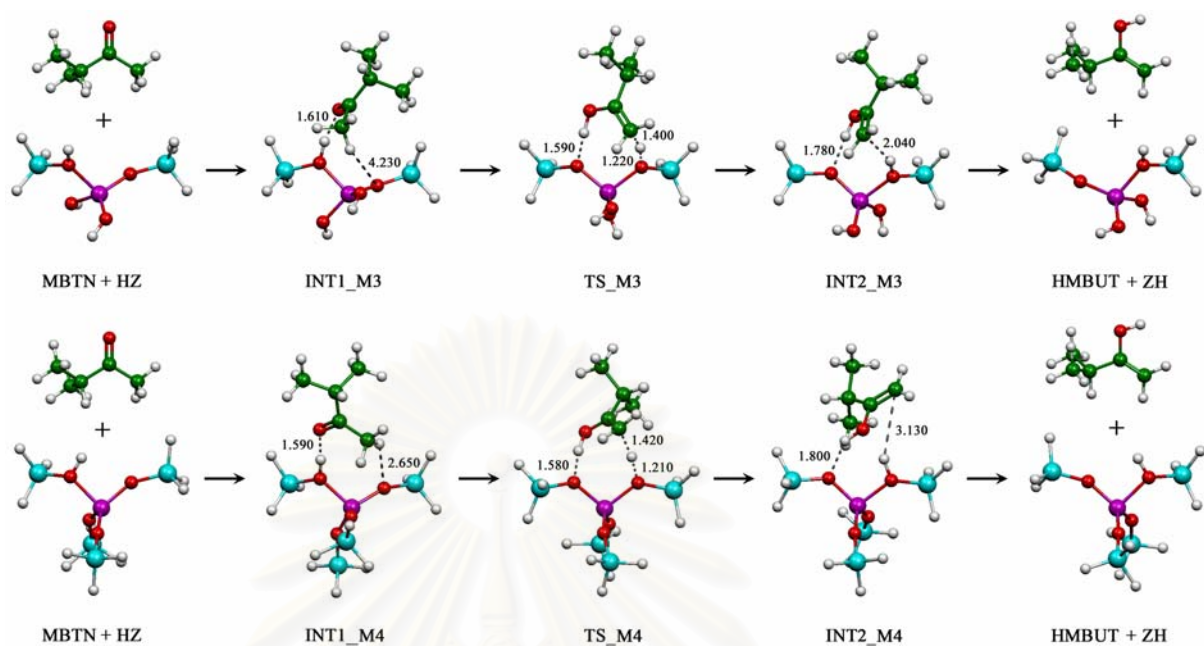


Figure 4.6 Reaction steps of keto-enol isomerization of reactant 3-methyl-2-butanone interacting with 3T (top) and 5T (bottom) cluster models.

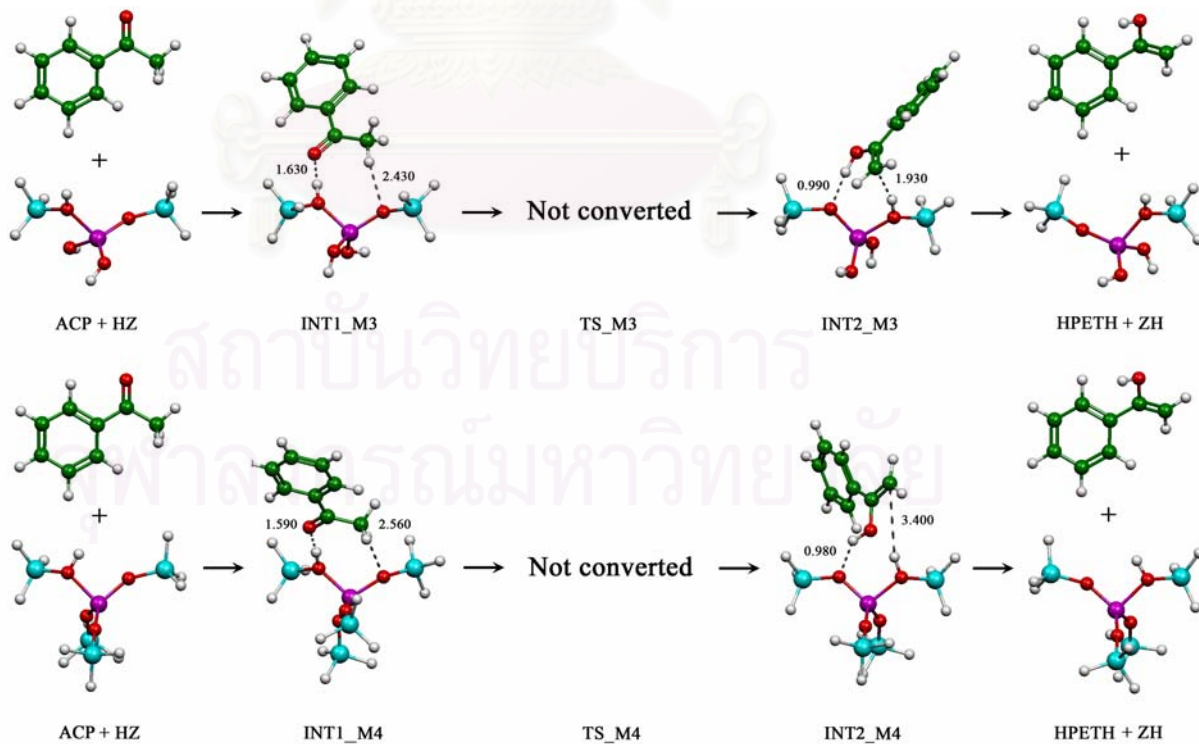


Figure 4.7 Reaction steps of keto-enol isomerization of reactant acetophenone interacting with 3T (top) and 5T (bottom) cluster models.

The IR spectroscopy is widely used in direct study of acidic hydroxyl groups in zeolites. In the region of the fundamental OH stretch frequencies of ZSM-5, there are two well-known IR absorption bands: The sharp peak at 3740 cm^{-1} that corresponds to terminal silanols [61], and somewhat broader peak at 3610 cm^{-1} which is assigned to bridging hydroxyl groups. [62]

The computed stretching vibrational frequencies of hydroxyl groups at the reaction-involved oxygen atoms (O2 and O3) and the selected geometry parameters (bond distances and bond angles) on the 5T and 3T clusters of H-ZSM-5 are tabulated in Table 4.5. Table 4.5 shows that the computed OH stretching vibrational frequencies of H-ZSM-5 at atoms O2 (3734.9 cm^{-1}) and O3 (3735.7 cm^{-1}) are almost the same positions. The computed stretching vibrational frequencies of hydroxyl groups at atoms O2 for reactant-side intermediate and O3 for product-side intermediate for all systems are hardly ever different but smaller than their corresponding isolated-H-ZSM-5 OH vibrational frequencies by approximately 700 cm^{-1} . Relative energies and thermodynamic quantities of related species of systems acetaldehyde, acetone, butanone, 2-pentanone, 3-methyl-2-butanone and acetophenone are listed in Table 4.6. The equilibrium constant of the reaction systems ACD, ACT, BTN, PTN and MBTN of the 5T and 3T (in parentheses) cluster models are $\log K = -13.35$ (-14.72), -14.46 (-16.33), -14.65 (-17.35), -14.70 (-16.42) and -16.89 (-17.32), respectively. The order of magnitudes of the equilibrium constant is in decreasing order: $\text{ACD} > \text{ACT} > \text{PTN} > \text{MBTN} > \text{BTN}$ for models 3 and $\text{ACD} > \text{ACT} > \text{BTN} > \text{PTN} > \text{MBTN}$ for models 4.

It can be observed that all reactants interact with the zeolite through a hydrogen bond between the carbonylic oxygen and the acid O2-H3 group of the zeolite. Consequently, the zeolitic O2-H3 distance increase considerably and the O2-H3 stretching vibrational frequencies are strongly downshifted. The shift of the Brønsted acid site, although smaller than the one that would be expected considering the proton affinity of all reactants. The enol form of all reactants interact with the zeolite through two hydrogen bonds: one in which the enol acts as proton donor and another in which it acts as proton acceptor. The first one occurs between the hydroxyl group and the O2 atom of the zeolite, and the second one, between the acid site O3-H1 of the zeolite and the π system of the enol. The frequency shift of the Brønsted

acid site, smaller than for the keto form. This is not surprising considering the larger hydrogen bond distances and the weaker interaction. The structure of the transition state can be observed that its geometry is closer to the product than to the reactant, as should be expected for an endothermic reactions (see 4.2 Reaction coordinate)

Finally, let us compare the results obtained with clusters 3T and 5T. It can be observed in Figure 4.2-4.7 that the geometry parameters related to the zeolite-reactant are very similar in all the stationary points. The main different interaction between the methyl group of reactant and the oxygens bonded to aluminum. This is due to the fact that in 3T cluster model these oxygens are of different nature (-OH and -OSiH₃), the presence of terminal -OH inducing the changes in the reactant orientation. On the other hand, the results obtained with 5T cluster model show that the dihedral angles defined by the Si1, O2, Al1, O3 and Si2 atoms are far from 180°, the value imposed in the 3T cluster model calculations to avoid unreal hydrogen bond interactions. The computed values of these dihedral angles, which range from 120° to 160° can, however, be the result of a lack of mechanical constraints in the zeolite. This aspect will be considered and discussed in the next section in which ONIOM2 calculations for 50/3T and 72/3T cluster models will be presented. The energy profiles obtained with 3T and 5T are very similar (see Table 4.6). The most remarkable is that the intermediate² and the transition structures are slightly more stable with the larger cluster.

Table 4.5 Computed stretching vibrational frequencies of hydroxyl groups at O2 and O3 atoms and the selected geometry parameters (bond distances and bond angles) on the 3T (model 3) and 5T (model 4) cluster models of H-ZSM-5.

System/parameter ^a	Vibrational frequencies at reaction states ^b				
	HZ	INT1	TS	INT2	ZH
ACD system					
ω (O2-H3) ^c	3734.9(3810.7)	3142.3(3206.1)	-	-	-
ω (O3-H1) ^c	-	-	-	3049.7(3316.1)	3735.7(3814.8)
r (C1-C2) ^d	-	1.490(1.494)	1.396(1.394)	1.350(1.349)	-
r (C1-O1) ^d	-	1.220(1.220)	1.290(1.290)	1.330(1.349)	-
r (C2-H1) ^d	-	-	1.370(1.370)	1.940(2.110)	-
r (O1-H3) ^d	-	1.640(1.660)	1.030(1.030)	0.990(0.990)	-
r (O2-H3) ^d	0.974(0.968)	1.000(1.000)	1.520(1.530)	1.760(1.760)	-
r (O3-H1) ^d	-	3.380(4.180)	1.260(1.260)	1.000(0.990)	0.974(0.968)
r (Al1-O2) ^d	1.948(1.911)	1.900(1.900)	1.790(1.800)	1.760(1.760)	1.728(1.712)
r (Al1-O3) ^d	1.720(1.711)	1.720(1.720)	1.840(1.840)	1.910(1.900)	1.940(1.890)
α (Si1-O2-Al1) ^e	123.800(111.660)	124.520(118.610)	126.560(127.920)	133.760(135.270)	153.180(161.510)
α (Si2-O3-Al1) ^e	153.410(155.580)	165.190(159.750)	126.860(127.320)	124.040(117.630)	123.530(110.440)
ACT system					
ω (O2-H3) ^c	3734.9(3810.7)	2996.2(3047.2)	-	-	-
ω (O3-H1) ^c	-	-	-	2961.5(3216.3)	3735.7(3814.8)
r (C1-C2) ^d	-	1.507(1.506)	1.397(1.397)	1.335(1.355)	-
r (C1-O1) ^d	-	1.230(1.230)	1.300(1.300)	1.380(1.340)	-
r (C2-H1) ^d	-	-	1.410(1.390)	3.060(2.030)	-
r (O1-H3) ^d	-	1.600(1.620)	1.020(1.020)	0.990(0.990)	-
r (O2-H3) ^d	0.974(0.968)	1.010(1.000)	1.580(1.580)	1.760(1.780)	-
r (O3-H1) ^d	-	3.160(3.770)	1.220(1.230)	1.010(0.990)	0.974(0.968)
r (Al1-O2) ^d	1.948(1.911)	1.890(1.900)	1.790(1.790)	1.760(1.760)	1.728(1.712)
r (Al1-O3) ^d	1.720(1.711)	1.720(1.720)	1.850(1.850)	1.900(1.900)	1.940(1.890)
α (Si1-O2-Al1) ^e	123.800(111.660)	124.270(118.920)	127.810(128.630)	131.960(134.420)	153.180(161.510)
α (Si2-O3-Al1) ^e	153.410(155.580)	168.410(155.580)	126.480(126.590)	124.930(117.970)	123.530(110.440)
BTN system					
ω (O2-H3) ^c	3734.9(3810.7)	2971.7(3012.7)	-	-	-
ω (O3-H1) ^c	-	-	-	2948.2(3222.7)	3735.7(3814.8)
r (C1-C2) ^d	-	1.508(1.508)	1.396(1.397)	1.335(1.350)	-
r (C1-O1) ^d	-	1.230(1.230)	1.300(1.300)	1.390(1.340)	-
r (C2-H1) ^d	-	-	1.410(1.400)	3.070(2.030)	-
r (O1-H3) ^d	-	1.600(1.610)	1.020(1.020)	0.990(0.990)	-
r (O2-H3) ^d	0.974(0.968)	1.010(1.010)	1.580(1.590)	1.780(1.780)	-
r (O3-H1) ^d	-	3.140(4.330)	1.210(1.220)	1.010(0.990)	0.974(0.968)
r (Al1-O2) ^d	1.948(1.911)	1.890(1.900)	1.790(1.790)	1.760(1.765)	1.728(1.712)
r (Al1-O3) ^d	1.720(1.711)	1.720(1.720)	1.850(1.850)	1.900(1.900)	1.940(1.890)
α (Si1-O2-Al1) ^e	123.800(111.660)	124.350(119.320)	127.790(128.140)	132.130(134.160)	153.180(161.510)
α (Si2-O3-Al1) ^e	153.41 (155.580)	168.430(157.780)	126.380 (126.730)	124.920(117.540)	123.530(110.440)
PTN system					
ω (O2-H3) ^c	3734.9(3810.7)	2953.9(2981.7)	-	-	-
ω (O3-H1) ^c	-	-	-	2949.0(3203.2)	3735.7(3814.8)
r (C1-C2) ^d	-	1.506(1.509)	1.396(1.397)	1.335(1.356)	-
r (C1-O1) ^d	-	1.230(1.230)	1.300(1.300)	1.390(1.340)	-
r (C2-H1) ^d	-	-	1.410(1.400)	3.060(2.020)	-
r (O1-H3) ^d	-	1.590(1.600)	1.020(1.020)	0.990(0.990)	-
r (O2-H3) ^d	0.974(0.968)	1.010(1.010)	1.580(1.590)	1.780(1.780)	-
r (O3-H1) ^d	-	3.680(4.190)	1.210(1.220)	1.010(0.990)	0.974(0.968)
r (Al1-O2) ^d	1.948(1.911)	1.890(1.900)	1.780(1.790)	1.760(1.760)	1.728(1.712)
r (Al1-O3) ^d	1.720(1.711)	1.720(1.720)	1.850(1.850)	1.900(1.900)	1.940(1.890)
α (Si1-O2-Al1) ^e	123.80(111.660)	123.960(119.720)	127.940(128.220)	132.220(133.940)	153.180(161.510)
α (Si2-O3-Al1) ^e	153.41 (155.580)	162.600(155.740)	126.410(126.590)	124.810(117.540)	123.530(110.440)

Table 4.5 (cont.)

System/parameter ^a	Vibrational frequencies at reaction states ^b				
	HZ	INT1	TS	INT2	ZH
MBTN system					
ω (O3-H1) ^c	-	-	-	2930.0(3368.6)	3735.7(3814.8)
r (C1-C2) ^d	-	1.508(1.509)	1.396 (1.396)	1.335(1.350)	-
r (C1-O1) ^d	-	1.230(1.230)	1.300 (1.300)	1.390(1.340)	-
r (C2-H1) ^d	-	-	1.420 (1.400)	3.130(2.040)	-
r (O1-H3) ^d	-	1.590(1.610)	1.020 (1.010)	0.980(0.990)	-
r (O2-H3) ^d	0.974(0.968)	1.010(1.010)	1.580 (1.590)	1.800(1.780)	-
r (O3-H1) ^d	-	2.650(4.230)	1.210 (1.220)	1.010(0.990)	0.974(0.968)
r (Al1-O2) ^d	1.948(1.911)	1.890(1.900)	1.780 (1.790)	1.760(1.760)	1.728(1.712)
r (Al1-O3) ^d	1.72(1.711)	1.720(1.720)	1.850 (1.850)	1.900(1.900)	1.940(1.890)
α (Si1-O2-Al1) ^e	123.80(111.660)	124.100(119.680)	127.920 (128.310)	132.840(134.269)	153.180(161.510)
α (Si2-O3-Al1) ^e	153.41 (155.580)	153.440(154.340)	126.650 (126.360)	125.460(117.320)	123.530(110.440)
ACP system					
ω (O2-H3) ^c	3734.9(3810.7)	2958.6(3116.2)	Not converted	-	-
ω (O3-H1) ^c	-	-	-	3043.4(3040.0)	3735.7(3814.8)
r (C1-C2) ^d	-	1.509(1.511)	-	1.338(1.362)	-
r (C1-O1) ^d	-	1.230(1.230)	-	1.380(1.340)	-
r (C2-H1) ^d	-	-	-	3.400(1.930)	-
r (O1-H3) ^d	-	1.590(1.630)	-	0.980(0.990)	-
r (O2-H3) ^d	0.974(0.968)	1.010(1.000)	-	1.840(1.740)	-
r (O3-H1) ^d	-	2.560(2.430)	-	1.000(1.000)	0.974(0.968)
r (Al1-O2) ^d	1.948(1.911)	1.890(1.890)	-	1.760(1.770)	1.728(1.712)
r (Al1-O3) ^d	1.72(1.711)	1.730(1.740)	-	1.900(1.900)	1.940(1.890)
α (Si1-O2-Al1) ^e	123.80(111.660)	124.080(117.080)	-	133.290(131.010)	153.180(161.510)
α (Si2-O3-Al1) ^e	153.41 (155.580)	152.700(143.900)	-	125.100(118.640)	123.530(110.440)

^a Atomic numbering are shown in Figure 3.1.

^b For 5T and 3T (in parenthesis) cluster models of H-ZSM-5.

^c Vibrational frequencies, in cm^{-1} .

^d Bond distance, in Å.

^e Angle, in degree.

Table 4.6 Relative energies and thermodynamic quantities of related species of various systems.

System/energy ^a	ΔE^{298} , ^b	ΔH^{298} , ^b	ΔG^{298} , ^b	ΔS^{298} , ^c	log K
ACD system					
ACD + HZ	0.00(0.00)	0.00(0.00)	0.00(0.00)	0.00(0.00)	
INT1_M4(M3)	-14.52(-14.76)	-14.92(-15.02)	-1.87(-3.75)	-43.79(-37.81)	
TS_M4(M3)	3.81(5.63)	2.70(4.82)	19.16(18.92)	-55.20(-47.29)	
INT2_M4(M3)	1.92(2.90)	1.37(2.09)	16.35(16.34)	-50.23(-47.79)	
HETH + ZH	17.75(17.21)	17.76(17.15)	18.63(17.20)	-2.95(-0.18)	-13.35 (-14.72)
ACT system					
ACT + HZ	0.00(0.00)	0.00(0.00)	0.00(0.00)	0.00(0.00)	
INT1_M4(M3)	-17.90(-17.94)	-16.90(-16.74)	-6.26(-9.02)	-35.68(-25.91)	
TS_M4(M3)	0.66(2.85)	0.72(3.17)	14.40(15.01)	-45.91(-39.72)	
INT2_M4(M3)	0.37(1.91)	0.79(2.61)	13.48(13.27)	-42.56(-35.74)	
HPRO + ZH	20.08(19.53)	20.52(19.91)	20.48(19.05)	0.13(2.90)	-14.46 (-16.33)
BTN system					
BTN + HZ	0.00(0.00)	0.00(0.00)	0.00(0.00)	0.00(0.00)	
INT1_M4(M3)	-16.43(-16.35)	-16.22(-16.05)	-4.35(-6.34)	-39.83(-32.56)	
TS_M4(M3)	1.46(3.69)	0.63(3.13)	16.82(17.25)	-54.32(-47.37)	
INT2_M4(M3)	1.43(2.99)	1.01(2.21)	15.63(17.34)	-49.05(-50.72)	
HBUT + ZH	18.75(18.20)	18.66(18.05)	20.05(18.62)	-4.67(-1.90)	-14.65 (-17.35)
PTN system					
PTN + HZ	0.00(0.00)	0.00(0.00)	0.00(0.00)	0.00(0.00)	
INT1_M4(M3)	-14.92(-14.89)	-15.80(-14.65)	-0.56(-3.47)	-51.14(-37.50)	
TS_M4(M3)	3.00(5.26)	2.14(4.65)	18.62(19.20)	-55.26(-48.80)	
INT2_M4(M3)	3.10(4.45)	2.14(3.68)	18.72(18.94)	-55.62(-51.18)	
HPEN + ZH	20.37(19.83)	20.19(19.58)	22.08(20.65)	-6.34(-3.58)	-14.70 (-16.42)
MBTN system					
MBTN + HZ	0.00(0.00)	0.00(0.00)	0.00(0.00)	0.00(0.00)	
INT1_M4(M3)	-16.48(-16.45)	-16.28(-16.12)	-4.20(-5.64)	-40.49(-35.15)	
TS_M4(M3)	2.12 (4.28)	1.32 (3.78)	17.63 (17.62)	-54.69 (-46.39)	
INT2_M4(M3)	3.03(3.71)	2.07(2.99)	18.84(18.00)	-56.24(-50.34)	
HMBUT + ZH	17.47(16.93)	17.23(16.63)	18.85(17.42)	-5.42(-2.65)	-16.89(-17.32)
ACP system					
ACP + HZ	0.00(0.00)	0.00(0.00)	0.00(0.00)	0.00(0.00)	
INT1_M4(M3)	-16.25(-14.99)	-16.44(-14.52)	-2.73(-4.49)	-45.98(-33.64)	
TS_M4(M3)		Not converted			
INT2_M4(M3)	3.61(4.03)	3.00(3.97)	17.87(17.00)	-49.89(-43.68)	
HPETH + ZH	19.89(19.34)	19.79(19.19)	20.89(19.46)	-3.68(-0.91)	No Value

^a For 5T (model 4) and 3T (model 3) (in parenthesis) cluster models of H-ZSM-5.

^b In kcal/mol. ^c In cal/mol K.

4.1.2 ONIOM calculations

In addition, the geometrical structures of the involved species in the systems acetaldehyde (ACD system), acetone (ACT system), butanone (BTN system), 2-pentanone (PTN system), 3-methyl-2-butanone (MBTN system) and acetophenone (ACP system) of the models 5 and 6 for ONIOM(B3LYP:AM1) method are shown in Figure 4.8, 4.9, respectively. Furthermore testing, the geometrical structure of ACD system was optimized by ONIOM(B3LYP:MNDO) method. For this method, it was found keto-enol isomerization reaction catalyzed by both 50/3T and 72/3T were not complete because the transition state was not converted. Geometrical data of this reactant in keto-enol isomerization reaction catalyzed by 50/3T and 72/3T are listed in Table A-3. Relative energies and thermodynamic quantities of related species of system acetaldehyde in keto-enol isomerization reaction catalyzed by 50/3T and 72/3T are listed in Table A-4.

The computed stretching vibrational frequencies of hydroxyl groups at the reaction-involved oxygen atoms (O2 and O3) and selected geometry parameters (bond distances and bond angles) on 50/3T cluster of H-ZSM-5 are tabulated in Table 4.7. Table 4.7 shows that the computed OH stretching vibrational frequencies of H-ZSM-5 at atoms O2 (3752.4 cm^{-1}) and O3 (3750.5 cm^{-1}) are almost the same positions. The computed stretching vibrational frequencies of hydroxyl groups at atoms O2 for reactant-side intermediate and O3 for product-side intermediate for all systems are hardly ever different but smaller than their corresponding isolated-H-ZSM-5 OH vibrational frequencies by approximately 700 cm^{-1} . Relative energies and thermodynamic quantities of related species of systems acetaldehyde, acetone, butanone, 2-pentanone, 3-methyl-2-butanone and acetophenone are listed in Table 4.8. The equilibrium constant of the reaction systems ACD, ACT, BTN, PTN and MBTN of the 50/3T cluster model are $\log K = -11.98, -13.80, -14.77, -13.68$ and -12.75 , respectively.

The computed stretching vibrational frequencies of hydroxyl groups at the reaction-involved oxygen atoms (O2 and O3) and selected geometry parameters (bond distances and bond angles) on 72/3T cluster of H-ZSM-5 are tabulated in Table 4.9. Table 4.9 shows that the computed OH stretching vibrational frequencies of H-ZSM-5

at atoms O2 (3696.6 cm^{-1}) and O3 (3765.8 cm^{-1}) are almost the same positions. The computed stretching vibrational frequencies of hydroxyl groups at atoms O2 for reactant-side intermediate and O3 for product-side intermediate for all systems are hardly ever different but smaller than their corresponding isolated-H-ZSM-5 OH vibrational frequencies by approximately 700 cm^{-1} . Relative energies and thermodynamic quantities of related species of systems acetaldehyde, acetone, butanone and 2-pentanone, 3-methyl-2-butanone and acetophenone are listed in Table 4.10. The equilibrium constant of the reaction systems ACD, ACT, BTN, PTN and MBTN of the 72/3T cluster model are $\log K = -10.09, -11.50, -11.83, -11.60$ and -10.11 , respectively.

The order of magnitudes of the equilibrium constant is in decreasing order: $\text{ACD} > \text{MBTN} > \text{PTN} > \text{ACT} > \text{BTN}$ for model 5 and $\text{ACD} > \text{MBTN} > \text{ACT} > \text{PTN} > \text{BTN}$ for model 6.

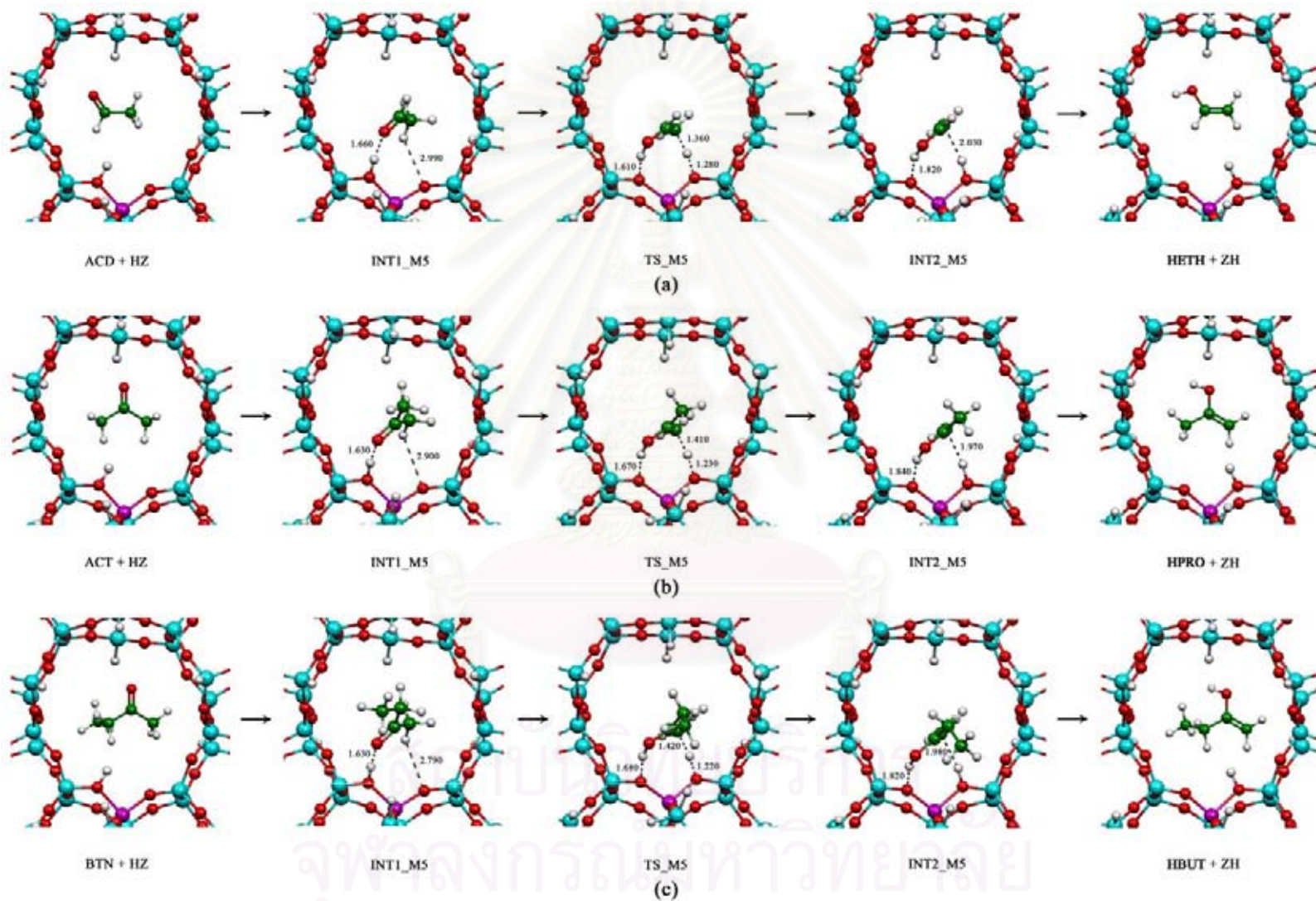


Figure 4.8 Reaction steps of keto-enol isomerization of reactants (a) acetaldehyde, (b) acetone, (c) butanone, (d) 2-pentanone, (e) 3-methyl-2-butanone and (f) acetophenone interacting with 50/3T cluster model of H-ZSM-5.

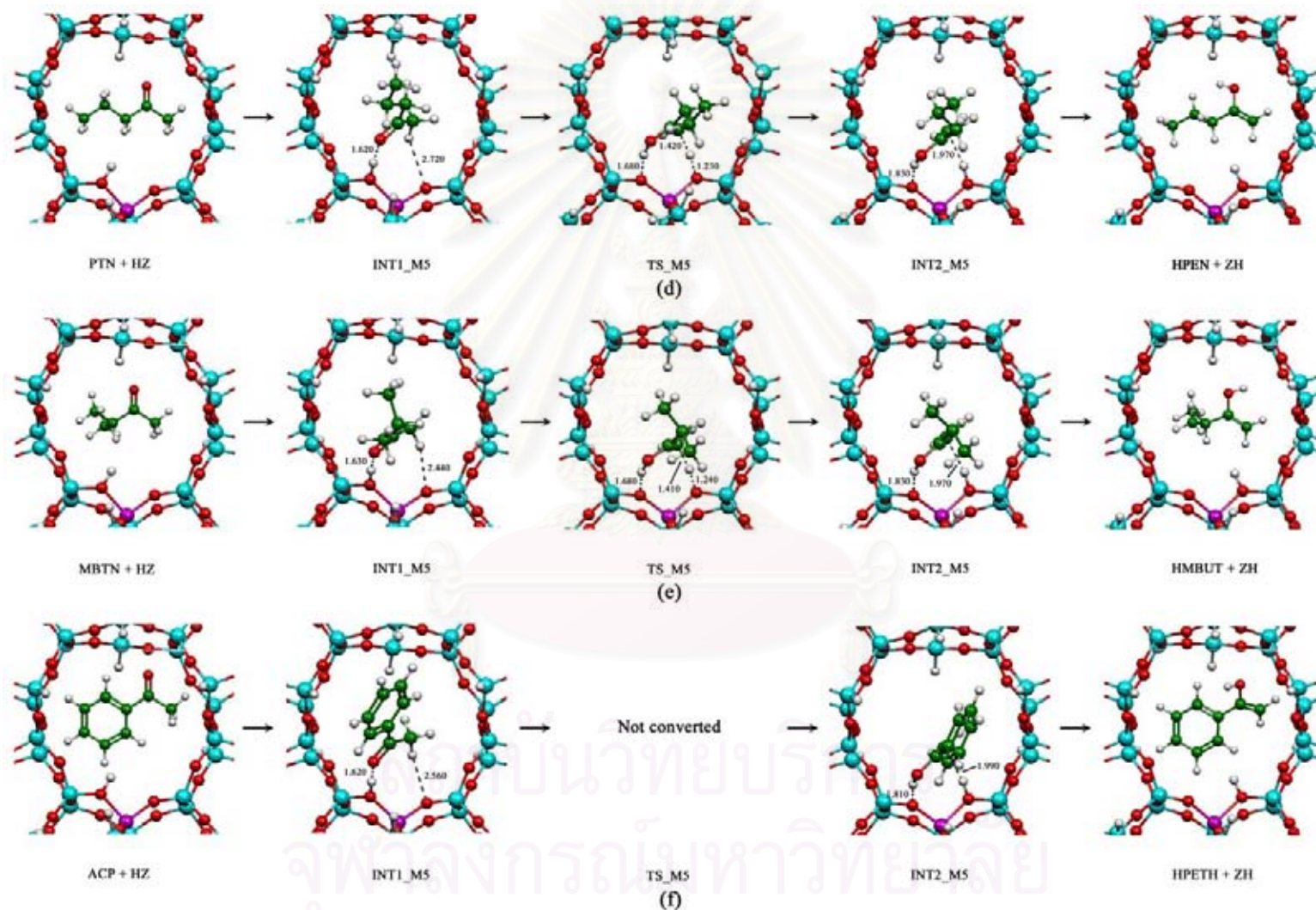


Figure 4.8 (cont.)

Table 4.7 Computed stretching vibrational frequencies of hydroxyl groups at O2 and O3 atoms and selected geometry parameters (bond distances and bond angles) on 50/3T (model 5) cluster model of H-ZSM-5.

System/parameter ^a	Vibrational frequencies at reaction states ^b				
	HZ	INT1	TS	INT2	ZH
ACD system					
ω (O2-H3) ^c	3752.4	3093.3	-	-	-
ω (O3-H1) ^c	-	-	-	3155.6	3750.5
r (C1-C2) ^d	-	1.494	1.390	1.340	-
r (C1-O1) ^d	-	1.220	1.290	1.340	-
r (C2-H1) ^d	-	-	1.360	2.030	-
r (O1-H3) ^d	-	1.660	1.020	0.990	-
r (O2-H3) ^d	0.973	1.000	1.610	1.820	-
r (O3-H1) ^d	-	2.990	1.280	1.000	0.973
r (Al1-O2) ^d	1.947	1.920	1.808	1.777	1.749
r (Al1-O3) ^d	1.740	1.740	1.850	1.910	1.940
α (Si1-O2-Al1) ^e	134.390	131.130	141.570	144.970	150.320
α (Si2-O3-Al1) ^e	151.370	155.390	135.820	133.880	135.940
ACT system					
ω (O2-H3) ^c	3752.4	2995.2	-	-	-
ω (O3-H1) ^c	-	-	-	3037.9	3750.5
r (C1-C2) ^d	-	1.500	1.390	1.350	-
r (C1-O1) ^d	-	1.230	1.310	1.340	-
r (C2-H1) ^d	-	-	1.410	1.970	-
r (O1-H3) ^d	-	1.630	1.010	0.980	-
r (O2-H3) ^d	0.973	1.010	1.670	1.840	-
r (O3-H1) ^d	-	2.900	1.230	1.000	0.973
r (Al1-O2) ^d	1.947	1.920	1.802	1.778	1.749
r (Al1-O3) ^d	1.740	1.750	1.860	1.910	1.940
α (Si1-O2-Al1) ^e	134.390	131.970	142.840	144.190	150.320
α (Si2-O3-Al1) ^e	151.370	154.520	135.220	134.310	135.940
BTN system					
ω (O2-H3) ^c	3752.4	2985.8	-	-	-
ω (O3-H1) ^c	-	-	-	3052.5	3750.5
r (C1-C2) ^d	-	1.500	1.390	1.350	-
r (C1-O1) ^d	-	1.230	1.310	1.340	-
r (C2-H1) ^d	-	-	1.420	1.980	-
r (O1-H3) ^d	-	1.630	1.010	0.980	-
r (O2-H3) ^d	0.973	1.010	1.680	1.820	-
r (O3-H1) ^d	-	2.790	1.220	1.000	0.973
r (Al1-O2) ^d	1.947	1.910	1.801	1.777	1.749
r (Al1-O3) ^d	1.740	1.750	1.860	1.910	1.940
α (Si1-O2-Al1) ^e	134.390	131.990	142.840	145.930	150.320
α (Si2-O3-Al1) ^e	151.370	154.760	135.170	133.430	135.940
PTN system					
ω (O2-H3) ^c	3752.4	2974.2	-	-	-
ω (O3-H1) ^c	-	-	-	3046.8	3750.5
r (C1-C2) ^d	-	1.507	1.394	1.356	-
r (C1-O1) ^d	-	1.230	1.310	1.340	-
r (C2-H1) ^d	-	-	1.420	1.970	-
r (O1-H3) ^d	-	1.620	1.010	0.980	-
r (O2-H3) ^d	0.973	1.010	1.680	1.830	-
r (O3-H1) ^d	-	2.720	1.230	1.000	0.973
r (Al1-O2) ^d	1.947	1.910	1.800	1.770	1.749
r (Al1-O3) ^d	1.740	1.750	1.860	1.910	1.940
α (Si1-O2-Al1) ^e	134.390	131.880	142.900	145.780	150.320
α (Si2-O3-Al1) ^e	151.370	154.960	135.160	133.820	135.940

Table 4.7 (cont.)

System/parameter ^a	Vibrational frequencies at reaction states ^b				
	HZ	INT1	TS	INT2	ZH
MBTN system					
ω (O3-H1) ^c	-	-	-	3037.5	3750.5
r (C1-C2) ^d	-	1.500	1.390	1.350	-
r (C1-O1) ^d	-	1.230	1.290	1.340	-
r (C2-H1) ^d	-	-	1.360	1.970	-
r (O1-H3) ^d	-	1.630	1.020	0.980	-
r (O2-H3) ^d	0.973	1.010	1.610	1.830	-
r (O3-H1) ^d	-	2.440	1.280	1.000	0.973
r (Al1-O2) ^d	1.947	1.919	1.808	1.778	1.749
r (Al1-O3) ^d	1.740	1.750	1.850	1.910	1.940
α (Si1-O2-Al1) ^e	134.390	132.750	141.570	145.440	150.320
α (Si2-O3-Al1) ^e	151.370	152.940	135.820	133.620	135.940
ACP system					
ω (O2-H3) ^c	3752.4	2970.5	Not converted	-	-
ω (O3-H1) ^c	-	-	-	3070.9	3750.5
r (C1-C2) ^d	-	1.500	-	1.360	-
r (C1-O1) ^d	-	1.230	-	1.340	-
r (C2-H1) ^d	-	-	-	1.990	-
r (O1-H3) ^d	-	1.620	-	0.980	-
r (O2-H3) ^d	0.973	1.010	-	1.810	-
r (O3-H1) ^d	-	2.560	-	1.990	0.973
r (Al1-O2) ^d	1.947	1.918	-	1.776	1.749
r (Al1-O3) ^d	1.740	1.750	-	1.920	1.940
α (Si1-O2-Al1) ^e	134.390	132.880	-	146.420	150.320
α (Si2-O3-Al1) ^e	151.370	153.500	-	133.190	135.940

^a Atomic numbering are shown in Figure 3.1.

^b For 50/3T cluster model of H-ZSM-5.

^c Vibrational frequencies, in cm^{-1} .

^d Bond distance, in Å.

^e Angle, in degree.

สถาบันวิทยบริการ
จุฬาลงกรณ์มหาวิทยาลัย

Table 4.8 Relative energies and thermodynamic quantities of related species of various systems.

System/energy ^a	ΔE^{298} , ^b	ΔH^{298} , ^b	ΔG^{298} , ^b	ΔS^{298} , ^c	log K
ACD system					
ACD + HZ	0.00	0.00	0.00	0.00	
INT1_M5	-11.23	-11.11	-0.66	-35.07	
TS_M5	8.16	7.33	20.76	-45.06	
INT2_M5	3.60	3.32	15.69	-41.51	
HETH + ZH	17.89	17.90	17.85	0.17	-11.98
ACT system					
ACT + HZ	0.00	0.00	0.00	0.00	
INT1_M5	-14.06	-12.94	-3.59	-31.36	
TS_M5	5.28	5.49	17.63	-40.74	
INT2_M5	3.39	4.02	15.24	-37.64	
HPRO + ZH	20.22	20.66	19.69	3.25	-13.80
BTN system					
BTN + HZ	0.00	0.00	0.00	0.00	
INT1_M5	-13.86	-13.56	-2.42	-37.35	
TS_M5	6.15	5.44	20.37	-50.10	
INT2_M5	4.30	4.07	17.73	-45.80	
HBUT + ZH	18.89	18.81	19.27	-1.55	-14.77
PTN system					
PTN + HZ	0.00	0.00	0.00	00.00	
INT1_M5	-12.13	-11.90	0.48	-41.52	
TS_M5	7.85	7.16	22.08	-50.05	
INT2_M5	5.84	5.65	19.14	-45.26	
HPEN + ZH	20.51	20.33	21.29	-3.22	-13.68
MBTN system					
MBTN + HZ	0.00	0.00	0.00	00.00	
INT1_M5	-12.00	-11.80	0.53	-21.09	
TS_M5	7.10	6.52	20.83	-48.01	
INT2_M5	5.09	4.94	17.93	-23.28	
HMBUT + ZH	17.62	17.38	18.06	-2.30	-12.75
ACP system					
ACP + HZ	0.00	0.00	0.00	00.00	
INT1_M5	-11.16	-10.71	0.51	-37.63	
TS_M5		Not converted			
INT2_M5	7.16	7.14	20.67	-45.40	
HPETH + ZH	20.03	19.94	20.10	-0.56	No Value

^a For 50/3T (model 5) cluster model of H-ZSM-5.

^b In kcal/mol. ^c In cal/mol K.

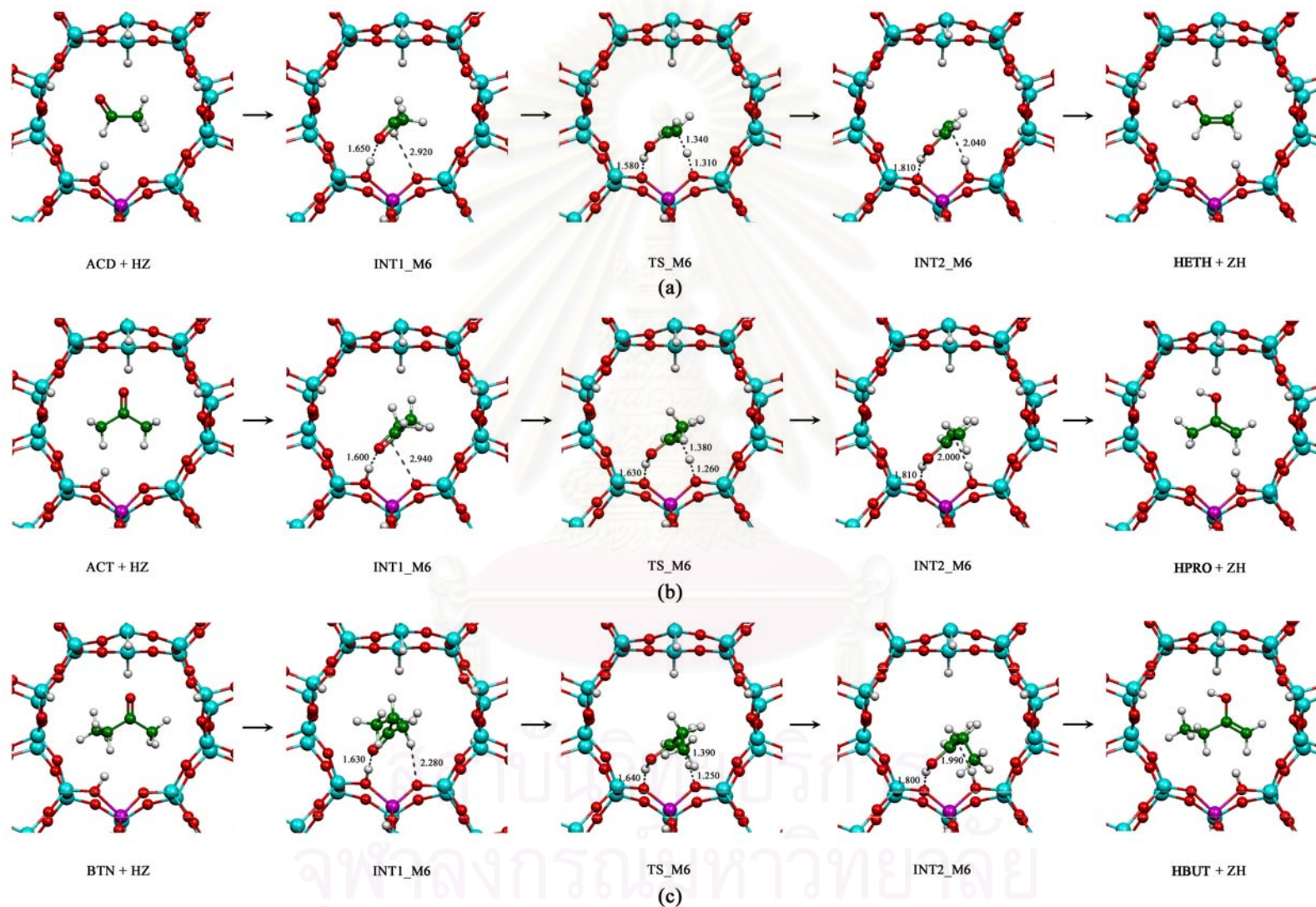


Figure 4.9 Reaction steps of keto-enol isomerization of reactants (a) acetaldehyde, (b) acetone, (c) butanone, (d) 2-pentanone, (e) 3-methyl-2-butanone and (f) acetophenone interacting with 72/3T cluster model of H-ZSM-5.

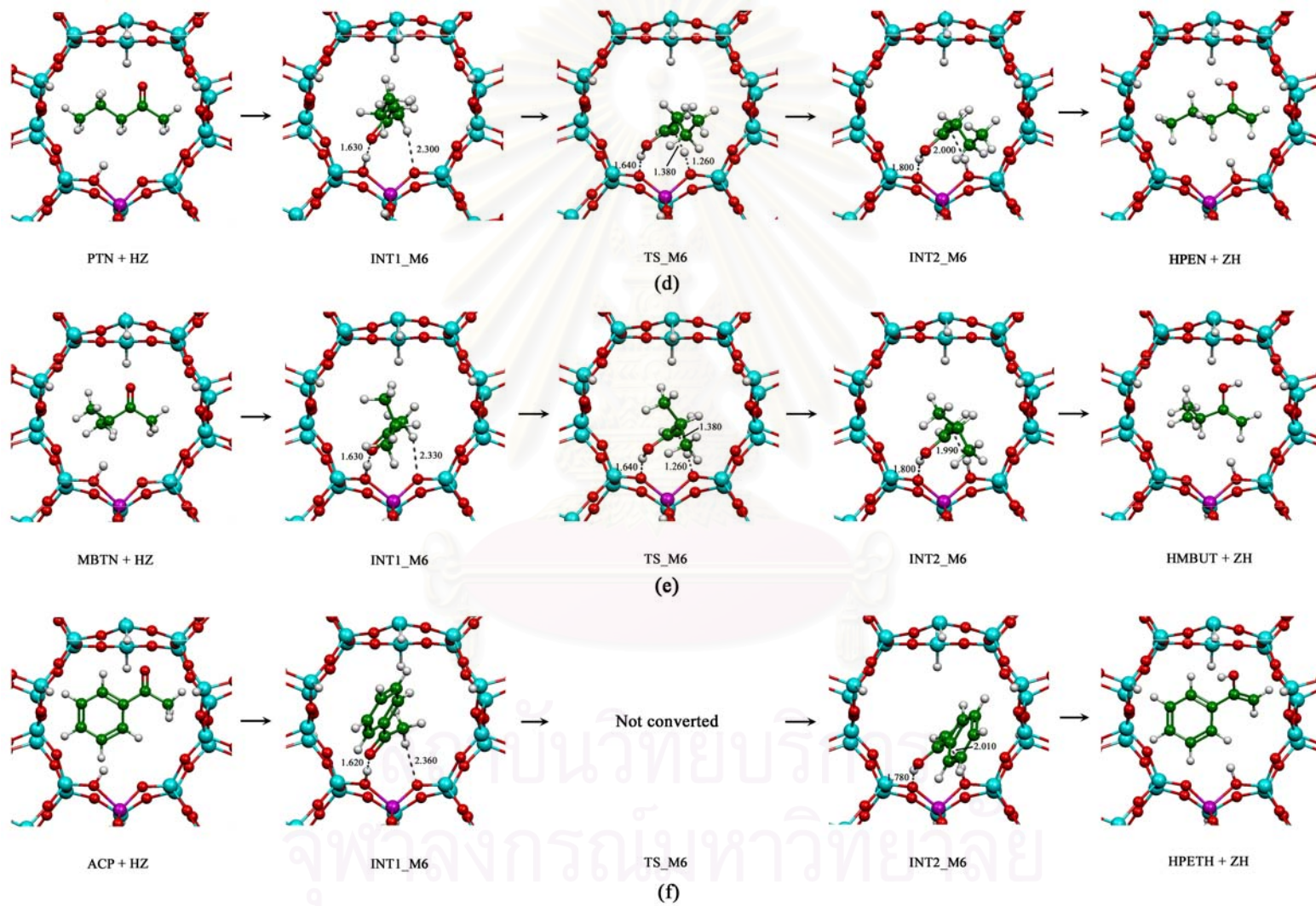


Figure 4.9 (cont.)

Table 4.9 Computed stretching vibrational frequencies of hydroxyl groups at O2 and O3 atoms and selected geometry parameters (bond distances and bond angles) on 72/3T (model 6) cluster model of H-ZSM-5.

System/parameter ^a	Vibrational frequencies at reaction states ^b				
	HZ	INT1	TS	INT2	ZH
ACD system					
ω (O2-H3) ^c	3696.6	3050.7	-	-	-
ω (O3-H1) ^c	-	-	-	3191.5	3765.8
R (C1-C2) ^d	-	1.490	1.390	1.340	-
R (C1-O1) ^d	-	1.220	1.290	1.340	-
R (C2-H1) ^d	-	-	1.340	2.040	-
R (O1-H3) ^d	-	1.650	1.030	0.990	-
R (O2-H3) ^d	0.977	1.010	1.580	1.810	-
R (O3-H1) ^d	-	2.920	1.310	1.000	0.972
R (Al1-O2) ^d	1.943	1.918	1.813	1.781	1.752
R (Al1-O3) ^d	1.760	1.750	1.850	1.910	1.930
α (Si1-O2-Al1) ^e	138.470	136.640	139.840	141.440	144.170
α (Si2-O3-Al1) ^e	135.250	137.870	132.130	131.530	133.190
ACT system					
ω (O2-H3) ^c	3696.6	2897.8	-	-	-
ω (O3-H1) ^c	-	-	-	3092.7	3765.8
R (C1-C2) ^d	-	1.500	1.390	1.350	-
R (C1-O1) ^d	-	1.230	1.300	1.340	-
R (C2-H1) ^d	-	-	1.380	2.000	-
R (O1-H3) ^d	-	1.600	1.010	0.990	-
R (O2-H3) ^d	0.977	1.010	1.630	1.810	-
R (O3-H1) ^d	-	2.940	1.260	1.000	0.972
R (Al1-O2) ^d	1.943	1.914	1.806	1.781	1.752
R (Al1-O3) ^d	1.760	1.760	1.850	1.910	1.930
α (Si1-O2-Al1) ^e	138.470	137.180	140.760	141.880	144.170
α (Si2-O3-Al1) ^e	135.250	137.910	131.830	131.750	133.190
BTN system					
ω (O2-H3) ^c	3696.6	2959.9	-	-	-
ω (O3-H1) ^c	-	-	-	3091.8	3765.8
R (C1-C2) ^d	-	1.507	1.390	1.350	-
R (C1-O1) ^d	-	1.230	1.300	1.340	-
R (C2-H1) ^d	-	-	1.390	1.990	-
R (O1-H3) ^d	-	1.630	1.010	0.990	-
R (O2-H3) ^d	0.977	1.010	1.640	1.800	-
R (O3-H1) ^d	-	2.280	1.250	1.000	0.972
R (Al1-O2) ^d	1.943	1.915	1.805	1.781	1.752
R (Al1-O3) ^d	1.760	1.760	1.850	1.910	1.930
α (Si1-O2-Al1) ^e	138.470	136.290	140.800	141.870	144.170
α (Si2-O3-Al1) ^e	135.250	137.580	131.780	131.330	133.190
PTN system					
ω (O2-H3) ^c	3696.6	2942.8	-	-	-
ω (O3-H1) ^c	-	-	-	3098.3	3765.8
R (C1-C2) ^d	-	1.500	1.390	1.350	-
R (C1-O1) ^d	-	1.230	1.310	1.340	-
R (C2-H1) ^d	-	-	1.380	2.000	-
R (O1-H3) ^d	-	1.630	1.010	0.990	-
R (O2-H3) ^d	0.977	1.010	1.640	1.800	-
R (O3-H1) ^d	-	2.300	1.260	1.000	0.972
R (Al1-O2) ^d	1.943	1.915	1.804	1.781	1.752
R (Al1-O3) ^d	1.760	1.760	1.850	1.910	1.930
α (Si1-O2-Al1) ^e	138.470	136.420	140.990	141.970	144.170
α (Si2-O3-Al1) ^e	135.250	137.510	131.570	131.190	133.190

Table 4.9 (cont.)

System/parameter ^a	Vibrational frequencies at reaction states ^b				
	HZ	INT1	TS	INT2	ZH
MBTN system					
ω (O2-H3) ^c	3696.6	2979.42	-	-	-
ω (O3-H1) ^c	-	-	-	3085.6	3765.8
R (C1-C2) ^d	-	1.500	1.390	1.350	-
R (C1-O1) ^d	-	1.230	1.310	1.340	-
R (C2-H1) ^d	-	-	1.380	1.990	-
R (O1-H3) ^d	-	1.630	1.010	0.990	-
R (O2-H3) ^d	0.977	1.010	1.640	1.800	-
R (O3-H1) ^d	-	2.330	1.260	1.000	0.972
R (Al1-O2) ^d	1.943	1.915	1.804	1.781	1.752
r (Al1-O3) ^d	1.760	1.760	1.850	1.910	1.930
α (Si1-O2-Al1) ^e	138.470	136.970	140.990	141.820	144.170
α (Si2-O3-Al1) ^e	135.250	137.420	131.570	131.380	133.190
ACP system					
ω (O2-H3) ^c	3696.6	2963.5	Not converted	-	-
ω (O3-H1) ^c	-	-	-	3107.3	3765.8
r (C1-C2) ^d	-	1.509	-	1.360	-
r (C1-O1) ^d	-	1.230	-	1.340	-
r (C2-H1) ^d	-	-	-	2.010	-
r (O1-H3) ^d	-	1.620	-	0.990	-
r (O2-H3) ^d	0.977	1.010	-	1.780	-
r (O3-H1) ^d	-	2.360	-	1.000	0.972
r (Al1-O2) ^d	1.943	1.910	-	1.780	1.752
r (Al1-O3) ^d	1.760	1.750	-	1.910	1.930
α (Si1-O2-Al1) ^e	138.470	136.830	-	142.020	144.170
α (Si2-O3-Al1) ^e	135.250	138.100	-	131.410	133.190

^a Atomic numbering are shown in Figure 3.1.

^b For 72/3T cluster model of H-ZSM-5.

^c Vibrational frequencies, in cm^{-1} .

^d Bond distance, in Å.

^e Angle, in degree.

Table 4.10 Relative energies and thermodynamic quantities of related species of various systems.

System/energy ^a	ΔE^{298} , ^b	ΔH^{298} , ^b	ΔG^{298} , ^b	ΔS^{298} , ^c	log K
<i>ACD system</i>					
ACD + HZ	0.00	0.00	0.00	0.00	
INT1_M6	-10.98	-10.73	-0.70	-33.65	
TS_M6	5.37	4.58	18.17	-45.57	
INT2_M6	-0.53	-1.29	13.07	-48.17	
HETH + ZH	14.44	14.50	14.20	1.01	-10.09
<i>ACT system</i>					
ACT + HZ	0.00	0.00	0.00	0.00	
INT1_M6	-13.96	-12.80	-3.52	-31.13	
TS_M6	2.31	2.69	14.10	-38.26	
INT2_M6	-0.87	-0.70	12.18	-43.22	
HPRO + ZH	16.77	17.27	16.05	4.08	-11.50
<i>BTN system</i>					
BTN + HZ	0.00	0.00	0.00	0.00	
INT1_M6	-14.16	-13.82	-2.38	-38.36	
TS_M6	3.24	2.77	15.98	-44.33	
INT2_M6	0.07	-0.48	13.77	-47.79	
HBUT + ZH	15.44	15.41	15.62	-0.72	-11.83
<i>PTN system</i>					
PTN + HZ	0.00	0.00	0.00	0.00	
INT1_M6	-12.52	-12.61	-0.70	-39.94	
TS_M6	5.12	4.52	18.96	-48.42	
INT2_M6	1.91	1.79	15.13	-44.75	
HPEN + ZH	17.06	16.93	17.65	-2.39	-11.60
<i>MBTN system</i>					
MBTN + HZ	0.00	0.00	0.00	0.00	
INT1_M6	-11.96	-11.67	0.21	-0.02	
TS_M6	4.10	3.12	18.78	-32.27	
INT2_M6	1.08	1.03	14.02	-0.02	
HMBUT + ZH	14.17	13.98	14.42	0.02	-10.11
<i>ACP system</i>					
ACP + HZ	0.00	0.00	0.00	0.00	
INT1_M6	-11.29	-11.28	1.71	-44.74	
TS_M6		Not converted			
INT2_M6	2.87	2.99	15.87	-44.37	
HPETH + ZH	16.58	16.54	16.46	0.27	No Value

^a For 72/3T (model 6) cluster model of H-ZSM-5.^b In kcal/mol. ^c In cal/mol K.

Figure 4.8 and 4.9 present the ONIOM2 optimized geometries corresponding to the stationary points of keto-enol isomerization inside H-ZSM-5. The comparison between the ONIOM2 results and the ones obtained with the 3T and 5T cluster models shows that there are not dramatic changes in the zeolite-reactant interaction when the cluster is increased to 50 and 72 tetrahedra with the ONIOM2 procedure. Nevertheless, there are some differences on the structure of the zeolite that are worth mentioning. On one hand, it can be observed that the 3T and 5T calculations provide values of the A11-O3-Si2 angle in HZ and in the HZ(keto) (or intermediate1) that are too large. This is due to the fact that 3T and 5T cluster models are too small to take into account the constraints induced by the zeolite framework. The A11-O3-Si2 angle is not so large in the transition state or the enol-adsorbed intermediate because the O3 atom is protonated or almost protonated. On the other hand, ONIOM2 calculations show that the dihedral angles defined by the Si1, O2, A11, O3, and Si2 atoms do not change very much along the HZ(keto) to HZ(enol) (or intermediate2) process, the largest variation being about 5-6°. However, for the 5T calculations the variations of the dihedral angles are much larger. This is again due to the larger flexibility of the 5T compared to 50/3T and 72/3T considered in the ONIOM calculations.

For comparison the results have also included the values obtained with 3T and 5T cluster models. It can be observed that ONIOM2 calculations provide a smaller interaction energy between reactant and the zeolite. This destabilization of the HZ(keto) intermediate is more important with B3LYP:AM1. In contrast, the HZ(enol) intermediate becomes slightly more stable in the ONIOM calculations. As a result, the reaction energy of the HZ(keto) to HZ(enol) process becomes smaller. Overall, it can explain that 3T and 5T cluster models provide a quite reasonable picture of the structure and energetics of the species involved in keto-enol isomerization of all reactants. However, enlarging the cluster with the ONIOM procedure allows us to introduce the characteristic building blocks of the zeolite, as well as to constrain the geometry optimizations of the active site by introducing the zeolite framework.

4.2 Molecular arrangement on different cluster models

Due to the molecular configurations of acetaldehyde interacting with H-ZSM-5 zeolite as four different clusters 3T, 5T, 50T and 72T, shown in Figure 4.2, 4.8 (a), 4.9 (a) respectively, the molecular arrangement of acetaldehyde on these clusters are quite similar. All cluster models employed for this system (ACD) should give the correct computational results, because the small molecule of acetaldehyde is hardly ever affected by double 10T membered ring of 50T and 72T cluster models. For the ACT system, the molecules of acetone and acetaldehyde are hardly different but the molecular arrangement of acetone on the 50/3T and 72/3T cluster models are quite different from the 5T and 3T models (see Figure 4.3, 4.8 (b), 4.9 (b), respectively). However, the molecular arrangements of the species interacting with 5T and 3T cluster models for ACT system are still different. As the molecules of butanone (BTN), 2-pentanone (PTN), 3-methyl-2-butanone (MBTN) and acetophenone (ACP) are bigger than the acetaldehyde and acetone, the molecular arrangements of butanone, 2-pentanone, 3-methyl-2-butanone and acetophenone (ACP) on the 50/3T and 72/3T cluster models are obviously different from the 5T and 3T models, see Figure 4.4, 4.8 (c), 4.9 (c), 4.5, 4.8 (d), 4.9 (d), 4.6, 4.8 (e), 4.9 (e), 4.7, 4.8 (f), 4.9 (f), respectively.

4.3 Reaction coordinate

The potential energy surfaces for keto-enol isomerization of acetaldehyde, acetone, butanone, 2-pentanone, 3-methyl-2-butanone and acetophenone in gas phase (model 1) and water-catalyzed (model 2) are shown in Figures 4.10 and 4.11, respectively. The potential energy surfaces for keto-enol isomerization of acetaldehyde, acetone, butanone, 2-pentanone, 3-methyl-2-butanone and acetophenone in the 3T (model 3) and 5T (model 4) are shown in Figures 4.12 and 4.13, respectively, and the potential energy surfaces for keto-enol isomerization of acetaldehyde, acetone, butanone, 2-pentanone, 3-methyl-2-butanone and acetophenone in the 50/3T (model 5) and 72/3T (model 6) clusters of H-ZSM-5 are shown in Figures 4.14 and 4.15, respectively. The activation of non-catalytic reactions

of systems ACD, ACT, BTN PTN, MBTN and ACP as shown in Figure 4.10 are 69.38, 65.92, 66.22, 67.87, 67.25 and 65.59 kcal/mol, respectively. Activation energies due to the activation steps of the water-catalyzed model of the systems ACD, ACT, BTN, PTN, MBTN and ACP as shown in Figure 4.11 are 38.07, 38.29, 39.30, 41.59, 38.28 and 39.63 kcal/mol, respectively. Activation energies due to the activation steps of the 5T and 3T (in parentheses) cluster models of the systems ACD, ACT, BTN, PTN and MBTN as shown in Figure 4.12 and 4.13 are 18.33 (20.39), 18.56 (20.79), 17.89 (20.04), 17.92 (20.15) and 18.60 (20.73) kcal/mol, respectively. Activation energies due to the activation steps of the 50/3T cluster model of the systems ACD, ACT, BTN, PTN and MBTN as shown in Figure 4.14 are 19.39, 19.34, 20.01, 19.98 and 19.10 kcal/mol, respectively, and activation energies due to the activation steps of the 72/3T cluster model of the systems ACD, ACT, BTN, PTN and MBTN as shown in Figure 4.15 are 16.30, 16.27, 17.40, 17.64 and 16.06 kcal/mol, respectively.

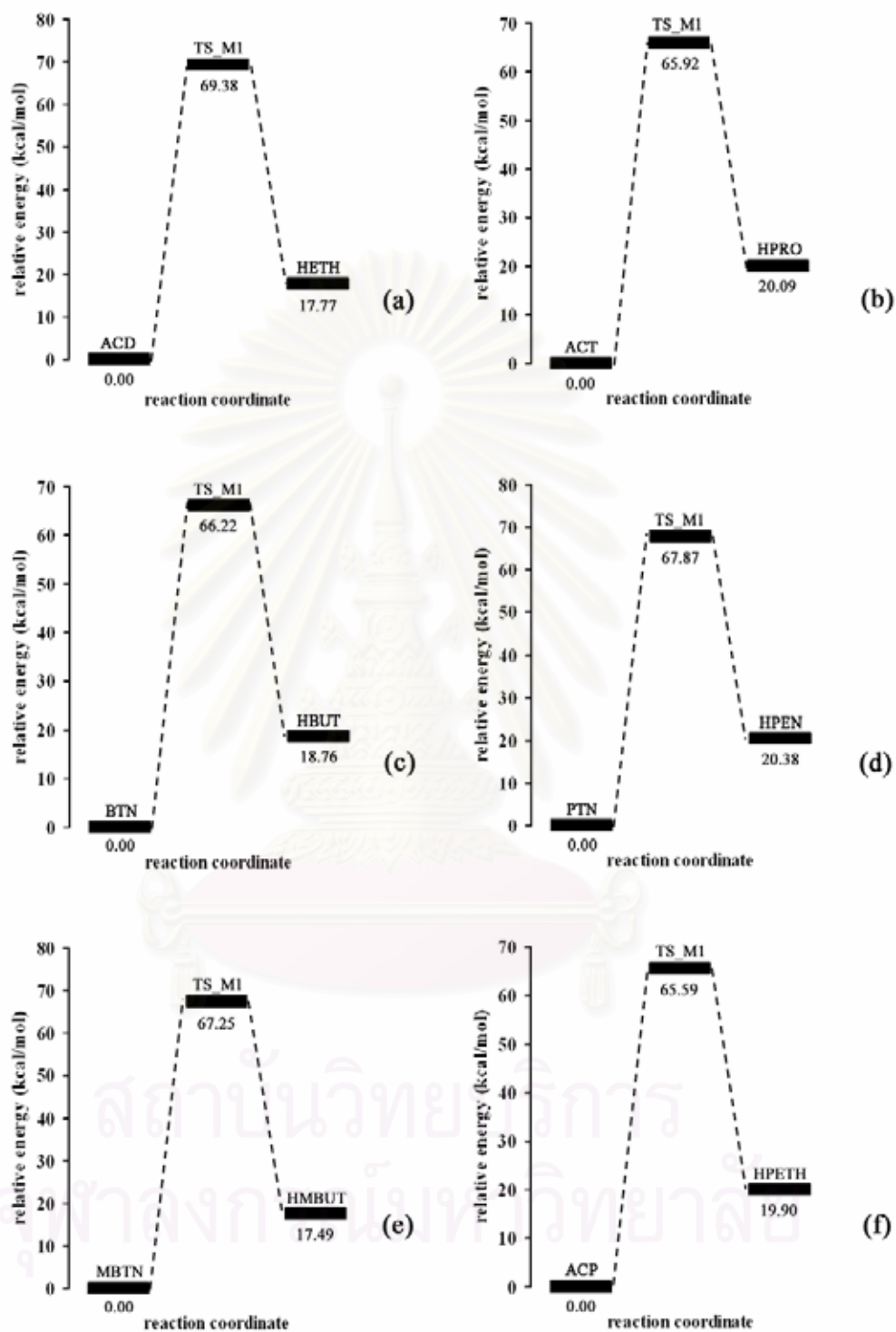


Figure 4.10 Potential energy surface for keto-enol isomerization of (a) acetaldehyde (b) acetone, (c) butanone, (d) 2-pentanone (e) 3-methyl-2-butanone and (f) acetophenone in gas phase (model 1).

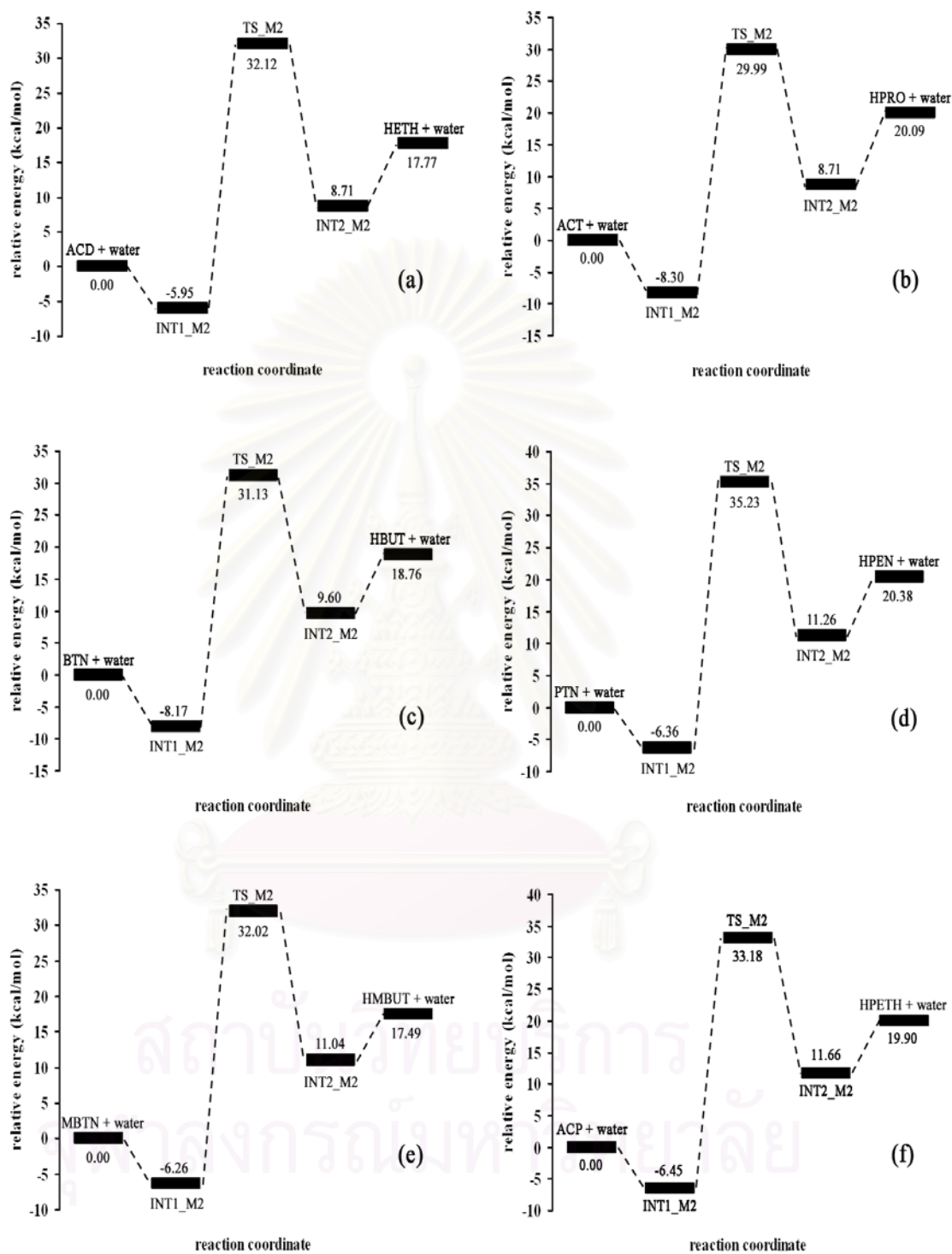


Figure 4.11 Potential energy surface for keto-enol isomerization of (a) acetaldehyde, (b) acetone, (c) butanone, (d) 2-pentanone, (e) 3-methyl-2-butanone and (f) acetophenone catalyzed by water (model 2).

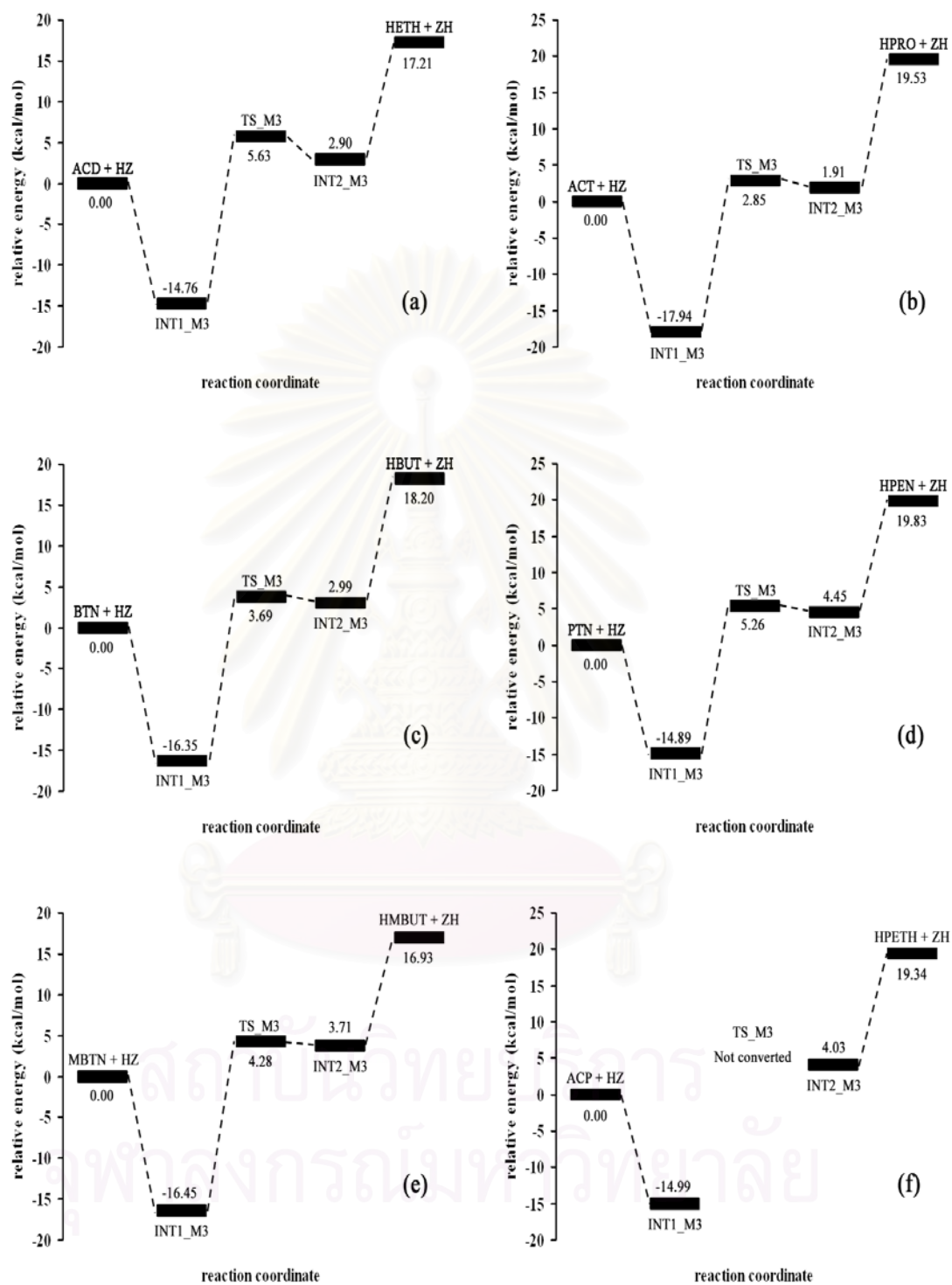


Figure 4.12 Potential energy surface for keto-enol isomerization of (a) acetaldehyde, (b) acetone, (c) butanone, (d) 2-pentanone, (e) 3-methyl-2-butanone and (f) acetophenone in the 3T cluster model of H-ZSM-5 (model 3).

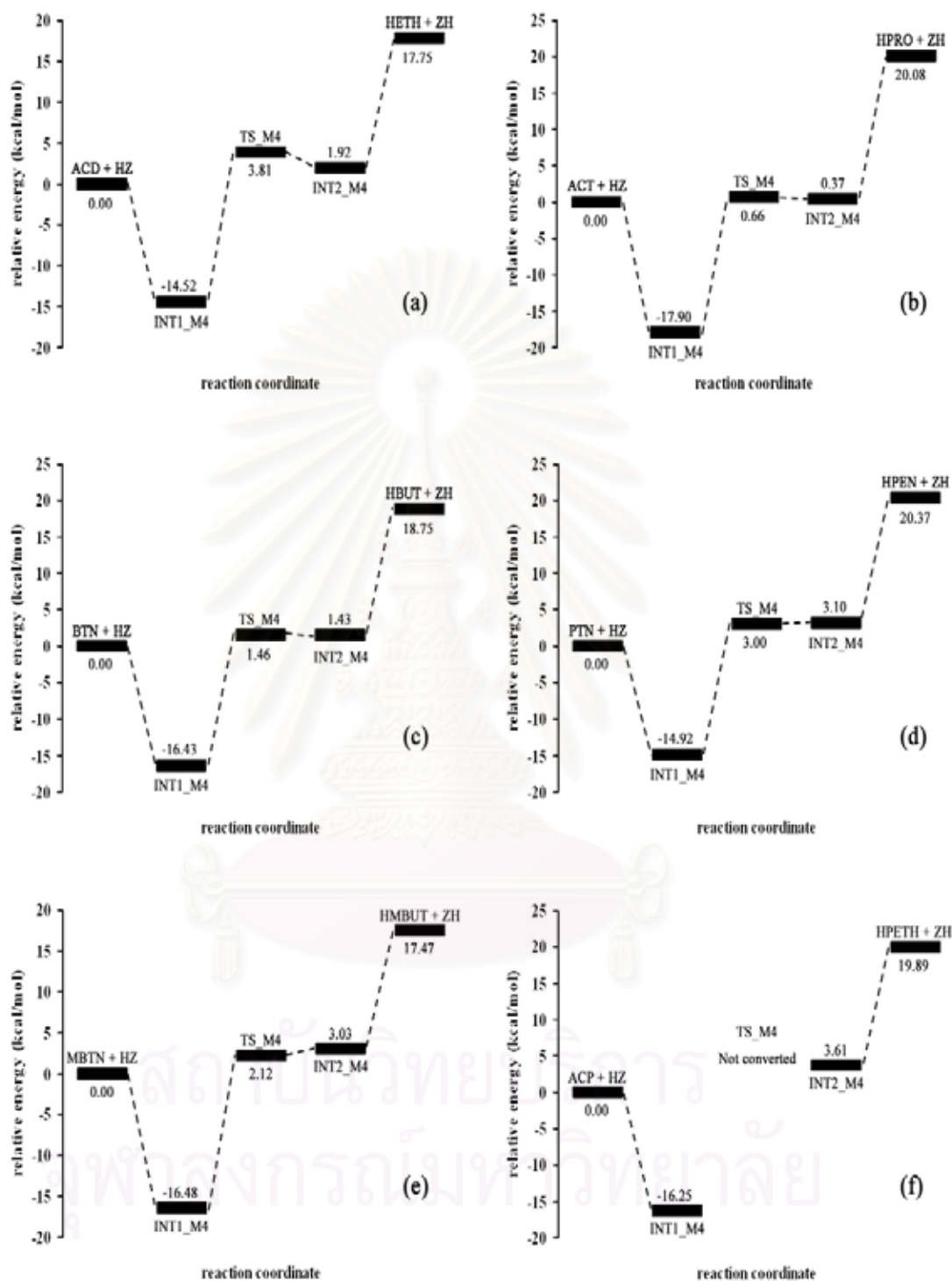


Figure 4.13 Potential energy surface for keto-enol isomerization of (a) acetaldehyde, (b) acetone, (c) butanone, (d) 2-pentanone, (e) 3-methyl-2-butanone and (f) acetophenone in the 5T cluster model of H-ZSM-5 (model 4).

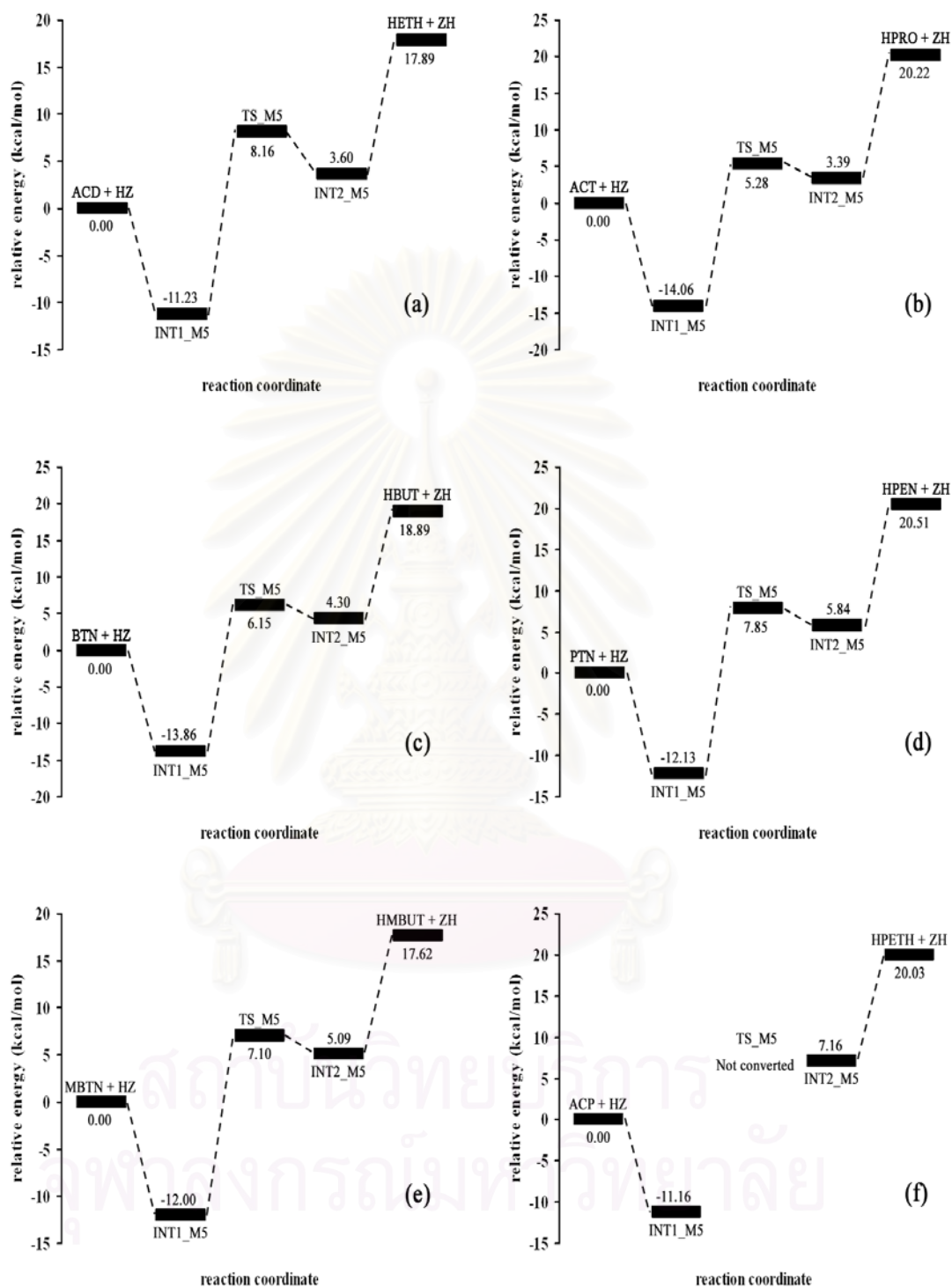


Figure 4.14 Potential energy surface for keto-enol isomerization of (a) acetaldehyde, (b) acetone, (c) butanone, (d) 2-pentanone, (e) 3-methyl-2-butanone and (f) acetophenone in the 50/3T cluster model of H-ZSM-5 (model 5).

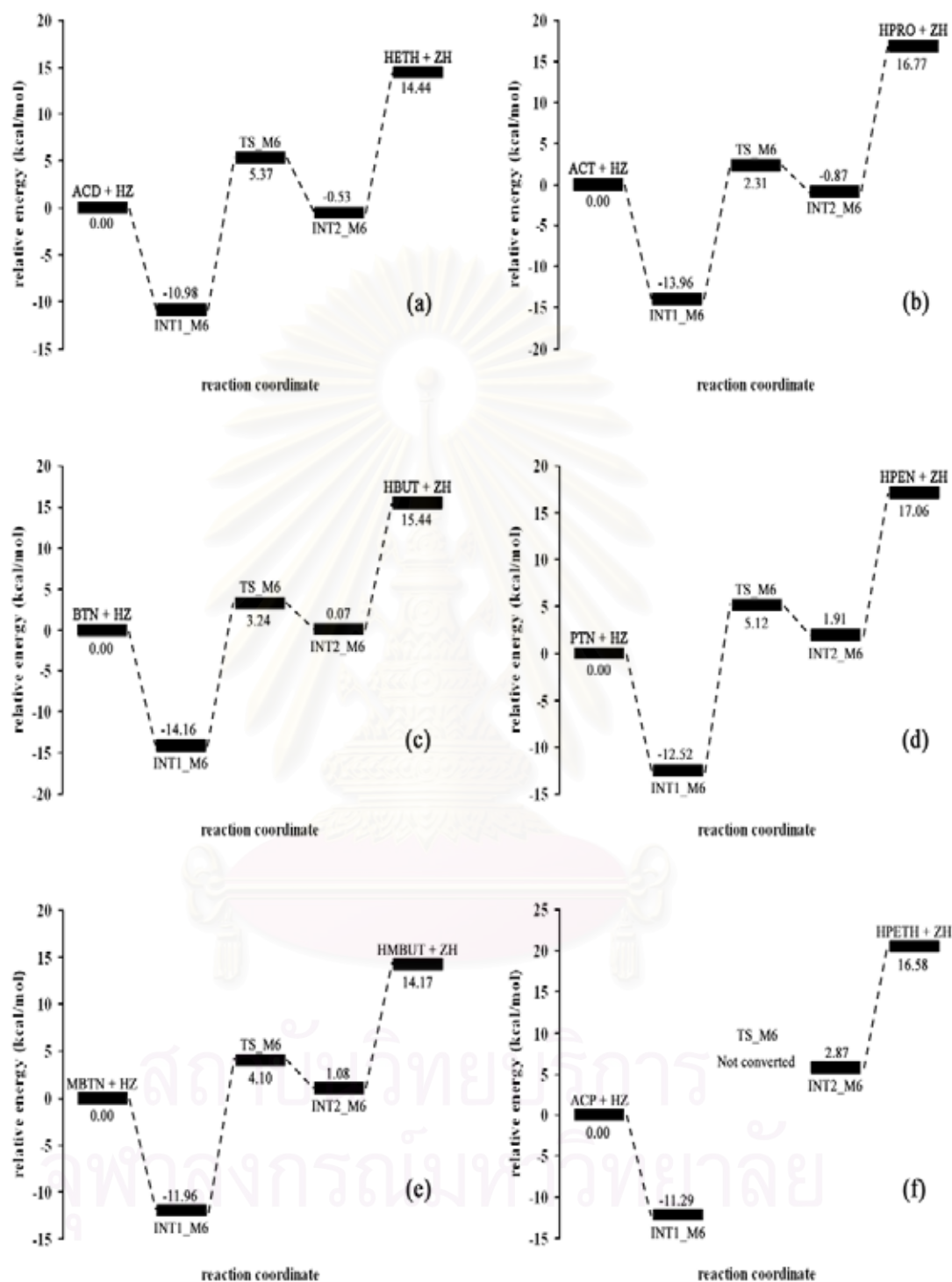


Figure 4.15 Potential energy surface for keto-enol isomerization of (a) acetaldehyde, (b) acetone, (c) butanone, (d) 2-pentanone, (e) 3-methyl-2-butanone and (f) acetophenone in the 72/3T cluster model of H-ZSM-5 (model 6).

Table 4.11 Activation energies of related model of various systems.

Model/Activation energies of system ^a	(ACD)	(ACT)	(BTN)	(PTN)	(MBTN)	(ACP)
Gas phase (model 1) ^b	69.38	65.92	66.22	67.87	67.25	65.59
Water catalyzed (model 2) ^b	38.07	38.29	39.30	41.59	38.28	39.63
H-ZSM-5 catalyzed						
3T (model 3) ^b	20.39	20.79	20.04	20.15	20.73	No
5T (model 4) ^b	18.33	18.56	17.89	17.92	18.60	No
50/3T (model 5) ^c	19.39	19.34	20.01	19.98	19.10	No
72/3T (model 6) ^c	16.30	16.27	17.40	17.64	16.06	No

^a in kcal/mol.

^b For DFT/B3LYP/6-31G(d) method.

^c For ONIOM(B3LYP/6-31G(d):AM1) method.

The comparison of activation energies of keto-enol isomerization in gas phase, catalyzed by water molecule and inside the zeolite using cluster models 3T, 5T, 50/3T and 72/3T of ACD, ACT, BTN, PTN, MBTN and ACP system as shown in Table 4.11. The order of the reaction energies for models 3 is in decreasing order: systems of ACT > MBTN > ACD > PTN > BTN, for models 4 is in decreasing order: systems of MBTN > ACT > ACD > PTN > BTN, for models 5 is in decreasing order: systems of BTN > PTN > ACD > ACT > MBTN and for models 6 is in decreasing order: systems of PTN > BTN > ACD > ACT > MBTN. As can be observed, the catalytic effect of the zeolite is much more important than that of water. The transition state of the reaction is largely stabilized with respect to the ground-state asymptote. Moreover, the energy barrier computed with respect to the keto intermediate is much lower for the zeolite-catalyzed than for the water-assisted or the gas-phase. This stronger catalytic effect is due to a smaller geometry reorganization of the system along the process and also to the high acidity of the zeolite, which facilitates the proton transfer to reactants. The real catalytic effect can be observed from the comparison between the activation free energy in the gas phase and inside the zeolite.

The Figure 4.16 shown the activation energy related to the quantum cluster sizes. The plot shows dramatic change in value between the 50T and 72T clusters. Therefore, the 72T cluster size is appropriate to over the important framework effects with the catalyzed for keto-enol isomerization.

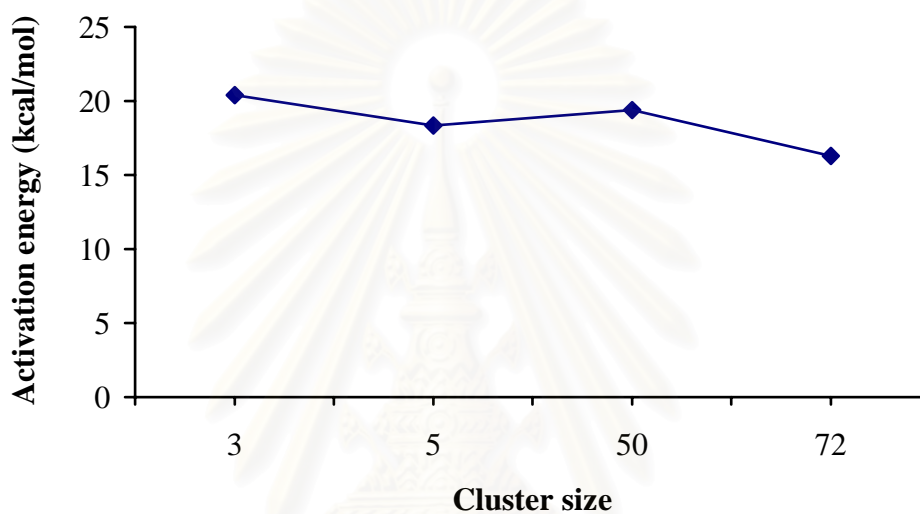


Figure 4.16 Activation energy of keto-enol isomerization of acetaldehyde in H-ZSM-5 zeolite plotted as a function of size of the cluster models.

In this work, the relative energies computed by DFT method with 3T and 5T cluster models show the underestimated values as compared to the 50/3T and 72/3T cluster models that computed by ONIOM method.

CHAPTER V

CONCLUSIONS AND SUGGESTIONS

Conversions of acetaldehyde (ACD) to hydroxyethylene (HETH), acetone (ACT) to 2-hydroxypropylene (HPRO), butanone (BTN) to 2-hydroxybutene (HBUT), 2-pentanone (PTN) to 2-hydroxypentene (HPEN), 3-methyl-2-butanone (MBTN) to 2-hydroxy-3-methylbutene (HMBUT) and acetophenone (ACP) to 2-hydroxyphenyethylene (HPETH) catalyzed by H-ZSM-5 have been theoretically studied using quantum chemical methods. Geometry optimizations reacting species in the acid sites of H-ZSM-5 catalyst of 3T and 5T cluster models have been computed at the DFT/B3LYP/6-31G(d) method. For the larger size of 50/3T and 72/3T cluster models employing the ONIOM(B3LYP/6-31G(d):AM1) calculations have been carried out. The vibrational frequencies of acid sites of H-ZSM-5, relative energies of all involved species, thermodynamic quantities and equilibrium constant of catalytic reactions have been obtained.

Results of keto-enol isomerization with all cluster models of H-ZSM-5 are very similar of ACD, ACT, BTN, PTN and MBTN systems. These results show that the keto-enol isomerization is endothermic reaction, which all systems can be decreased their activation energies by H-ZSM-5 catalyst. For ACP system catalyzed by H-ZSM-5, keto-enol isomerization was not complete because of the steric and electronic effect of ACP system. The activation energies of all systems ACD, ACT, BTN, PTN and MBTN catalyzed by H-ZSM-5 are obviously lower than non catalytic and water-catalyzed models. The activation energies obtained from the activation steps of the 72/3T cluster model of the ACD, ACT, BTN, PTN and MBTN systems are 16.30, 16.27, 17.40, 17.64 and 16.06 kcal/mol, respectively. It can be seen that the 72/3T cluster model is more important catalytic effect than other cluster models. The 72/3T of ONIOM calculation model is an appropriate tool for the electronic calculation in the H-ZSM-5 catalyst system. The catalytic effect is much larger than that produced by water molecule, due to the larger acidity of the zeolite and to smaller geometry reorganizations along the process. As catalytic ability of H-ZSM-5 depending on the activation of these conversion reactions, the H-ZSM-5 can be applied in the production of some unsaturated alcohols.

Suggestions for further work:

1. The aldol condensation on H-ZSM-5 assumes that the first step is keto-enol isomerization. Next step, the enol reacting with an aldehyde or ketone molecule that is coordinated to a Brønsted acid site of the zeolite should be studied for further work.

2. As the results according to ONIOM(B3LYP/6-31G(d):AM1) method are in good results for ONIOM2 level, the ONIOM3 method for three-layer such as ONIOM(B3LYP/6-31G(d):HF/3-21G:AM1) or ONIOM(B3LYP/6-31G(d):HF/STO-3G:AM1) should be employed for getting more reliable results.



สถาบันวิทยบริการ
จุฬาลงกรณ์มหาวิทยาลัย

REFERENCES

1. Hölderich, W.; Hesse, M. and Näumann, F. Zeolites: Catalysts for organic synthesis. Angew. Chem., Int. Ed. Engl. 27 (1988): 226.
2. Corma, A. Inorganic solid acids and their use in acid-catalyzed hydrocarbon reaction. Chem. Rev. 95 (1995): 559.
3. Ghobarkar, H.; Schäf, O. and Guth, U. Zeolites-from kitchen to space. Prog. Solid St. Chem. 27 (1999): 29.
4. Sen, S. E.; Smith, S. M. and Sullivan, K. A. Organic transformations using zeolites and zeotype materials. Tetrahedron 55 (1999): 12657.
5. Valyon, J.; Onyestyák, G. and Rees, L. V. C. Study of the dynamics of NH₃ adsorption in ZSM-5 zeolites and the acidity of the sorption sites using the frequency-response technique. J. Phys. Chem. B 102 (1998): 8994.
6. Farneth, W. E. and Gorte, R. J. Methods for characterizing zeolite acidity. Chem. Rev. 95 (1995): 615.
7. Yin, F.; Blumenfeld A. L.; Gruver, V. and Fripiat, J. J. NH₃ as a probe molecule for NMR and IR study of zeolite catalyst acidity. J. Phys. Chem. B 101 (1997): 1824.
8. Paukshtis, E. A.; Malysheva, L. V. and Stepanov, V. G. Interaction of aromatics with Brønsted sites in zeolites: Demarcation line between regions of stable existence of H-complexes and ion pairs for various types of bases. React. Kinet. Catal. Lett. 65 (1998): 75.
9. Barthos, R.; Lónyi, F.; Onyestyák, G. and Valyon, J. An IR, FR, and TPD study on the acidity of H-ZSM-5, sulfated zirconia, and sulfated zirconia-titania using ammonia as the probe molecule. J. Phys. Chem. B 104 (2000): 7311.
10. Lónyi, F. and Valyon, J. A TPD and IR study of the surface species formed from ammonia on zeolite H-ZSM-5, H-mordenite and H-beta. Thermochim. Acta 373 (2001): 53.
11. Lónyi, F. and Valyon, J. On the interpretation of the NH₃-TPD patterns of H-ZSM-5 and H-mordenite. Microporous Mesoporous Mater. 47 (2001): 293.

12. Bore'ave, A.; Auroux, A. and Guimon, C. Nature and strength of acid sites in HY zeolites: a multitechnical approach. Micropor. Mater. 11 (1997): 275.
13. Kao, H.-M. and Grey, C. P. Probing the Brønsted and Lewis acidity of zeolite HY: A $^1\text{H}/^{27}\text{Al}$ and $^{15}\text{N}/^{27}\text{Al}$ TRAPDOR NMR study of monomethylamine adsorbed on HY. J. Phys. Chem. 100 (1996): 5105.
14. Jacobs, W. P. J. H.; de Haan, J. W.; van de Ven, L. J. M. and van Santen, R. A. Interaction of ammonia with Brønsted acid sites in different cages of zeolite Y as studied by proton MAS NMR. J. Phys. Chem. 97 (1993): 10394.
15. Kapustin, G. I. and Brueva, T. R. A simple method for determination of heats of ammonia adsorption on catalysts from thermodesorption data. Thermochim. Acta 379 (2001): 71.
16. Katada, N.; Igi, H.; Kim, J.-H. and Niwa, M. Determination of the acidic properties of zeolite by theoretical analysis of temperature-programmed desorption of ammonia based on adsorption equilibrium. J. Phys. Chem. B 101 (1997): 5969.
17. Brueva, T. R.; Mishin, I. V. and Kapustin, G. I. Distribution of acid-site strengths in hydrogen zeolites and relationship between acidity and catalytic activity. Thermochim. Acta 379 (2001): 15.
18. Parrillo, D. J. and Gorte, R. J. Characterization of acidity in H-ZSM-5, H-ZSM-12, H-Mordenite, and H-Y using microcalorimetry. J. Phys. Chem. 97 (1993): 8786.
19. Lee, C.; Parrillo, D. J.; Gorte, R. J. and Farneth, W. E. Relationship between differential heats of adsorption and Brønsted acid strengths of acidic zeolites: H-ZSM-5 and H-Mordenite. J. Am. Chem. Soc. 118 (1996): 3262.
20. Zecchina, A.; Geobaldo, F.; Spoto, G.; Bordiga, S.; Ricchiardi, G.; Buzzoni, R. and Petrini, G. FTIR investigation of the formation of neutral and ionic hydrogen-bonded complexes by interaction of H-ZSM-5 and H-Mordenite with CH_3CN and H_2O : Comparison with the H-NAFION superacidic system. J. Phys. Chem. 100 (1996): 16584.

21. Pazé, C.; Bordiga, S.; Lamberti, C.; Salvalaggio, M.; Zecchina, A. and Bellussi, G. Acidic properties of H- β zeolite as probed by bases with proton affinity in the 118-204 kcal mol⁻¹ range: A FTIR investigation. J. Phys. Chem. B 101 (1997): 4740.
22. Morokuma, K. ONIOM and its applications to material chemistry and catalyze. Bull. Korean Chem. Soc. 24 (2003): 797-801.
23. Breck, D. W. Zeolite molecular sieves. Union Carbide Corporation: Tarrytown New York (1984): pp. 312, 373, 529-588.
24. Streitwieser and Heathcock, Jr. C. H. Introduction to organic chemistry. University of California: Berkley (1977): pp. 360-365, 385-388.
25. Kubelkova, L.; Cejka, J. and Novakova, J. Surface reactivity of ZSM-5 zeolites in interaction with ketones at ambient temperature (a FTIR study). Zeolite 11(1) (1991): 48-53.
26. Xu, T.; Munson, E. J. and Haw, F. Toward a systematic chemistry of organic reactions in zeolites: In situ NMR studies of ketones. J. Am. Chem. Soc. 116 (1994): 1962-1972.
27. Dumitriu, E.; Hulea, V.; Fechetu, I.; Auroux, A.; Lacaze, J. and Guimon, C. The aldol condensation of lower aldehydes over MFI zeolites with different acidic properties. Micropor. Mater. 43 (2001): 341-359.
28. Sepa, J.; Lee, C.; Gorte, R. J.; White, D.; Kassab, E.; Evleth, E. M.; Jessri, H. and Allavena, M. Carbonyl ¹³C shielding tensors and heats of adsorption of acetone adsorbed in silicalite and the 1:1 stoichiometric complex in H-ZSM-5. J. Phys. Chem. 100 (1996): 18515-18523.
29. Kassab, E.; Jessri, H.; Allavena, M. and White, D. Ab initio calculations of carbonyl adsorption complexes at zeolitic Brønsted sites simulated by model clusters: role of modeling. J. Phys. Chem. A. 103 (1999): 2766-2774.
30. Monfort, X.-S.; Bertran, J.; Branchadell, V. and Sodupe, M. Keto-enol isomerization of acetaldehyde in HZSM5. A theoretical study using the ONIOM2 method. J. Phys. Chem. B 106 (2002): 10220-10226.

31. Biaglow, I.; Gorte, R. J.; Kokotailo, G. T. and White, D. A probe of Brønsted site acidity in zeolites: ^{13}C chemical shift of acetone. J. Catal. 148 (1994): 779-786.
32. Böhlman, W. and Michel, D. ^1H MAS NMR studies of molecules adsorbed on activated zeolites. J. Catal. 202 (2001): 421-426.
33. Xu, M.; Wang, W. and Hunger, M. Formation of acetone enol on acidic zeolite ZSM-5 evidenced by H/D exchange. Chem. Commun. 1 (2003): 722-723.
34. Panov, G. and Fripiat, J. J. Acetone condensation reaction on acid catalysts. J. Catal. 178 (1998): 188-197.
35. Barich, D. H.; Nicholas, J. B.; Xu, T. and Haw, J. F. Theoretical and experimental study of the ^{13}C chemical shift tensors of acetone complexes with Brønsted and Lewis Acids. J. Am. Chem. Soc. 120 (1998): 12342-12350.
36. Santiago, L.-R.; Vendrell, O.; Tejero, I.; Sodupe, M. and Bertran, J. Solvent-assisted catalysis in the enolization of acetaldehyde radical cation. Chem. Phys. Letters 334 (2001): 112-118.
37. Khaliullin, R. Z.; Bell, A. T. and Kazansky, V. B. An experimental and density functional theory study of the interactions of CH_4 with H-ZSM-5. J. Phys. Chem. A 105 (2001): 10454.
38. Panjan, W. and Limtrakul, J. The influence of the framework on adsorption properties of ethylene/H-ZSM-5 system: An ONIOM study. J. Mol. Struct. 654 (2003): 35-45.
39. Raksakoon, C. and Limtrakul, J. Adsorption of aromatic hydrocarbon onto H-ZSM-5 zeolite investigated by ONIOM study. J. Mol. Struct. (Theochem) 631 (2003): 147-156.
40. Milas, I. and Nascimento, M. A. C. The dehydrogenation and cracking reactions of isobutene over the ZSM-5 zeolite. Chem. Phys. Letters 373 (2003): 379.
41. Bhan, A.; Joshi, Y. V.; Delgass, W. N. and Thomson, K. T. DFT investigation of alkoxide formation from olefins in H-ZSM-5. J. Phys. Chem. B 107 (2003): 10476.

42. Sillar, K. and Burk, P. Computational study of vibrational frequencies of bridging hydroxyl groups in zeolite ZSM-5. Chem. Phys. Letters 393 (2004): 285.
43. Sillar, K. and Burk, P. Hybrid quantum chemical and density functional theory (ONIOM) study of the acid sites in zeolite ZSM-5. J. Phys. Chem. B 108 (2004): 9893.
44. Zheng, X. and Blowers, P. An ab initio study of ethane conversion reactions on zeolites using the complete basis set composite energy method. J. Mol. Catal. A: Chemical 229 (2005): 77-85.
45. Lewars, E. Computational chemistry: Introduction to the theory and applications of molecular and quantum mechanics. Trent University: Peterborough, Ontario (2003).
46. HyperChem 7.0 user manual. Hypercube, Inc., URL – <http://www.hyper.com>.
47. Chem3D 5.0 user manual. CambridgeSoft, MA., URL – <http://www.camsoft.com>.
48. Atkins, P. W. Quanta 2nd ed. Oxford University: (1991).
49. Becke, D. Density-functional exchange-energy approximation with correct asymptotic behavior. Phys. Rev. A 38 (1988): 3098.
50. Lee, C.; Yang, W. and Parr, R.G. Development of the Colle-Salvetti correlation-energy formula into a functional of the electron density. Phys. Rev. B 37 (1988): 785.
51. Maseras, F. and Morokuma, K. IMOMO: A new integrated ab initio + molecular mechanics geometry optimization scheme of equilibrium structures and transition states. J. Comput. Chem. 16 (1995): 1170.
52. Humbel, S.; Sieber, S. and Morokuma, K. The IMOMO method: Integration of different levels of molecular orbital approximations for geometry optimization of large systems: Test for n-butane conformation and S_N2 reaction : RCl + Cl⁻. J. Chem. Phys. 105 (1996): 1959.
53. Vreven, T. and Morokuma, K. On the application of the IMOMO (Integrated Molecular Orbital + Molecular Orbital) method. J. Comput. Chem. 21 (2000): 1419.

54. Remko, M.; Walsh, O.A. and Richards, W.G. Theoretical study of molecular structure, tautomerism, and geometrical isomerism of moxonidine: Two-layered ONIOM calculations. J. Phys. Chem. A. 105 (2001): 6926.
55. Remko, M. The gas-phase acidities of substituted hydroxamic and silahydroxamic acids: A comparative ab initio study. J. Phys. Chem. A. 106 (2002): 5005.
56. Peng, C.; Ayala, P. Y.; Schlegel, H. B. and Frisch, M. J. Using redundant internal coordinates to optimize equilibrium geometries and transition states. J. Comp. Chem. 17 (1996): 49.
57. Gonzales, C. and Schlegel, H.B. An improved algorithm for reaction path following. J. Chem. Phys. 90 (1989): 2154.
58. Frisch, M. J.; Trucks, G. W.; Schlegel, H. B.; Scuseria, G. E.; Robb, M. A.; Cheeseman, J. R.; Montgomery, J. A.; Jr.; Vreven, T.; Kudin, K. N.; Burant, J. C.; Millam, J. M.; Iyengar, S. S.; Tomasi, J.; Barone, V.; Mennucci, B.; Cossi, M.; Scalmani, G.; Rega, N.; Petersson, G. A.; Nakatsuji, H.; Hada, M.; Ehara, M.; Toyota, K.; Fukuda, R.; Hasegawa, J.; Ishida, M.; Nakajima, T.; Honda, Y.; Kitao, O.; Nakai, H.; Klene, M.; Li, X.; Knox, J. E.; Hratchian, H. P.; Cross, J. B.; Adamo, C.; Jaramillo, J.; Gomperts, R.; Stratmann, R. E.; Yazyev, O.; Austin, A. J.; Cammi, R.; Pomelli, C.; Ochterski, J. W.; Ayala, P. Y.; Morokuma, K.; Voth, G. A.; Salvador, P.; Dannenberg, J. J.; Zakrzewski, V. G.; Dapprich, S.; Daniels, A. D.; Strain, M. C.; Farkas, O.; Malick, D. K.; Rabuck, A. D.; Raghavachari, K.; Foresman, J. B.; Ortiz, J. V.; Cui, Q.; Baboul, A. G.; Clifford, S.; Cioslowski, J.; Stefanov, B. B.; Liu, G.; Liashenko, A.; Piskorz, P.; Komaromi, I.; Martin, R. L.; Fox, D. J.; Keith, T.; Al-Laham, M. A.; Peng, C. Y.; Nanayakkara, A.; Challacombe, M.; Gill, P. M. W.; Johnson, B.; Chen, W.; Wong, M. W.; Gonzalez, C. and Pople, J. A. Gaussian 03. Revision B.03: Gaussian, Inc., Pittsburgh PA, (2003).
59. Schaftenaar, G. MOLDEN 3.7. CAOS/CAMM Center: Nijmegen Toernooiveld, Nijmegen, Netherlands, (1991).
60. Flükiger, P.; Lüthi, H.P.; Portmann, S. and Weber, J. MOLEKEL 4.3. Swiss Center for Scientific Computing: Manno, Switzerland, (2000).

61. Zholobenko, V.L.; Kustov, L.M.; Borovkov, V.Yu.; Kazansky, V.B. A new type of acidic hydroxyl groups in ZSM-5 zeolite and in mordenite according to diffuse reflectance IR-spectroscopy. Zeolites 8 (1988): 175.
62. Datka, J.; Gil, B.; Baran, P. Heterogeneity of OH groups in HZSM-5 zeolites: splitting of OH and OD bands in low-temperature IR spectra. Micropor. Mesopor. Mater. 58 (2003): 291.



สถาบันวิทยบริการ
จุฬาลงกรณ์มหาวิทยาลัย



APPENDICES

สถาบันวิทยบริการ
จุฬาลงกรณ์มหาวิทยาลัย



Appendix A

สถาบันวิทยบริการ
จุฬาลงกรณ์มหาวิทยาลัย

Crystal structure of H-ZSM-5 zeolite

Table A-1 Unit cell of 72T cluster.

Number	SybylType	Xfrac	Yfrac	Zfrac	Number	SybylType	Xfrac	Yfrac	Zfrac
1	H	-0.1481	-0.462	-1.9695	123	O	-9.8199	-4.1576	1.5559
2	O	-0.5484	-0.0858	-1.1822	124	O	-9.0194	-1.5313	1.3427
3	Al	-0.21	1.6945	-1.128	125	O	-10.5226	0.7263	-3.1429
4	Si	-1.5059	-1.1777	-0.4885	126	O	-10.3335	-3.8596	-2.8184
5	O	1.6372	1.636	-1.0444	127	O	-8.9881	-1.5151	-3.0813
6	O	-0.7443	2.4647	-2.5679	128	O	-9.2032	0.1324	-0.8288
7	O	-0.7393	2.4633	0.3142	129	O	-7.5874	-3.3094	2.9804
8	O	-3.1276	-0.9746	-0.9872	130	H	-8.6994	-3.4998	-4.7841
9	O	-0.977	-2.7318	-1.0157	131	O	4.7747	-5.866	1.6045
10	O	-1.4538	-1.1744	1.2258	132	O	-0.0969	-10.2866	1.3332
11	Si	2.7388	2.6621	-0.4098	133	O	3.9223	-8.4001	1.1853
12	Si	-1.4441	3.3994	-3.8121	134	O	4.7342	-5.8208	-3.4092
13	Si	-1.3362	3.3862	1.6164	135	O	-0.0282	-10.1072	-3.1942
14	Si	-4.7828	-0.7525	-1.2016	136	O	3.869	-8.3479	-3.0401
15	Si	-1.0048	-4.4196	-1.1148	137	O	3.691	-6.6209	-0.9094
16	Si	-1.5252	-1.2142	2.9115	138	H	-1.6487	-9.2575	-5.0218
17	O	4.214	2.0794	-1.0553	139	O	-2.2791	-9.1432	0.1464
18	O	2.4813	4.2691	-0.8998	140	O	-2.1825	-9.104	2.848
19	O	2.8328	2.6167	1.2966	141	O	-2.3724	-8.8876	-2.5686
20	O	-0.945	2.6053	3.0777	142	H	-5.7921	7.4401	-4.6987
21	O	-0.56	0.0013	3.5956	143	O	-2.3283	10.0526	1.3486
22	O	-5.3616	0.115	0.1313	144	O	-3.6919	7.7316	1.497
23	O	-5.1968	0.0898	-2.6166	145	O	-2.2489	10.0099	-2.9389
24	O	-0.1276	-5.1369	0.1458	146	O	-3.7264	7.7706	-3.103
25	O	-0.3075	-4.9619	-2.5639	147	O	-2.2428	8.3062	-0.8012
26	H	-1.413	2.74	-5.0895	148	H	6.684	0.0761	-5.0782
27	O	-0.5829	4.9066	1.6598	149	O	7.3678	-1.4171	1.2116
28	O	-2.9964	3.6404	1.3919	150	O	8.9387	0.7738	1.0028
29	O	-0.6077	4.8881	-3.9453	151	O	7.3598	-1.5497	-3.169
30	O	-3.0446	3.7481	-3.3283	152	O	8.7397	0.7376	-3.5573
31	O	-5.5816	-2.2425	-1.2537	153	O	-4.03	-7.2314	3.5468
32	O	-2.5959	-4.974	-0.9235	154	O	-5.2885	-4.7018	3.6205
33	O	-3.0979	-0.9336	3.4891	155	H	-6.9448	-3.859	5.4286
34	O	-1.0578	-2.738	3.4867	156	Si	-6.796	8.6674	-0.7832
35	Si	-0.0484	1.5534	4.0736	157	Si	7.6559	4.7755	3.7687
36	Si	5.868	1.8389	-1.2741	158	Si	5.4929	7.1963	2.7453
37	Si	2.1852	5.9272	-1.0993	159	Si	-3.4797	-8.8053	3.9265
38	Si	2.9065	2.6792	2.987	160	Si	-11.1382	-5.1584	1.1502
39	Si	0.1678	6.3853	-3.75	161	Si	-12.1578	0.8844	-3.6002
40	Si	0.2452	6.3768	1.5976	162	Si	-11.7984	-4.2565	-2.0589
41	Si	-6.0065	0.9946	1.4263	163	Si	5.8806	-5.0703	2.6309
42	Si	-6.0931	1.1561	-3.5988	164	Si	1.0821	-11.3766	0.7795
43	Si	-4.6521	-0.5805	4.0767	165	Si	4.0749	-10.0292	1.6639

Table A-1 (cont.)

Number	SybylType	Xfrac	Yfrac	Zfrac	Number	SybylType	Xfrac	Yfrac	Zfrac
44	Si	-6.5037	-3.6535	-1.1297	166	Si	5.986	-5.19	-4.3813
45	Si	0.4215	-6.0507	1.4581	167	Si	1.0638	-11.2754	-2.6204
46	Si	0.4818	-5.9258	-3.7172	168	Si	4.0882	-9.9868	-3.4548
47	Si	-4.547	3.9127	0.7728	169	Si	-2.848	11.5874	-3.1974
48	Si	-4.5624	3.9743	-2.6122	170	Si	-2.951	11.61	1.6668
49	Si	-4.0198	-5.7159	-0.3828	171	Si	9.621	4.6006	-3.9472
50	Si	-1.0054	-4.3708	3.9511	172	Si	9.7494	4.6359	1.1173
51	H	-0.2531	1.754	5.4801	173	Si	10.3528	1.4434	0.3649
52	O	6.659	3.3357	-1.3516	174	Si	7.8291	-2.991	0.7978
53	O	3.686	6.7167	-1.0387	175	Si	10.1945	1.4216	-3.0172
54	O	1.5799	1.8612	3.6547	176	Si	7.877	-3.0456	-2.5682
55	O	4.3959	2.0768	3.526	177	H	-8.2283	8.7777	-0.7566
56	O	2.7965	4.2773	3.5492	178	O	-6.0781	10.2183	-0.7891
57	O	1.3664	6.2266	-2.5481	179	O	-4.2439	11.8158	0.5612
58	O	1.2231	6.3906	0.2119	180	O	-4.1851	11.7686	-2.1398
59	O	1.2861	6.4436	2.9384	181	H	8.2527	5.1273	5.0297
60	O	6.451	0.9636	0.0497	182	O	6.6018	6.0019	3.241
61	O	6.2077	0.9313	-2.6713	183	H	5.8926	8.4836	3.248
62	O	-7.693	0.8184	1.3404	184	O	8.8533	4.6494	2.5653
63	O	-7.7071	0.8756	-3.1062	185	H	-4.5447	-9.7635	3.7249
64	O	-5.4349	0.3376	2.8799	186	O	-13.0186	-0.192	-2.5836
65	O	-7.4777	-3.5276	0.2487	187	O	-12.704	-2.8307	-1.8358
66	O	-7.5705	-3.7312	-2.45	188	O	-11.5177	-4.8529	-0.4906
67	H	-5.945	0.916	-5.0063	189	H	-10.7846	-6.5532	1.3024
68	O	-5.5097	2.6028	1.2537	190	H	-12.5286	-5.2179	-2.8382
69	O	-5.5426	2.7058	-3.174	191	H	-12.3489	0.5136	-4.9855
70	O	2.0794	-6.3348	1.2874	192	H	-12.6236	2.2343	-3.3699
71	O	-0.3756	-7.5494	1.4489	193	O	2.6143	-10.8242	1.2691
72	O	2.0537	-6.255	-3.1512	194	O	2.6235	-10.7903	-3.0957
73	O	-0.3388	-7.4153	-3.8023	195	O	1.0373	-11.3593	-0.9227
74	H	0.5197	-5.282	-5.0003	196	H	5.176	-4.2525	3.5921
75	O	0.0082	-5.2313	2.8829	197	H	6.7055	-6.0444	3.313
76	H	0.7475	6.8365	-4.9846	198	H	6.7802	-6.2608	-4.9437
77	O	-0.9042	7.6179	1.4905	199	H	4.2875	-10.1112	3.0935
78	O	-5.1046	5.4064	1.3485	200	H	5.1726	-10.6565	0.9609
79	O	-0.9811	7.5024	-3.1681	201	H	5.1702	-10.5686	-2.6916
80	O	-5.1593	5.4826	-3.1085	202	H	0.8547	-12.7017	1.2867
81	O	-4.5126	3.9611	-0.9214	203	H	0.7551	-12.5648	-3.179
82	O	-3.9577	-7.3349	-0.8837	204	H	5.4112	-4.3866	-5.4396
83	O	-5.3995	-4.9266	-0.9647	205	H	4.3574	-10.1051	-4.8726
84	O	-5.5129	-2.0418	4.2573	206	O	6.868	-4.0973	1.6347
85	O	-2.5602	-4.9802	3.6185	207	O	6.9692	-4.217	-3.3818
86	O	-4.031	-5.6341	1.3143	208	H	-3.2988	11.7575	-4.5624
87	H	-0.5969	-4.5332	5.3162	209	H	-1.9316	12.6117	1.4421
88	H	-4.6081	0.1086	5.3367	210	H	-1.827	12.5653	-2.8883
89	Si	2.5834	5.9254	3.912	211	H	9.092	4.6374	-5.2931
90	Si	6.011	1.8038	3.9749	212	O	10.3734	3.0737	0.8351

Table A-1 (cont.)

Number	SybylType	Xfrac	Yfrac	Zfrac	Number	SybylType	Xfrac	Yfrac	Zfrac
91	Si	7.475	4.8177	-1.3785	213	O	11.6801	0.5586	0.9295
92	Si	5.2518	7.2439	-0.6495	214	O	9.4267	-3.2673	1.2964
93	Si	-3.3355	-8.893	-1.1623	215	O	10.1836	3.0305	-3.5556
94	Si	-9.1652	0.1019	0.8762	216	O	11.4543	0.5336	-3.7183
95	Si	-8.476	-3.1237	1.5514	217	O	9.5096	-3.2902	-2.9578
96	Si	-9.0812	0.0839	-2.5163	218	O	10.3133	1.376	-1.3315
97	Si	-8.8776	-3.1822	-3.396	219	O	7.7368	-3.132	-0.887
98	Si	-6.3751	-3.5045	4.1586	220	H	10.7967	5.6168	1.1561
99	Si	3.6245	-6.7833	0.7744	221	H	10.6998	5.5543	-3.8097
100	Si	-1.2118	-9.017	1.4578	222	H	-3.0033	-8.8759	5.2909
101	Si	3.5718	-6.741	-2.5897	223	Si	-5.249	11.7011	-0.8105
102	Si	-1.1277	-8.9189	-3.7249	224	Si	-13.4805	-1.365	-1.4287
103	Si	-5.2851	7.1529	-3.3868	225	Si	12.4195	-0.6602	-4.4627
104	Si	-2.2676	8.419	0.8898	226	Si	11.1578	-3.5976	-3.2681
105	Si	-5.2348	7.0553	1.7366	227	Si	12.7667	-0.6204	1.5115
106	Si	-2.2634	8.3675	-2.4924	228	Si	10.994	-3.5143	1.9187
107	Si	7.1976	0.0461	-3.7392	229	H	-6.1817	12.7942	-0.8515
108	Si	7.3476	0.2724	1.3068	230	H	-14.9142	-1.5472	-1.5159
109	Si	-4.0068	-5.6181	3.0062	231	H	-13.1042	-0.937	-0.0991
110	O	-6.224	7.8387	0.5874	232	H	12.2982	-0.5792	-5.9026
111	O	-6.2656	7.8762	-2.1921	233	H	11.2885	-4.6626	-4.2398
112	H	2.342	6.1727	5.3054	234	O	11.9112	-2.0865	1.7095
113	H	6.1097	1.1952	5.271	235	O	11.8466	-2.1802	-3.9318
114	O	6.3831	6.094	-1.1997	236	H	13.8394	-0.8163	0.5611
115	O	6.8231	3.3021	3.9331	237	H	13.2982	-0.2074	2.7927
116	O	4.0015	6.7233	3.4063	238	H	11.6426	-4.5993	1.2151
117	O	5.3942	7.2609	1.0488	239	H	10.9212	-3.8105	3.3343
118	H	5.5227	8.5373	-1.2113	240	H	13.8004	-0.4999	-4.0632
119	O	8.6276	4.8868	-0.1363	241	H	11.8486	-3.9392	-2.0444
120	O	8.3735	4.9101	-2.8188	242	H	-5.7437	7.2506	3.0641
121	O	6.7429	0.8351	2.7813	243	H	-3.4573	11.71	3.0187
122	H	-4.3677	-9.8841	-1.2687	244	H	-12.2798	-4.8411	1.9815
					245	H	-10.3058	0.7462	1.4583

Table A-2 Dipole moment of all reactants and all products.

Reactant	Dipole moment (Debye)	Product	Dipole moment (Debye)
acetaldehyde (C ₂ H ₄ O)	2.72	hydroxyethylene (C ₂ H ₄ O)	1.97
acetone (C ₃ H ₆ O)	2.69	2-hydroxypropylene (C ₃ H ₆ O)	2.34
butanone (C ₄ H ₈ O)	2.75	2-hydroxybutene (C ₄ H ₈ O)	2.13
2-pentanone (C ₅ H ₁₀ O)	2.80	2-hydroxypentene (C ₅ H ₁₀ O)	2.30
3-methyl-2-butanone (C ₅ H ₁₀ O)	2.65	2-hydroxy-3-methylbutene (C ₅ H ₁₀ O)	2.38
acetophenone (C ₈ H ₈ O)	3.12	2-hydroxyphenylethylene (C ₈ H ₈ O)	2.01

ONIOM(B3LYP/6-31G(d):MND0) Calculations

Table A-3 Computed stretching vibrational frequencies of hydroxyl groups at O2 and O3 atoms and selected geometry parameters (bond distances and bond angles) on 50/3T (model 5) and 72/3T (model 6) cluster models of H-ZSM-5.

System/parameter ^a	Vibrational frequencies at reaction states ^b				
	HZ	INT1	TS	INT2	ZH
<i>ACD system</i>					
ω (O2-H3) ^c	3601.9(3664.2)	3177.7(3195.0)	Not converted	-	-
ω (O3-H1) ^c	-	-	-	3154.6(3130.9)	3700.9(3653.2)
r (C1-C2) ^d	-	1.493(1.490)	-	1.350(1.352)	-
r (C1-O1) ^d	-	1.220(1.220)	-	1.330(1.330)	-
r (C2-H1) ^d	-	-	-	1.990(1.980)	-
r (O1-H3) ^d	-	1.680(1.680)	-	0.990(0.990)	-
r (O2-H3) ^d	0.982(0.978)	1.000(1.000)	-	1.710(1.720)	-
r (O3-H1) ^d	-	2.220(2.310)	-	1.000(1.000)	0.976(0.978)
r (Al1-O2) ^d	1.940(1.954)	1.910(1.920)	-	1.770(1.770)	1.740(1.753)
r (Al1-O3) ^d	1.750(1.740)	1.750(1.740)	-	1.900(1.920)	1.920(1.940)
α (Si1-O2-Al1) ^e	136.140(136.690)	135.940(135.040)	-	135.144(138.510)	135.833(140.910)
α (Si2-O3-Al1) ^e	126.690(141.050)	127.750(141.640)	-	128.910(133.940)	130.010(137.330)

^a Atomic numbering are shown in Figure 3.1.

^b For 72/3T and 50/3T cluster models (in parenthesis) of H-ZSM-5.

^c Vibrational frequencies, in cm^{-1} .

^d Bond distance, in Å.

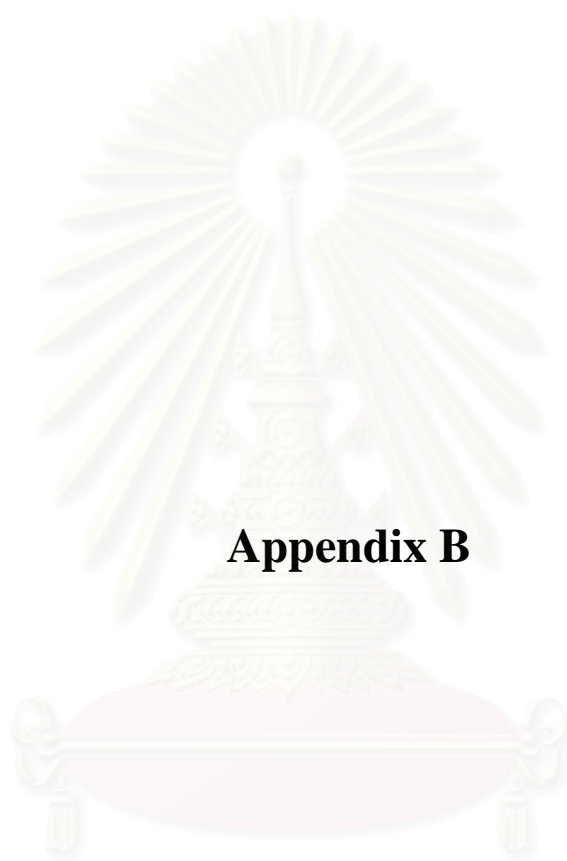
^e Angle, in degree.

Table A-4 Relative energies and thermodynamic quantities of related species of various systems.

System/energy ^a	ΔE^{298} , ^b	ΔH^{298} , ^b	ΔG^{298} , ^b	ΔS^{298} , ^c	log K
<i>ACD system</i>					
ACD + HZ	0.00(0.00)	0.00(0.00)	0.00(0.00)	0.00(0.00)	
INT1_M6(M5)	-8.02 (-8.17)	-7.81 (-7.90)	2.89 (1.79)	-35.88 (-32.52)	
TS_M6(M5)		Not converted			
INT2_M6(M5)	0.50 (3.59)	0.30 (3.25)	12.75 (16.41)	-41.79 (-44.13)	
HETH + ZH	15.79 (17.75)	15.87 (17.75)	15.80 (17.85)	0.21 (-0.35)	No Value

^a For 72/3T (model 6) and 50/3T (model 5) cluster models (in parenthesis) of H-ZSM-5.

^b In kcal/mol. ^c In cal/mol K.



Appendix B

สถาบันวิทยบริการ
จุฬาลงกรณ์มหาวิทยาลัย

The electrostatic potential represented over an electronic isodensity surface of $\rho = 0.01 \text{ e}\text{\AA}^{-3}$, computed by MOLEKEL 4.3 software are shown.

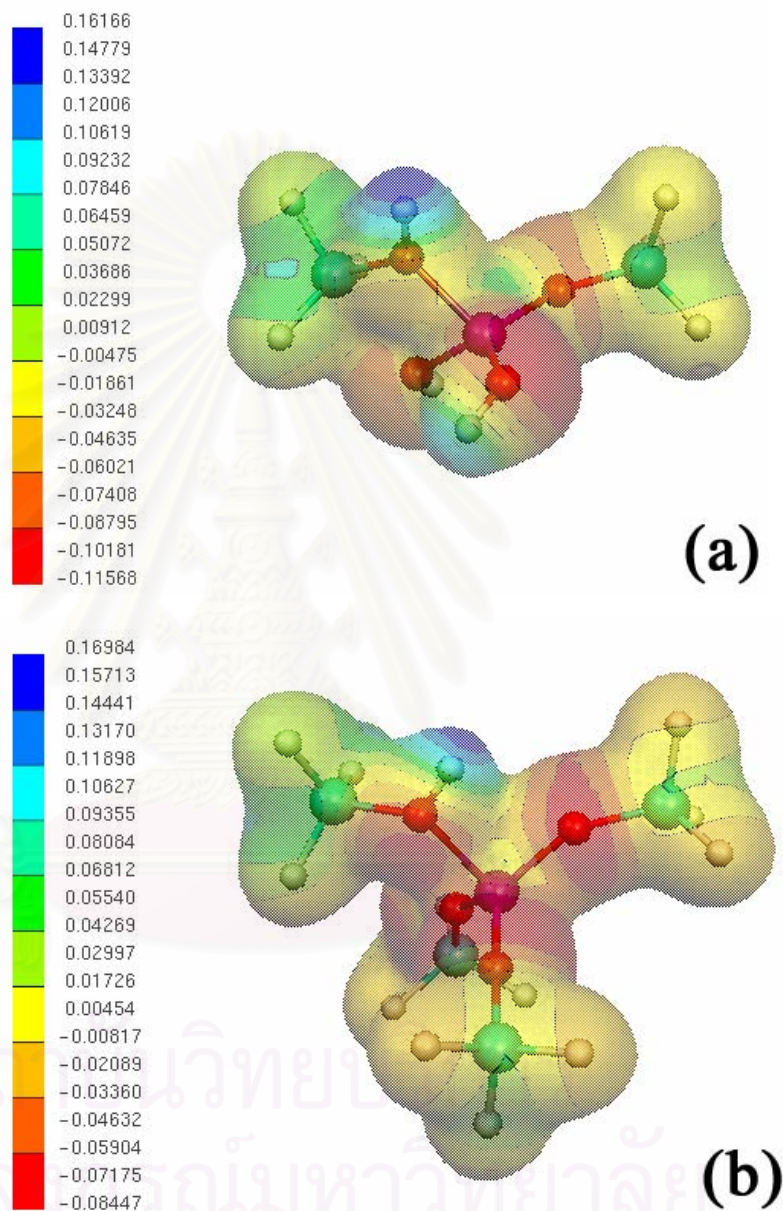


Figure B-1 Front views of the molecular electrostatic potential (in au) presented over electronic isodensity ρ (in $\text{e}\text{\AA}^{-3}$) surfaces of volume V_s (in \AA^{-3}). All figures correspond to the cutoff value of $\rho = 0.01 \text{ e}\text{\AA}^{-3}$, (a) 3T, $V_s = 88.05$, $\phi_{<} = -0.11568$ and $\phi_{>} = 0.16166$; (b) 5T, $V_s = 126.92$, $\phi_{<} = -0.08447$ and $\phi_{>} = 0.16984$. The surface map color legend within the grid value, $\phi_{<} < \phi_{>}$, of the molecular species are shown at the left side of their structures.

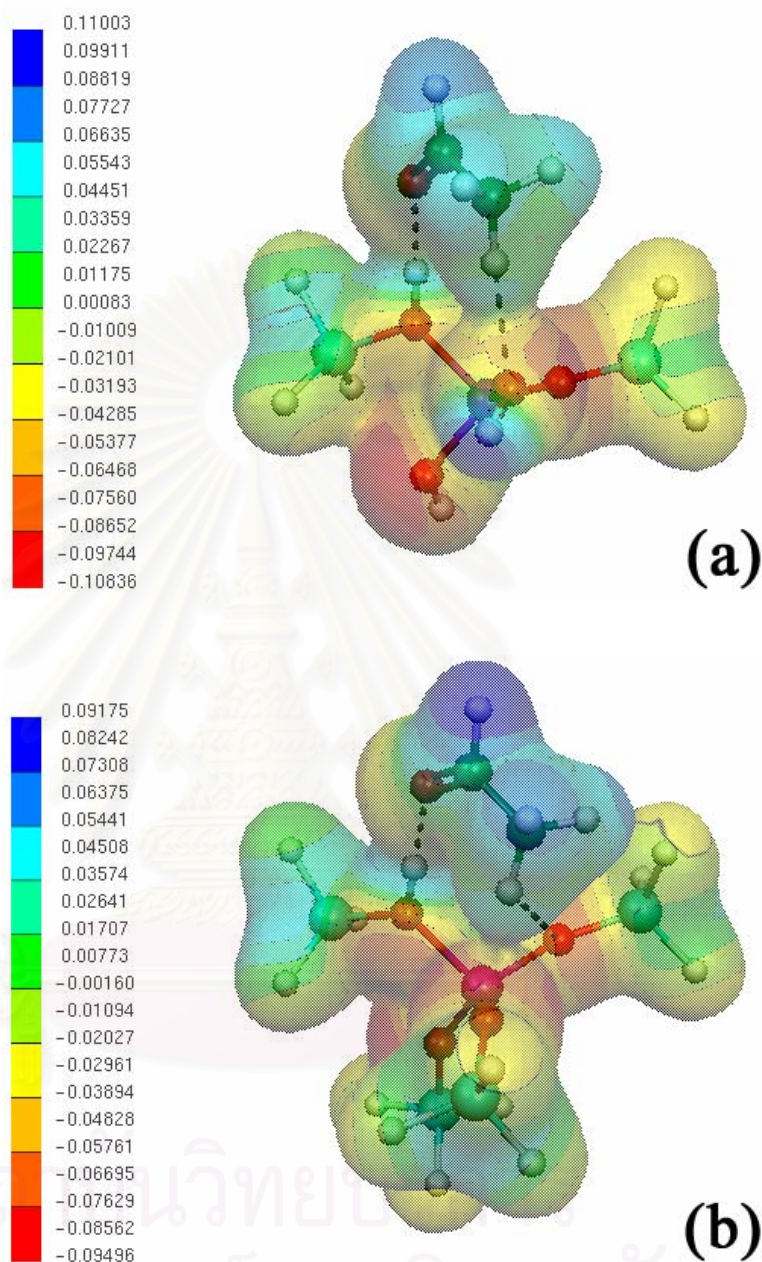


Figure B-2 Front views of the molecular electrostatic potential (in au) presented over electronic isodensity ρ (in $\text{e}\text{\AA}^{-3}$) surfaces of volume V_s (in \AA^{-3}). All figures correspond to the cutoff value of $\rho = 0.01 \text{ e}\text{\AA}^{-3}$, (a) 3T-acetaldehyde, $V_s = 118.91$, $\phi_{<} = -0.10836$ and $\phi_{>} = 0.11003$; (b) 5T-acetaldehyde, $V_s = 157.08$, $\phi_{<} = -0.09495$ and $\phi_{>} = 0.09175$. The surface map color legend within the grid value, $\phi_{<}$ to $\phi_{>}$, of the molecular species are shown at the left side of their structures.

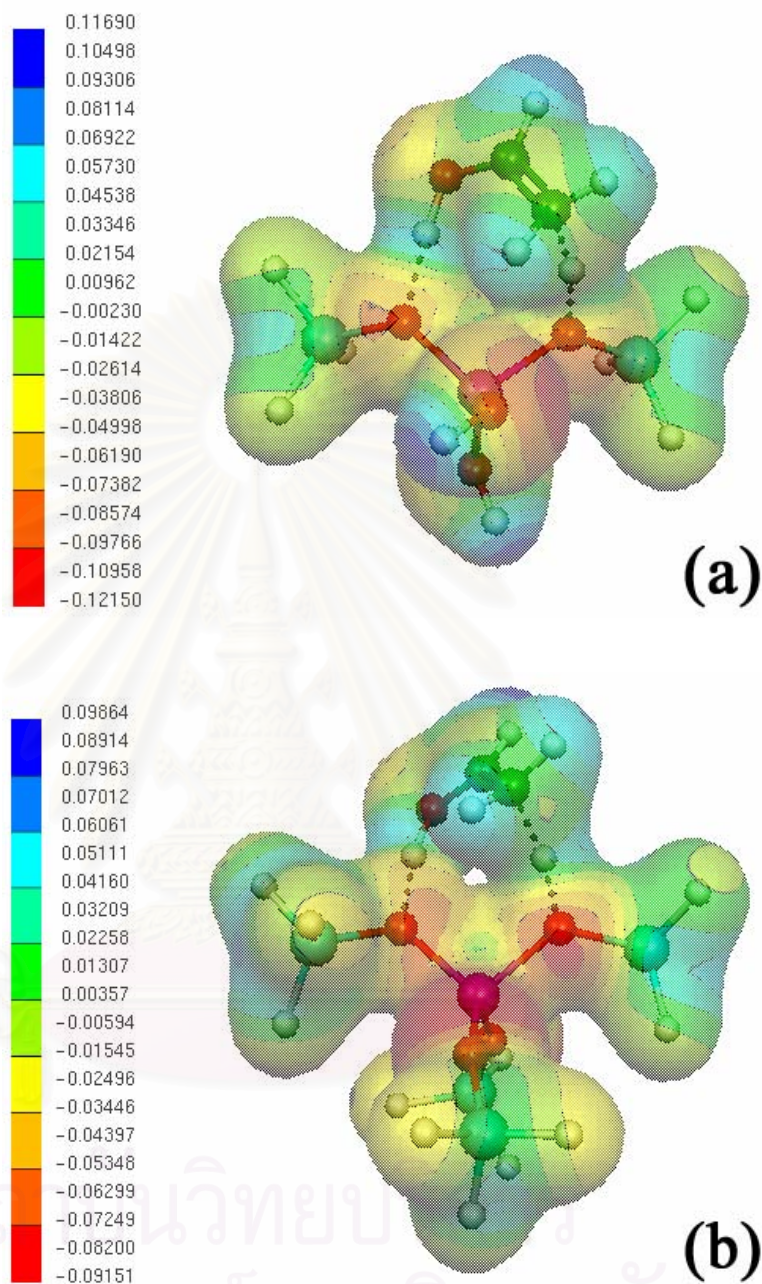


Figure B-3 Front views of the molecular electrostatic potential (in au) presented over electronic isodensity ρ (in $\text{e}\text{\AA}^{-3}$) surfaces of volume V_s (in \AA^{-3}). All figures correspond to the cutoff value of $\rho = 0.01 \text{ e}\text{\AA}^{-3}$, (a) 3T-TS, $V_s = 118.34$, $\phi_{<} = -0.12149$ and $\phi_{>} = 0.11690$; (b) 5T-TS, $V_s = 156.93$, $\phi_{<} = -0.09150$ and $\phi_{>} = 0.09864$. The surface map color legend within the grid value, $\phi_{<}$ to $\phi_{>}$, of the molecular species are shown at the left side of their structures.

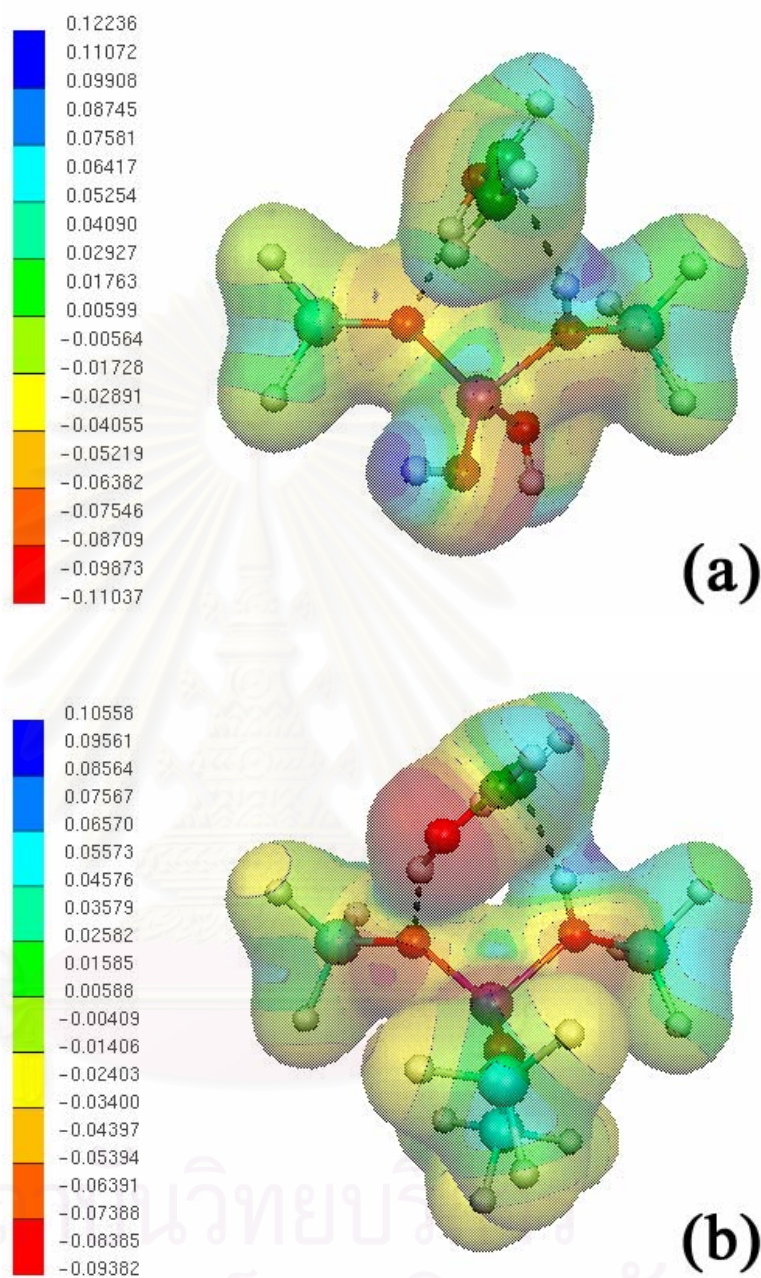
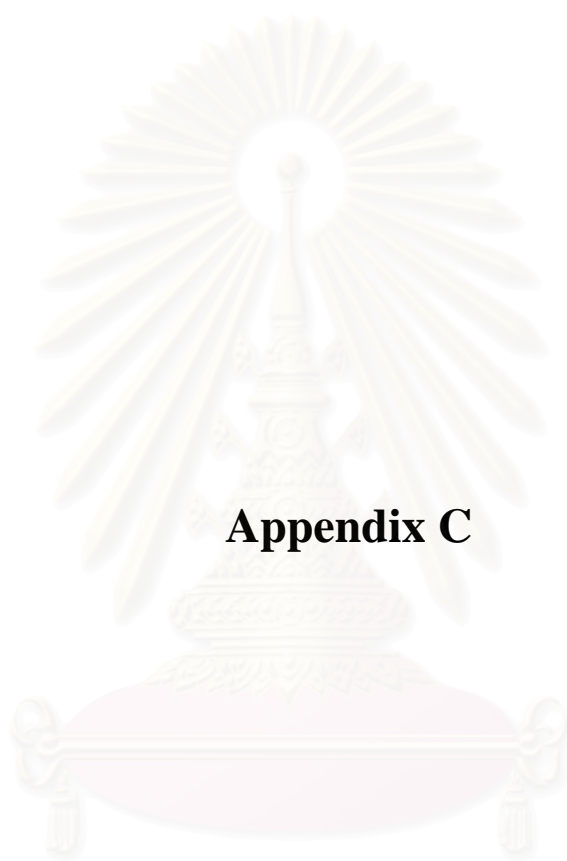
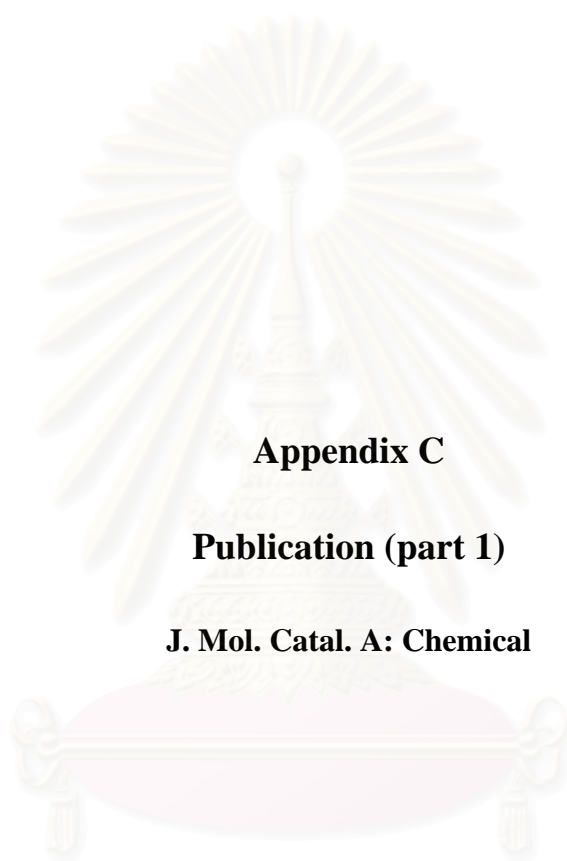


Figure B-4 Front views of the molecular electrostatic potential (in au) presented over electronic isodensity ρ (in $\text{e}\text{\AA}^{-3}$) surfaces of volume V_s (in \AA^{-3}). All figures correspond to the cutoff value of $\rho = 0.01 \text{ e}\text{\AA}^{-3}$, (a) 3T-hydroxyethylene, $V_s = 119.24$, $\phi_{<} = -0.11036$ and $\phi_{>} = 0.12235$; (b) 5T-hydroxyethylene, $V_s = 157.43$, $\phi_{<} = -0.09382$ and $\phi_{>} = 0.10558$. The surface map color legend within the grid value, $\phi_{<}$ to $\phi_{>}$, of the molecular species are shown at the left side of their structures.



Appendix C

สถาบันวิทยบริการ
จุฬาลงกรณ์มหาวิทยาลัย



Appendix C

Publication (part 1)

J. Mol. Catal. A: Chemical

สถาบันวิทยบริการ
จุฬาลงกรณ์มหาวิทยาลัย

Theoretical study of conversion reactions of ketone to hydroxyalkylene in cluster models of zeolite H-ZSM-5

Attasak Rattanasumrit, Vithaya Ruangpornvisuti*

*Supramolecular Chemistry Research Unit, Department of Chemistry, Faculty of Science,
Chulalongkorn University, Bangkok 10330, Thailand*

Received 9 March 2005; received in revised form 13 June 2005; accepted 13 June 2005
Available online 18 July 2005

Abstract

Conversions of acetaldehyde to hydroxyethylene, acetone to 2-hydroxypropylene, butanone to 2-hydroxybutene and 2-pentanone to 2-hydroxypentene catalyzed by H-ZSM-5 have been theoretically studied using quantum chemical methods. Geometry optimizations of the local structures of species reacting with H-ZSM-5 zeolite using 3T-DFT and 5T-DFT cluster models computed at B3LYP/6-31G(d) level and 50/3T-ONIOM2 cluster model computed at ONIOM(B3LYP/6-31G(d):AM1) level have been carried out. Three steps of the reaction mechanism were found and thermodynamic properties of each reaction steps and equilibrium constants of overall reaction have been obtained. The overall reaction of the conversion for all systems is endothermic reaction. The activation energies of all conversion reactions derived at three different methods are reported.

© 2005 Elsevier B.V. All rights reserved.

Keywords: Ketone; Hydroxyalkylene; ZSM-5 zeolite; Cluster; DFT; ONIOM

1. Introduction

The few last decade up to present, zeolites have played very important role in the petroleum and petrochemical industries. They have been known as the one of the most important heterogeneous catalysts [1–4]. Therefore, zeolites were widely studied for their acidic properties of Brønsted acid sites [5,6] using several techniques [7–21]. The hydrogen-bonded complexes due to the interaction between waters and Brønsted acids of zeolites were studied [20–22]. ZSM-5 (Zeolite SOCONY Mobile-5) is one of the most useful catalysts that have been widely used in the petroleum and petrochemical industries. H-ZSM-5 was widely used in the conversion of light alkanes to aromatics with low selectivity because of cracking side reactions [23–29]. The catalysts of exchanged cations on H-ZSM-5 were used in many reactions. The Zn/H-ZSM-5 was used to increase propane conversion turnover rates, hydrogen formation rates, and

selectivity to aromatics [30]. The methane reactions in Mo/H-ZSM5 were investigated [31] and the Co/H-ZSM-5 was used for propane conversion to propene and to C6–C8 aromatics for dehydrogenation and dehydrocyclization of alkanes [32]. The siting and coordination of Cu⁺ ions in zeolite ZSM-5 have been studied by a combined quantum mechanics and interatomic potential function technique [33]. The reaction pathways and the energetics for the direct methane-methanol and benzene-phenol conversions that occur on the surface of Fe-ZSM-5 zeolite were analyzed using density functional theory (DFT) computations [34]. The coordination of divalent metal cations to ZSM-5 has been investigated using gradient-corrected DFT method. Coordination at both isolated charge-exchange sites and pairs of charge-exchange sites was considered for many divalent transition metal cations [35].

Protolytic cracking of ethane in ZSM-5 zeolites has been investigated using quantum-chemical techniques and a cluster model of the zeolite acid site. An aluminosilicate cluster model containing five tetrahedral atoms was used to locate all of the stationary points along a reaction

* Corresponding author. Tel.: +66 2218 7644; fax: +66 2254 1309.
E-mail address: vithaya.r@chula.ac.th (V. Ruangpornvisuti).

path for ethane cracking at the HF/6-31G(d), B3LYP/6-31G(d), and MP2(FC)/6-31G(d) levels of theory [36]. A theoretical study of the cracking reaction of thiophene by small zeolitic cluster catalysts has been reported and it has been shown that the cracking of thiophene was catalyzed by Lewis basic oxygen atoms [37]. The isomerization and transalkylation reactions of aromatic species catalyzed by acidic zeolite were theoretically studied using the cluster DFT calculations. All different reported mechanisms of isomerization and transalkylation have been investigated and analyzed [38]. The structures and electronic properties of the Brønsted acid site in B, Al or Ga isomorphously substituted ZSM-5 zeolites were studied by ab initio Hartree-Fock (HF) and DFT methods [39]. The interactions of methane with Brønsted acid sites in H-ZSM-5 were investigated both experimentally and theoretically [40]. The dehydrogenation and cracking reactions of isobutane over zeolite H-ZSM-5 represented by double-ring 20T cluster were studied at the DFT/B3LYP level of theory [41]. The propene, 1-hexene, and 3-hexene protonation over representative H-ZSM-5 clusters to give covalent alkoxide intermediates were theoretically studied using DFT method [42]. The vibrational frequencies, structural, energetic, and spectroscopic properties of the acid sites of zeolite ZSM-5 were studied [43,44] using three-layered ONIOM(B3LYP/6-311+G(d, p):HF/3-21G(d):MNDO) method. To rationalize and get more understanding on the experiments of conversion reaction of aldehyde to unsaturated alcohols, the aim of this work is therefore to theoretically study the reaction mechanisms of the conversion reactions of acetaldehyde to hydroxyethylene, acetone to 2-hydroxypropylene, butanone to 2-hydroxybutene and 2-pentanone to 2-hydroxypentene catalyzed by H-ZSM-5 using various cluster models. These conversion reactions have been theoretically investigated employing the calculations at B3LYP/6-31G(d) level of theory for 3T, 5T cluster models and ONIOM(B3LYP/6-31G(d):AM1) level of theory for 50T cluster model. The energetics and thermodynamic quantities of these catalytic reactions of all models have been determined and compared with non-catalytic and water-catalyzed models.

2. Computational details

2.1. Zeolite cluster models

Three sizes of the H-ZSM-5 clusters 3T, 5T and 50T are modeled as the molecular catalyst interacting with the adsorbent. These H-ZSM-5 cluster models were employed in the computation of the interaction between the modeled structure and interacting species. The 3T and 5T, respectively defined as the structures $\text{H}_3\text{Si}(\text{OH})\text{Al}(\text{OH})_2(\text{O})\text{SiH}_3$ and $\text{H}_3\text{Si}(\text{OH})\text{Al}(\text{O SiH}_3)_2(\text{O})\text{SiH}_3$ are shown in Fig. S1 (Supplementary data). The 50T cluster consisting of forty-nine silicon and one aluminum tetrahedral (Si/Al = 49) shown in Fig. S2 (Supplementary data) is modeled with the integrated

molecular orbital + molecular orbital (IMOMO) method [45] which is implemented as the two-layered ONIOM(MO:MO) methodology [46]. The geometries of these clusters were prepared from the ZSM-5 crystal lattice structure reported in the literature [47]. The 50T cluster employed with the two-layered ONIOM calculation is finally called as the 50/3T-ONIOM2 model.

2.2. Methods of calculation

Full geometry optimizations of the configuration of species interacting with the 3T and 5T clusters were carried out for all stationary points using DFT method. The DFT calculations have been performed with the Becke's three parameters hybrid density functional using the Lee, Yang and Parr correlation functional (B3LYP) [48–50]. Geometry optimizations of the 50T cluster model have been carried out using the hybrid ONIOM methodology [51,52], known as the 50/3T-ONIOM2 calculation model. The ONIOM2(MO:MO) approach employed for the 50T cluster subdivides the real system in two different layers, each one being described at a high and low levels of theory. The active site of H-ZSM-5 zeolite and reacting compounds called as the model system is described at the highest level of theory whereas the rest of the zeolite is computed at a lower level. The real and model systems of H-ZSM-5 zeolite and reacting compounds used for the two-layered ONIOM(MO:MO) calculations are shown in Fig. S2 (Supplementary data). The energies computed at the B3LYP/6-31G(d) for 3T (3T-DFT) and 5T (5T-DFT) cluster models and the ONIOM2(B3LYP/6-31G(d):AM1) [53,54] for 50/3T model have been carried out with the zero-point vibration energy corrections.

The transition-state structures of 3T-DFT and 5T-DFT cluster models optimized at B3LYP/6-31G(d) level of theory have been located using the reaction coordinate method referred to the synchronous transit-guided quasi-newton (STQN) calculation [55]. The transition states were confirmed by one imaginary frequency. The intrinsic reaction coordinate (IRC) method [56] was used to track minimum energy paths from transition structures to the corresponding minimum. For 50/3T-ONIOM2 calculation model, the transition structures of all related species have been located using the B3LYP/6-31G(d)-optimized transition structure of the 3T cluster model as an initial geometry of the computation. The reaction energy ΔE^{298} , standard enthalpy ΔH^{298} and Gibbs free energy changes ΔG^{298} of all reactions have been derived from the frequency calculations at B3LYP/6-31G(d) level of theory. The reaction entropies ΔS^{298} of all reactions were derived from individual value of entropy of related species obtained at the same level of theory. All computations were performed using the GAUSSIAN 03 program package [57]. The MOLDEN 3.7 program [58] was utilized to observe molecular energies and geometries convergence via the Gaussian output files. The molecular graphics of all species were generated with the MOLEKEL program [59].

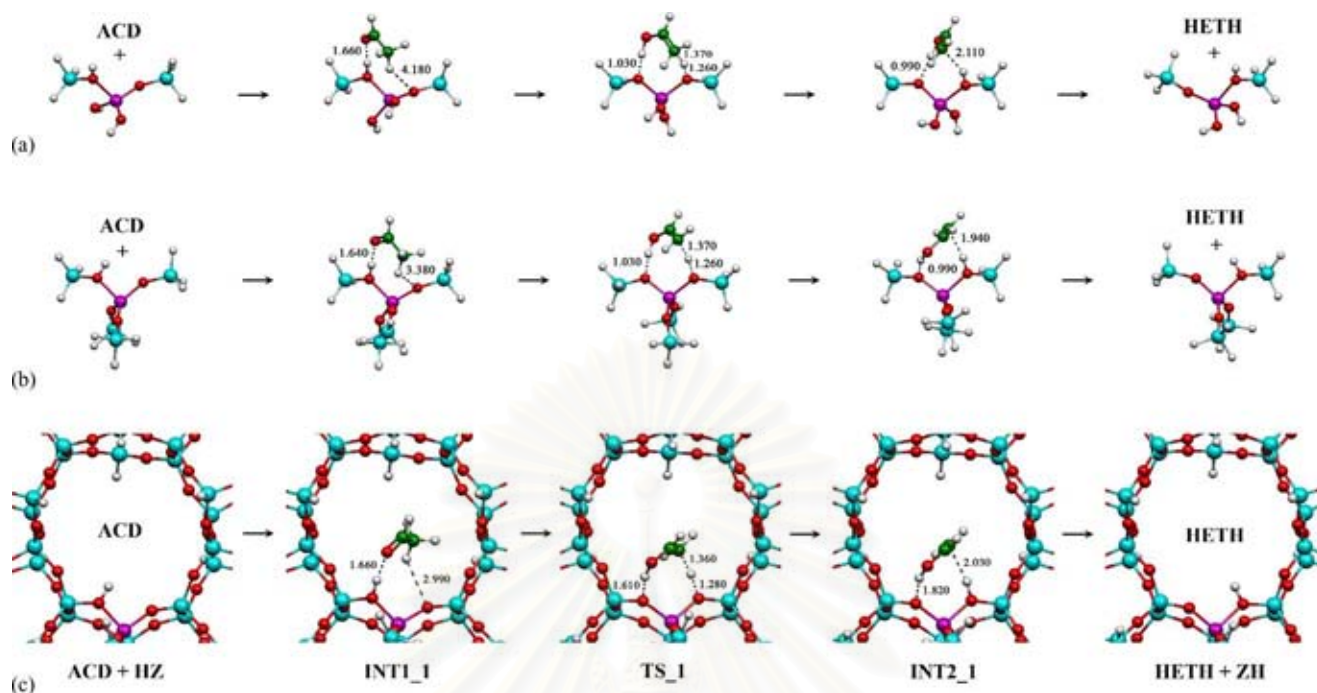


Fig. 1. Reaction steps for acetaldehyde conversion on (a) 3T-DFT, (b) 5T-DFT and (c) 50/3T ONIOM2 cluster models.

3. Results and discussion

Conversion reactions of acetaldehyde (ACD) to hydroxyethylene (HETH), acetone (ACT) to 2-hydroxypropylene (HPRO), butanone (BTN) to 2-hydroxybutene (HBUT) and 2-pentanone (PTN) to 2-hydroxypentene (HPEN) were investigated on the 3T, 5T and 50T clusters of H-ZSM-5 catalyst compared to non-catalytic and water-catalyzed models. The systems of conversion reactions according to the reactants acetaldehyde, acetone, butanone and 2-pentanone are also designated as ACD, ACT, BTN and PTN systems, respectively. Relative energies and thermodynamic properties of all systems and models were computed from the frequency calculations at the B3LYP/6-31G(d) level of theory.

3.1. Geometrical structures, energetics and thermodynamic quantities

The geometrical structures of reactants acetaldehyde, acetone, butanone and 2-pentanone were optimized at B3LYP/6-31G(d) level of theory. Geometrical data for these reactants, their corresponding transition-state structures and products of non-catalytic (gas phase) and water-catalyzed models are listed in Table S1 and S2 (Supplementary data), respectively; their atomic numbering are shown in Fig. S1. The geometrical structures of the involved species of the systems acetaldehyde (ACD), acetone (ACT), butanone (BTN) and 2-pentanone (PTN) employing the 3T-DFT and 5T-DFT calculation models are shown in Figs. 1a–b, 2a–b, 3a–b and 4a–b, respectively.

The computed stretching vibrational frequencies of hydroxyl groups at the reaction-involved oxygen atoms (O_2 and O_3) and the selected geometry parameters (bond distance and bond angle) on the 3T and 5T clusters of H-ZSM-5 zeolite are tabulated in Table S3. Table S3 shows that the computed OH stretching vibrational frequencies of H-ZSM-5 at atoms O_2 (3734.9 cm^{-1}) and O_3 (3735.7 cm^{-1}) are almost the same positions. The computed stretching vibrational frequencies of hydroxyl groups at atoms O_2 for reactant-side intermediate and O_3 for product-side intermediate for all systems are hardly ever different but smaller than their corresponding isolated-H-ZSM-5 OH vibrational frequencies by approximate 700 cm^{-1} . Relative energies and thermodynamic quantities of related species of systems acetaldehyde, acetone, butanone and 2-pentanone for 3T and 5T cluster model are listed in Table 1. The order of the reaction energies for all models is in decreasing order: systems $PTN > ACT > BTN > ACD$. The conversion constants of the reaction systems ACD, ACT, BTN and PTN of the 5T and 3T (in parentheses) cluster models are $\log K = -13.35$ (-14.72), -14.46 (-16.33), -14.65 (-17.35) and -14.70 (-16.42), respectively.

The computed stretching vibrational frequencies of hydroxyl groups at the reaction-involved oxygen atoms (O_2 and O_3) and selected geometry parameters (bond distances and bond angles) on 50T cluster of H-ZSM-5 are tabulated in Table S4. It shows that the computed OH stretching vibrational frequencies of H-ZSM-5 at atoms O_2 (3752.4 cm^{-1}) and O_3 (3750.5 cm^{-1}) are almost the same positions. The computed stretching vibrational frequencies of hydroxyl groups at atoms O_2 for reactant-side interme-

Table 1
Relative energies and thermodynamic quantities of related species of various systems on 3T and 5T cluster models

System/energy ^a	$\Delta E^{\ddagger b}$	ΔE^{298c}	ΔH^{298c}	ΔG^{298c}	ΔS^{298d}	log K
ACD system						
ACD + HZ	–	0.00(0.00)	0.00(0.00)	0.00(0.00)	0.00(0.00)	
INT1_1	–	–14.52(–14.76)	–14.92(–15.02)	–1.87(–3.75)	–43.79(–37.81)	
TS_1	18.33(20.39)	3.81(5.63)	2.70(4.82)	19.16(18.92)	–55.20(–47.29)	
INT2_1	–	1.92(2.90)	1.37(2.09)	16.35(16.34)	–50.23(–47.79)	
HETH + ZH	–	17.75(17.21)	17.76(17.15)	18.63(17.20)	–2.95(–0.18)	–13.35 (–14.72)
ACT system						
ACT + HZ	–	0.00(0.00)	0.00(0.00)	0.00(0.00)	0.00(0.00)	
INT1_2	–	–17.90(–17.94)	–16.90(–16.74)	–6.26(–9.02)	–35.68(–25.91)	
TS_2	18.56(20.79)	0.66(2.85)	0.72(3.17)	14.40(15.01)	–45.91(–39.72)	
INT2_2	–	0.37(1.91)	0.79(2.61)	13.48(13.27)	–42.56(–35.74)	
HPRO + ZH	–	20.08(19.53)	20.52(19.91)	20.48(19.05)	0.13(2.90)	–14.46 (–16.33)
BTN system						
BTN + HZ	–	0.00(0.00)	0.00(0.00)	0.00(0.00)	0.00(0.00)	
INT1_3	–	–16.43(–16.35)	–16.22(–16.05)	–4.35(–6.34)	–39.83(–32.56)	
TS_3	17.89(20.04)	1.46(3.69)	0.63(3.13)	16.82(17.25)	–54.32(–47.37)	
INT2_3	–	1.43(2.99)	1.01(2.21)	15.63(17.34)	–49.05(–50.72)	
HBUT + ZH	–	18.75(18.20)	18.66(18.05)	20.05(18.62)	–4.67(–1.90)	–14.65 (–17.35)
PTN system						
PTN + HZ	–	0.00(0.00)	0.00(0.00)	0.00(0.00)	0.00(0.00)	
INT1_4	–	–14.92(–14.89)	–15.80(–14.65)	–0.56(–3.47)	–51.14(–37.50)	
TS_4	17.92(20.15)	3.00(5.26)	2.14(4.65)	18.62(19.20)	–55.26(–48.80)	
INT2_4	–	3.10(4.45)	2.14(3.68)	18.72(18.94)	–55.62(–51.18)	
HPEN + ZH	–	20.37(19.83)	20.19(19.58)	22.08(20.65)	–6.34(–3.58)	–14.70 (–16.42)

^a For 5T and 3T (in parenthesis) cluster models of H-ZSM-5, computed at B3LYP/6-31G(d) level of theory.

^b Activation energy, in kcal mol^{–1}.

^c In kcal mol^{–1}.

^d In cal mol^{–1} K^{–1}.

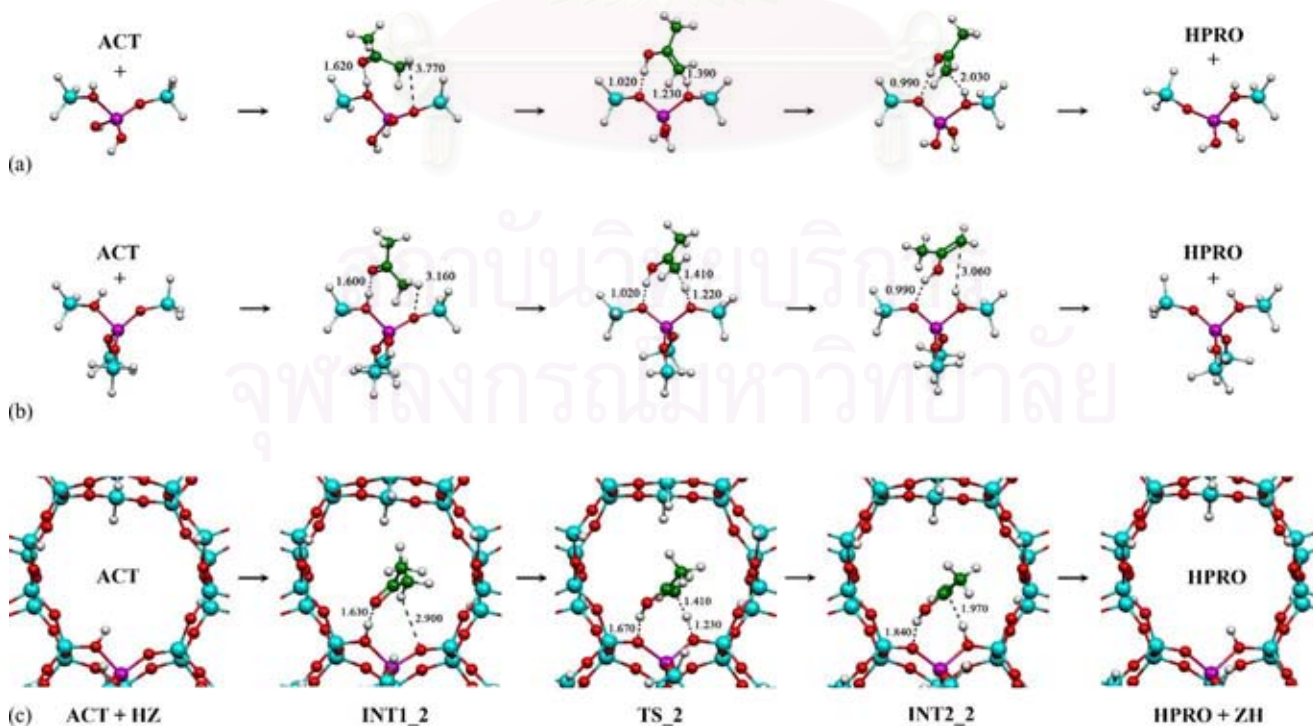


Fig. 2. Reaction steps for acetone conversion on (a) 3T-DFT, (b) 5T-DFT and (c) 50/3T ONIOM2 cluster models.

Table 2

Relative energies and thermodynamic quantities of related species of various systems on 50T cluster model

System/energy ^a	$\Delta E^{\ddagger b}$	ΔE^{298c}	ΔH^{298c}	ΔG^{298c}	ΔS^{298d}	log <i>K</i>
ACD system						
ACD + HZ	–	0.00	0.00	0.00	0.00	
INT1.1	–	–11.23	–11.11	–0.66	–35.07	
TS_1	19.39	8.16	7.33	20.76	–45.06	
INT2.1	–	3.60	3.32	15.69	–41.51	
HETH + ZH	–	17.89	17.90	17.85	0.17	–11.98
ACT system						
ACT +	–	0.00	0.00	0.00	0.00	
INT1.2	–	–14.06	–12.94	–3.59	–31.36	
TS_2	19.34	5.28	5.49	17.63	–40.74	
INT2.2	–	3.39	4.02	15.24	–37.64	
HPRO + ZH	–	20.22	20.66	19.69	3.25	–13.80
BTN system						
BTN + HZ	–	0.00	0.00	0.00	0.00	
INT1.3	–	–13.86	–13.56	–2.42	–37.35	
TS_3	20.01	6.15	5.44	20.37	–50.10	
INT2.3	–	4.30	4.07	17.73	–45.80	
HBUT + ZH	–	18.89	18.81	19.27	–1.55	–14.77
PTN system						
PTN + HZ	–	0.00	0.00	0.00	00.00	
INT1.4	–	–12.13	–11.90	0.48	–41.52	
TS_4	19.98	7.85	7.16	22.08	–50.05	
INT2.4	–	5.84	5.65	19.14	–45.26	
HPEN + ZH	–	20.51	20.33	21.29	–3.22	–13.68

^a For 50/3T cluster model of H-ZSM-5, computed at ONIOM2(B3LYP/6-31G(d):AM1) level of theory.^b Activation energy, in kcal mol^{–1}.^c In kcal mol^{–1}.^d In cal mol^{–1} K^{–1}.

diolate and O₃ for product-side intermediate for all systems are hardly ever different but smaller than their corresponding isolated-H-ZSM-5 OH vibrational frequencies by approximate 700 cm^{–1}. Relative energies and thermodynamic quantities of related species of systems acetaldehyde, acetone, butanone and 2-pentanone are listed in Table 2. The conversion constants of the reaction systems ACD, ACT, BTN and PTN of the 50T cluster model are log *K* = –11.98, –13.80, –14.77 and –13.68, respectively. Relative energies and thermodynamic quantities of related species of various systems on the 50T cluster model are listed in Table 2. The geometrical structures of the involved species of the systems ACD, ACT, BTN and PTN of the 50/3T-ONIOM2 model are shown in Figs. 1c, 2c, 3c and 4c, respectively. The order of magnitudes of the conversion constants is in decreasing order: ACD > ACT > BTN > PTN for 3T-DFT and 5T-DFT calculation models and ACD > PTN > ACT > BTN for 50/3T-ONIOM2 calculation model.

3.2. Molecular arrangement on different cluster models

Due to the molecular configurations of acetaldehyde interacting with H-ZSM-5 zeolite as three different clusters 3T, 5T and 50T, shown in Fig. 1, the molecular arrangement of acetaldehyde on these clusters are quite similar. All cluster models employed for this system (ACD) should give the correct computational results, because the small molecule

of acetaldehyde is hardly ever affected by double 10T-membered ring of 50T cluster. For the ACT system, the molecules of acetone and acetaldehyde are hardly different but the molecular arrangement of acetone on the 50/3T cluster model are quite different from the 5T and 3T models (see Fig. 2). However, the molecular arrangements of the species interacting with 5T and 3T cluster models for ACT system are still different. As the molecules of butanone (BTN) and 2-pentanone (PTN) are bigger than the acetaldehyde and acetone, the molecular arrangements of butanone and 2-pentanone on the 50/3T cluster model are obviously different from the 5T and 3T models, see Figs. 3 and 4. The 50/3T-ONIOM2 calculation model is an appropriate tool for the electronic calculation in the H-ZSM-5 catalyst system.

3.3. Reaction coordinate

The potential energy surfaces for keto-enol isomerization of acetaldehyde, acetone, butanone and 2-pentanone of non-catalytic shown in Fig. S3 (Supplementary data), water-catalyzed in Fig. S4 (Supplementary data) and 3T-DFT, 5T-DFT and 50/3T-ONIOM2 in Fig. 5 are presented. The activation of non-catalytic reactions of systems ACD, ACT, BTN and PTN, shown in Fig. S3 (Supplementary data) are 69.38, 65.92, 66.22 and 67.87 kcal/mol, respectively. Activation energies due to the activation steps of the water-catalyzed model of the systems ACD, ACT, BTN and PTN, shown in

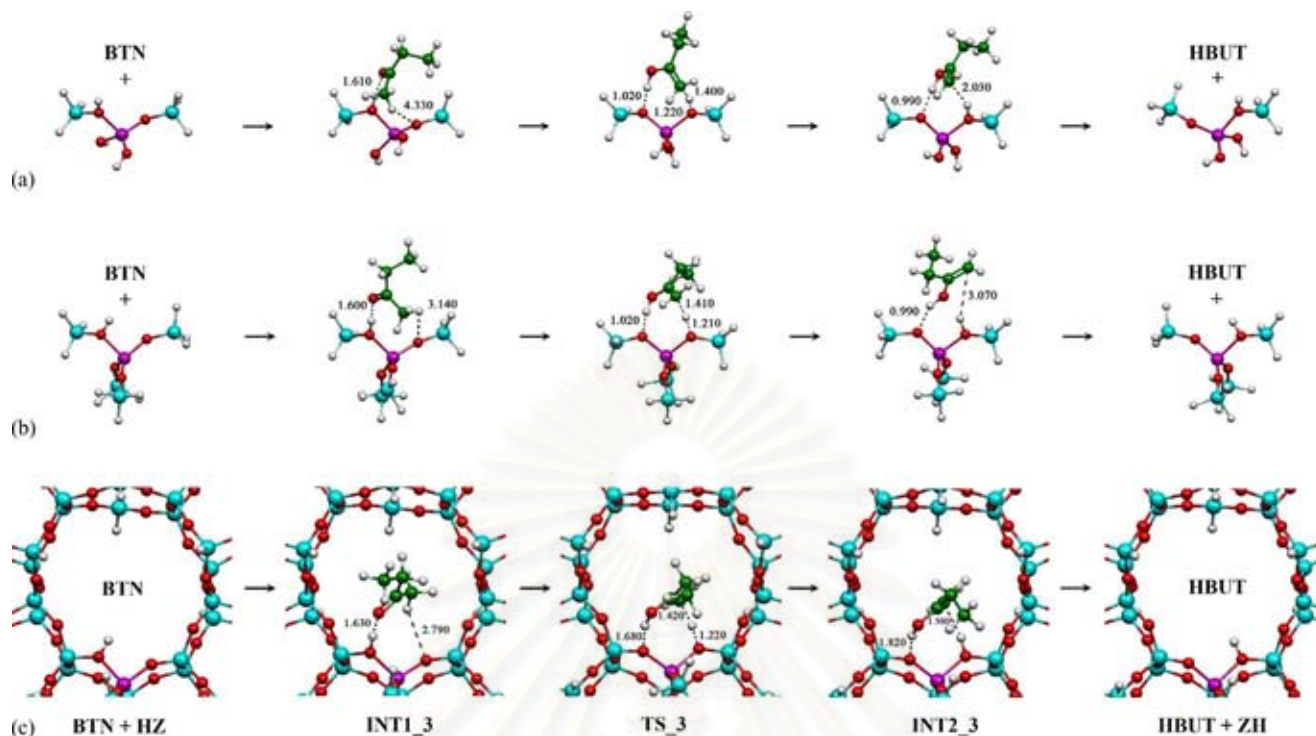


Fig. 3. Reaction steps for butanone conversion on (a) 3T-DFT, (b) 5T-DFT and (c) 50/3T ONIOM2 cluster models.

Fig. S4 (Supplementary data) are 38.07, 38.29, 39.30 and 41.59 kcal/mol, respectively. Activation energies due to the activation steps of the 5T and 3T (in parentheses) cluster models of the systems ACD, ACT, BTN and PTN shown in Fig. 5 are 18.33 (20.39), 18.56 (20.79), 17.89 (20.04) and

17.92 (20.15) kcal/mol, respectively. Activation energies due to the activation steps of the 50T cluster model of the systems ACD, ACT, BTN and PTN shown in Fig. 5 are 19.39, 19.34, 20.01 and 19.98 kcal/mol, respectively. In this work, the relative energies computed by the 3T-DFT and 5T-DFT

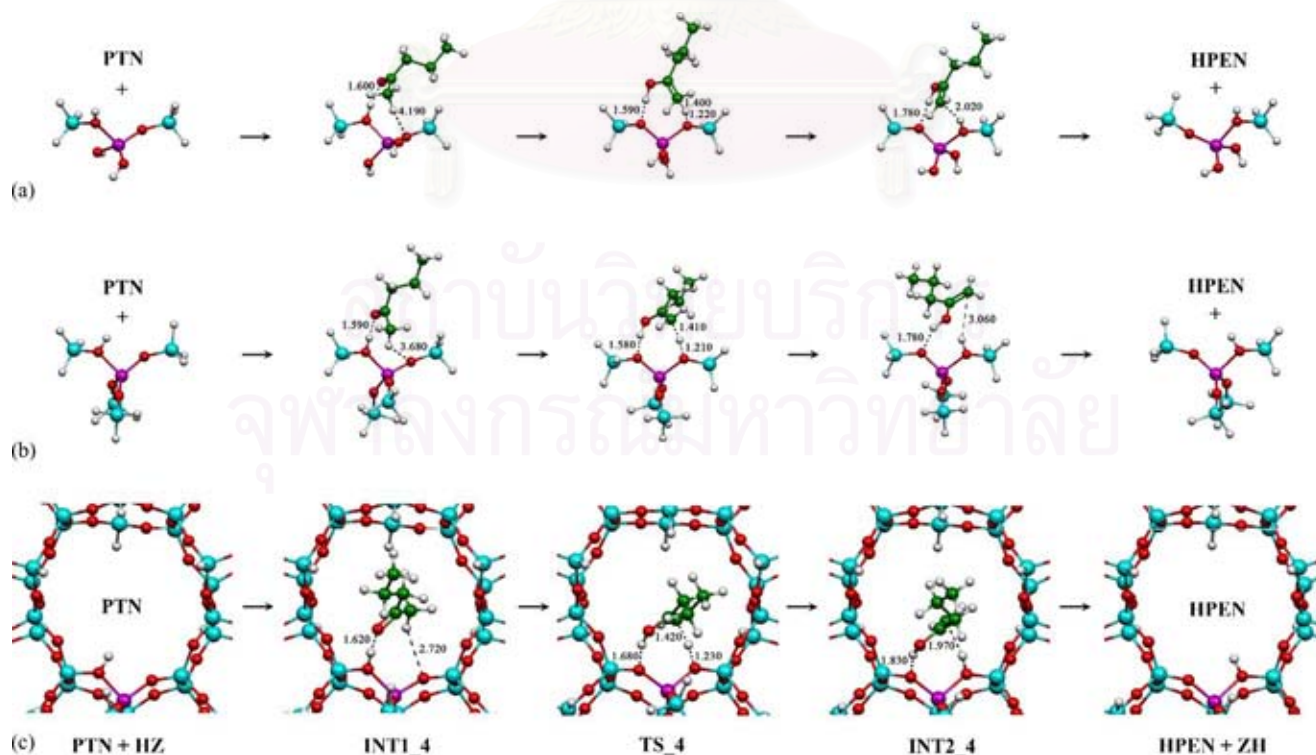


Fig. 4. Reaction steps for 2-pentanone conversion on (a) 3T-DFT, (b) 5T-DFT and (c) 50/3T ONIOM2 cluster models.

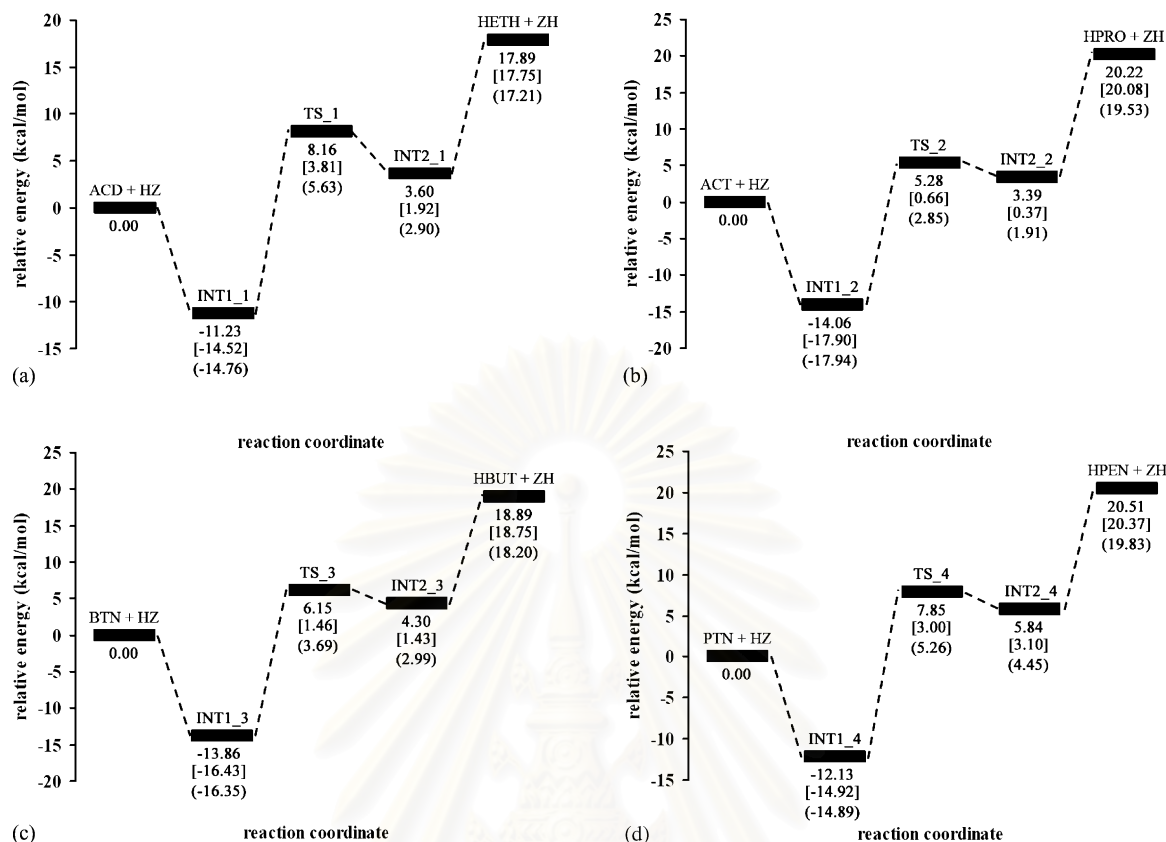


Fig. 5. Potential energy surface for keto-enol isomerization of (a) acetaldehyde, (b) acetone, (c) butanone and (d) 2-pentanone on three cluster models of H-ZSM-5. Relative energies are derived from the 50/3T-ONIOM2, 5T-DFT [in bracket] and 3T-DFT (in parenthesis).

models show the underestimated values as compared to the 50/3T-ONIOM2 model.

4. Conclusion

Conversions of acetaldehyde to hydroxyethylene, acetone to 2-hydroxypropylene, butanone to 2-hydroxybutene and 2-pentanone to 2-hydroxypentene catalyzed by H-ZSM-5 have been theoretically studied using 3T-DFT and 5T-DFT cluster models computed at the B3LYP/6-31G(d) level and 50/3T-ONIOM cluster model computed at the ONIOM(B3LYP/6-31G(d):AM1) level have been carried out. The activation energies of all systems ACD, ACT, BTN and PTN catalyzed by H-ZSM-5 zeolite are obviously lower than non catalytic and water-catalyzed models. As catalytic ability of H-ZSM-5 zeolite depending on the activation of these conversion reactions, the H-ZSM-5 can be applied in the production of some unsaturated alcohols. The 50/3T-ONIOM2 calculation model is an appropriate tool for the electronic calculation in the H-ZSM-5 catalyst system.

Acknowledgements

Authors gratefully acknowledge the financial assistance from Rachadapisek Sompoch Endowment Fund, Chula-

longkorn University. We are also thankful to the Thailand Research Fund (TRF) for giving an encouragement of present work.

Appendix A. Supplementary data

Supplementary data associated with this article can be found, in the online version, at doi:10.1016/j.molcata.2005.06.012.

References

- [1] W. Hölderich, M. Hesse, F. Nümann, *Angew. Chem. Int. Ed. Engl.* 27 (1988) 226.
- [2] A. Corma, *Chem. Rev.* 95 (1995) 559.
- [3] H. Ghobarkar, O. Schäf, U. Guth, *Prog. Solid St. Chem.* 27 (1999) 29.
- [4] S.E. Sen, S.M. Smith, K.A. Sullivan, *Tetrahedron* 55 (1999) 12657.
- [5] J. Valyon, G. Onyestyák, L.V.C. Rees, *J. Phys. Chem. B* 102 (1998) 8994.
- [6] W.E. Farneth, R.J. Gorte, *Chem. Rev.* 95 (1995) 615.
- [7] F. Yin, A.L. Blumenfeld, V. Gruver, J.J. Fripiat, *J. Phys. Chem. B* 101 (1997) 1824.
- [8] E.A. Paukshtis, L.V. Malysheva, V.G. Stepanov, *React. Kinet. Catal. Lett.* 65 (1998) 145.
- [9] R. Barthos, F. Lónyi, G. Onyestyák, J. Valyon, *J. Phys. Chem. B* 104 (2000) 7311.

- [10] F. Lónyi, J. Valyon, *Thermochim. Acta* 373 (2001) 53.
- [11] F. Lónyi, J. Valyon, *Microporous Mesoporous Mater.* 47 (2001) 293.
- [12] A. Boreňave, A. Auroux, C. Guimon, *Micropor. Mater.* 11 (1997) 275.
- [13] H.-M. Kao, C.P. Grey, *J. Phys. Chem.* 100 (1996) 5105.
- [14] W.P.J.H. Jacobs, J.W. de Haan, L.J.M. van de Ven, R.A. van Santen, *J. Phys. Chem.* 97 (1993) 10394.
- [15] G.I. Kapustin, T.R. Brueva, *Thermochim. Acta* 379 (2001) 71.
- [16] N. Katada, H. Igi, J.-H. Kim, M. Niwa, *J. Phys. Chem. B* 101 (1997) 5969.
- [17] T.R. Brueva, I.V. Mishin, G.I. Kapustin, *Thermochim. Acta* 379 (2001) 15.
- [18] D.J. Parrillo, R.J. Gorte, *J. Phys. Chem.* 97 (1993) 8786.
- [19] C. Lee, D.J. Parrillo, R.J. Gorte, W.E. Farneth, *J. Am. Chem. Soc.* 118 (1996) 3262.
- [20] A. Zecchina, F. Geobaldo, G. Spoto, S. Bordiga, G. Ricchiardi, R. Buzzoni, G. Petrini, *J. Phys. Chem.* 100 (1996) 16584.
- [21] C. Pazé, S. Bordiga, C. Lamberti, M. Salvalaggio, A. Zecchina, G. Bellussi, *J. Phys. Chem. B* 101 (1997) 4740.
- [22] H. Jobic, A. Tuel, M. Krossner, J. Sauer, *J. Phys. Chem.* 100 (1996) 19545.
- [23] H. Kitagawa, Y. Sendoda, Y. Ono, *J. Catal.* 101 (1986) 12.
- [24] M. Shibata, H. Kitagawa, Y. Sendoda, Y. Ono, *Proceedings of the Seventh International Zeolite Conference*, Elsevier, Tokyo, 1986, p. 717.
- [25] M.S. Scurrell, *Appl. Catal.* 41 (1988) 89.
- [26] Y. Ono, K. Kanae, *J. Chem. Soc. Faraday Trans.* 87 (1991) 663.
- [27] R. Shigeishi, A. Garforth, I. Harris, J. Dwyer, *J. Catal.* 130 (1991) 423.
- [28] M. Guisnet, N.S. Gnep, D. Aittaleb, J.Y. Doyemet, *Appl. Catal.* 87 (1992) 255.
- [29] M. Guisnet, N.S. Gnep, F. Alario, *Appl. Catal.* 89 (1992) 1.
- [30] J.A. Biscardi, G.D. Meitzner, E. Iglesia, *J. Catal.* 179 (1998) 192.
- [31] W. Ding, S. Li, G.D. Meitzner, E. Iglesia, *J. Phys. Chem. B* 105 (2001) 506.
- [32] W. Li, S.Y. Yu, G.D. Meitzner, E. Iglesia, *J. Phys. Chem. B* 105 (2001) 1176.
- [33] D. Nachtigallova, P. Nachtigall, M. Sierka, J. Sauer, *Phys. Chem. Chem. Phys.* 1 (1999) 2019.
- [34] K. Yoshizawa, Y. Shiota, T. Yumura, T. Yamabe, *J. Phys. Chem. B* 104 (2000) 734.
- [35] M.J. Rice, A.K. Chakraborty, A.T. Bell, *J. Phys. Chem. B* 104 (2000) 9987.
- [36] S.A. Zygmunt, L.A. Curtiss, P. Zapol, L.E. Iton, *J. Phys. Chem. B* 104 (2000) 1944.
- [37] X. Rozanska, R.A. van Santen, F. Hutschkay, *J. Catal.* 200 (2001) 79.
- [38] X. Rozanska, X. Saintigny, R.A. van Santen, F. Hutschkay, *J. Catal.* 202 (2001) 141.
- [39] S.P. Yuan, J.G. Wang, Y.W. Li, S.Y. Peng, *J. Mol. Catal. A Chem.* 178 (2002) 267.
- [40] R.Z. Khaliullin, A.T. Bell, V.B. Kazansky, *J. Phys. Chem. A* 105 (2001) 10454.
- [41] I. Milas, M.A.C. Nascimento, *Chem. Phys. Lett.* 373 (2003) 379.
- [42] A. Bhan, Y.V. Joshi, W.N. Delgass, K.T. Thomson, *J. Phys. Chem. B* 107 (2003) 10476.
- [43] K. Sillar, P. Burk, *Chem. Phys. Lett.* 393 (2004) 285.
- [44] K. Sillar, P. Burk, *J. Phys. Chem. B* 108 (2004) 9893.
- [45] S. Humbel, S. Sieber, K. Morokuma, *J. Chem. Phys.* 105 (1996) 1959.
- [46] S. Dapprich, I. Komaromi, K.S. Byun, K. Morokuma, M.J. Frisch, *J. Mol. Struct. (THEOCHEM)* 462 (1999) 1.
- [47] H.V. Koningsveld, H.V. Bekkum, J.C. Jansen, *Acta. Cryst. B* 43 (1987) 127.
- [48] A.D. Becke, *Phys. Rev. A* 38 (1988) 3098.
- [49] C. Lee, W. Yang, R.G. Parr, *Phys. Rev. B* 37 (1988) 785.
- [50] A.D. Becke, *J. Chem. Phys.* 98 (1993) 5648.
- [51] F. Maseras, K. Morokuma, *J. Comput. Chem.* 16 (1995) 1170.
- [52] T. Vreven, K. Morokuma, *J. Comp. Chem.* 21 (2000) 1419.
- [53] M. Remko, O.A. Walsh, W.G. Richards, *J. Phys. Chem. A* 105 (2001) 6926.
- [54] M. Remko, *J. Phys. Chem. A* 106 (2002) 5005.
- [55] C. Peng, P.Y. Ayala, H.B. Schlegel, M.J. Frisch, *J. Comp. Chem.* 17 (1996) 49.
- [56] C. Gonzalez, H.B. Schlegel, *J. Chem. Phys.* 90 (1989) 2154.
- [57] M.J. Frisch, G.W. Trucks, H.B. Schlegel, G.E. Scuseria, M.A. Robb, J.R. Cheeseman, J.A. Montgomery Jr., T. Vreven, K.N. Kudin, J.C. Burant, J.M. Millam, S.S. Iyengar, J. Tomasi, V. Barone, B. Men- nucci, M. Cossi, G. Scalmani, N. Rega, G.A. Petersson, H. Nakatsuji, M. Hada, M. Ehara, K. Toyota, R. Fukuda, J. Hasegawa, M. Ishida, T. Nakajima, Y. Honda, O. Kitao, H. Nakai, M. Klene, X. Li, J.E. Knox, H.P. Hratchian, J.B. Cross, C. Adamo, J. Jaramillo, R. Gom- perts, R.E. Stratmann, O. Yazyev, A.J. Austin, R. Cammi, C. Pomelli, J.W. Ochterski, P.Y. Ayala, K. Morokuma, G.A. Voth, P. Salvador, J.J. Dannenberg, V.G. Zakrzewski, S. Dapprich, A.D. Daniels, M.C. Strain, O. Farkas, D.K. Malick, A. D. Rabuck, K. Raghavachari, J.B. Foresman, J.V. Ortiz, Q. Cui, A.G. Baboul, S. Clifford, J. Cioslowski, B.B. Stefanov, G. Liu, A. Liashenko, P. Piskorz, I. Komaromi, R.L. Martin, D.J. Fox, T. Keith, M.A. Al-Laham, C.Y. Peng, A. Nanayakkara, M. Challacombe, P.M. W. Gill, B. Johnson, W. Chen, M.W. Wong, C. Gonzalez, J.A. Pople, *Gaussian 03*, Revision B.03, Gaussian Inc., Pittsburgh PA, 2003.
- [58] G. Schaftenaar, *MOLDEN 3.7*, CAOS/CAMM Center, Nijmegen Toernooiveld, Nijmegen, The Netherlands, 1991.
- [59] *MOLEKEL 4.3*: Swiss Center for Scientific Computing, Manno (Switzerland), 2000.



Appendix C

Presentation Abstract (part 2)

(Poster Session). 30th Congress on Science and Technology of Thailand, 19-21
October 2004: Impact Exhibition and Convention Center, Muang Thong Thani,
Nonthaburi, Thailand.

สถาบันวิทยบริการ
จุฬาลงกรณ์มหาวิทยาลัย

การศึกษาปฏิกิริยา คีโ-อินอล ไอโซเมอไรเซชัน ของสารประกอบอะซีทัลดีไฮด์และอะซีโตนใน
ซีโอไลต์ชนิดเอช-แซดเอสเอ็ม-5 โดยวิธีทฤษฎีเดนซิตีฟังก์ชันนอลและอนเนียม

INVESTIGATION OF THE KETO-ENOL ISOMERIZATION OF ACETAL- DEHYDE AND ACETONE IN H-ZSM-5 BY DFT AND ONIOM METHODS

อัครศักดิ์ รัตนสัมฤทธิ์ และ วิทยา เรืองพรวิสุทธิ*

Attasak Rattanasumrit and Vithaya Ruangpornvisuti*

**Supramolecular Chemistry Research Unit, Department of Chemistry,
Faculty of Science, Chulalongkorn University 10330 Bangkok, Thailand,
e-mail address : attasakthailand@hotmail.com**

บทคัดย่อ: การศึกษาปฏิกิริยา คีโ-อินอล ไอโซเมอไรเซชัน ของสารประกอบอะซีทัลดีไฮด์และสารประกอบ
อะซีโตนในซีโอไลต์ชนิดเอช-แซดเอสเอ็ม-5 ศึกษาแบบจำลองคลัสเตอร์ขนาด 3T และ 5T โดยวิธีทฤษฎีเดนซิตี
ฟังก์ชันนอล (DFT) ชนิด B3LYP/6-31G(d) และแบบจำลองคลัสเตอร์ที่มีขนาดใหญ่ คือ 72T โดยวิธี
ONIOM2(B3LYP/6-31G(d):AM1) และ ONIOM2(B3LYP/6-31G(d):MNDO) ซึ่งกำหนดคลัสเตอร์ขนาด 3T
และ 5T เป็นบริเวณของการคำนวณโดยทฤษฎีสูง พบว่าการดูดซับสารผลิตภัณฑ์บนซีโอไลต์มีการลดลงของ
พลังงานจากสภาวะทรานซิชันซึ่งมีค่าสูงกว่าพลังงานของการดูดซับสารตั้งต้นบนซีโอไลต์ โดยแบบจำลอง
คลัสเตอร์ขนาด 3T ให้ค่าพลังงานกระตุ้นและค่าคงที่อัตราเร็วของสารตั้งต้นเชิงซ้อนเท่ากับ 20.39 kcal/mol
และ $\log K = -14.72$ ตามลำดับ

Abstract: This study is focused to keto-enol isomerization of acetaldehyde and acetone inside H-ZSM-5. The H-ZSM-5 clusters of 3T and 5T have been studied using a density functional theory (DFT) at B3LYP/6-31G(d). Level of theory for the enlarging cluster of 72T, we have used the two-layer ONIOM2(B3LYP/6-31G(d):AM1) and ONIOM2(B3LYP/6-31G(d):MNDO) approaches, and its active site (cluster 3T and 5T) were treated as high theoretical area. We found the reaction energy of HZ(enol), which decreased from transition state but still higher than HZ(keto). Due to the 3T cluster model, activation energy and rate constant of complex reactant are 20.39 kcal/mol and $\log K = -14.72$, respectively.

Methodology: $\text{HZ+keto} \longrightarrow \text{HZ(keto)} \longrightarrow \text{TS} \longrightarrow \text{HZ(enol)} \longrightarrow \text{HZ+enol}$

Two distinctive strategies have been adopted to model H-ZSM-5. The first one presents the active site of the aluminosilicate by different clusters, and the second strategy uses the hybrid ONIOM methodology. Geometry optimization of 3T and 5T clusters and harmonic vibrational frequencies have been computed using the non local hybrid three-parameter B3LYP density functional approach and the 6-31G(d) basis set. The model in ONIOM2 method are 3T and 5T clusters, described using the B3LYP functional and the 6-31G(d) basis set. For the low-level part we have tested two different semi-empirical methods: AM1 and MNDO. All calculations have been performed by using Gaussian03 program.

Results, Discussion and Conclusion: For the results with cluster 3T and 5T are very alike both the reactants are acetaldehyde and acetone. Enlarging the size of the cluster to 72T with the ONIOM2 approach destabilizes the keto intermediate and stabilizes the HZ(enol), which presents in a decrease of the reaction energy from transition state but still higher than the HZ(keto).

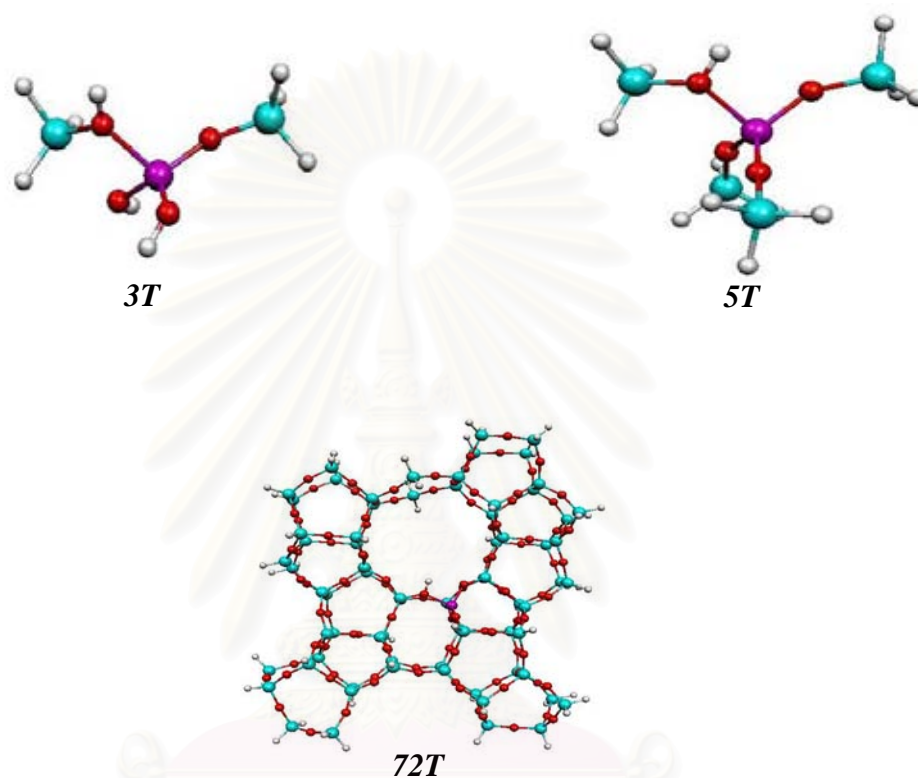


Figure C-1 3T, 5T and 72T cluster models of H-ZSM-5.

Reference: [1]. Xavier Solans-Monfort, Joan Bertran, Vicenc Branchadell, and Mariona Sodupe*, *J. Phys. Chem. B* **2002**, *106*, 10220-10226.
[2]. Keiji Morokuma, *Bull. Korean Chem. Soc.* **2003**, Vol.24, No.6, 797-801.

Keywords: keto-enol isomerization, H-ZSM-5, DFT, ONIOM2



Appendix C

Presentation Abstract (part 2)

**(Poster Session). 2nd Asian Pacific Conference on Theoretical &
Computational Chemistry (APCTCC2), 2-6 May 2005:
Chulalongkorn University, Bangkok, Thailand**

สถาบันวิทยบริการ
จุฬาลงกรณ์มหาวิทยาลัย

Theoretical study of conversion reactions of ketone to hydroxyalkylene in cluster models of H-ZSM-5 zeolite

Attasak Rattanasumrit and Vithaya Ruangpornvisuti*

Supramolecular Chemistry Research Unit, Department of Chemistry, Faculty of Science, Chulalongkorn University 10330 Bangkok, Thailand,
e-mail address : attasakthailand@hotmail.com

Abstract: Conversions of acetaldehyde to hydroxyethylene, acetone to 2-hydroxypropylene, butanone to 2-hydroxybutene and 2-pentanone to 2-hydroxypentene catalyzed by H-ZSM-5 have been theoretically studied using quantum chemical methods. Geometry optimizations reacting species in the acid sites of H-ZSM-5 catalyst of 3T and 5T cluster models (Figure C-2) employing the DFT/B3LYP/6-31G(d) method and of 50T cluster model (Figure C-2) employing the ONIOM(B3LYP/6-31G(d):AM1) calculations have been carried out. The vibrational frequencies of acid sites of H-ZSM-5, relative energies of all involved species, thermodynamic quantities and equilibrium constant of catalytic reactions have been obtained. The estimated activation energies of all conversion reactions are presented.

Methodology: $\text{HZ+keto} \longrightarrow \text{HZ(keto)} \longrightarrow \text{TS} \longrightarrow \text{HZ(enol)} \longrightarrow \text{ZH+enol}$

Two distinctive strategies have been adopted to model H-ZSM-5. The first one presents the active site of the aluminosilicate by different clusters, and the second strategy uses the hybrid ONIOM methodology. Geometry optimization of 3T and 5T clusters and harmonic vibrational frequencies have been computed using the non local hybrid three-parameter B3LYP density functional approach and the 6-31G(d) basis set. The model in ONIOM2 method is 3T cluster, described using the B3LYP functional and the 6-31G(d) basis set. For the low-level part we have tested semi-empirical method: AM1. All calculations have been performed by using GAUSSIAN 03 program package.

Results, Discussion and Conclusion: For the results with cluster 3T and 5T are very alike of all the reactants. Enlarging the size of the cluster to 50T with the ONIOM2 approach destabilizes the keto intermediate and stabilizes the HZ(enol), which presents in a decrease of the reaction energy from transition state but still higher than the HZ(keto).

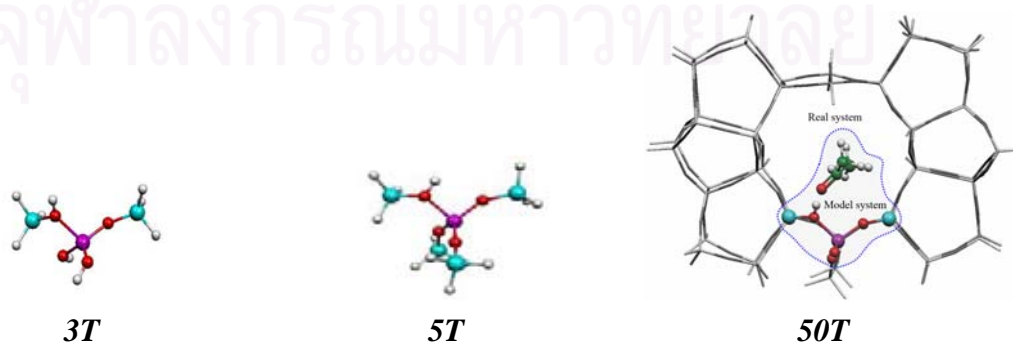


Figure C-2 3T, 5T and 50T cluster models of H-ZSM-5.

CURRICULUM VITAE

NAME, NICKNAME : Mr. Attasak Rattanasumrit, Tom

BIRTH DATE : January 15th, 1982

BIRTH PLACE : Chainat Province, Thailand

EDUCATION : YEAR INSTITUTION DEGREE/DIPLOMA

1999	Suankularb Wittayalai Nonthaburi	High School
2003	Kasetsart Univ.	B.S. (Chemistry)
2005	Chulalongkorn Univ.	M.S. (Petrochemistry and Polymer Science)

ADDRESS : 297/128, Moo 9, Bangkrasor, Muang, Nonthaburi,
11000, Thailand. Tel. 02-5808219

E-MAIL : attasakthailand@hotmail.com

PUBLICATION

[1] Attasak Rattanasumrit and Vithaya Ruangpornvisuti*, Theoretical study of conversion reactions of ketone to hydroxyalkylene in cluster models of zeolite H-ZSM-5. J. Mol. Catal A-Chem 229 (2005): 68-75.

[2] Vithaya Ruangpornvisuti* and Attasak Rattanasumrit., ONIOM study of the ketone to hydroxyalkylene conversion on cluster model of zeolite H-ZSM-5. J. Catal letter. (submitted)

PRESENTATION

[1] Attasak Rattanasumrit and Vithaya Ruangpornvisuti*, Investigation of keto-enol isomerization of acetaldehyde and acetone in H-ZSM-5 using DFT and ONIOM methods. (Poster Session): 30th Congress on Science and Technology of Thailand, 19-21 October 2004. Impact Exhibition and Convention Center, Muang Thong Thani, Nonthaburi, Thailand.

[2] Attasak Rattanasumrit and Vithaya Ruangpornvisuti*, Theoretical study of conversion reactions of ketone to hydroxyalkylene in cluster models of H-ZSM-5 zeolite. (Poster Session): 2nd Asian Pacific Conference on Theoretical & Computational Chemistry (APCTCC2), 2-6 May 2005. Chulalongkorn University, Bangkok, Thailand.